

新制

工

1335

**STUDIES ON PHASE SEPARATION IN SILOXANE  
SOL-GEL SYSTEMS IN CONFINED GEOMETRY**

**KAZUYOSHI KANAMORI**

**2005**

**STUDIES ON PHASE SEPARATION IN SILOXANE  
SOL-GEL SYSTEMS IN CONFINED GEOMETRY**

**KAZUYOSHI KANAMORI**

**2005**

# CONTENTS

GENERAL INTRODUCTION .....	1
CHAPTER 1: METHODOLOGY .....	9
CHAPTER 2: STRUCTURES IN A TWO-DIMENSIONAL MOLD .....	32
2.1 Three-Dimensional Observation of Phase-Separated MTMS-Derived Gels and Comparison with TMOS-Derived Ones: Global Geometry .....	32
2.2 Local Geometrical Analysis of Structural Deformation in MTMS-Derived Phase-Separating Gels: Effect of Wetting, Gravity, and Viscoelasticity .....	52
CHAPTER 3: STRUCTURES IN A ONE-DIMENSIONAL MOLD .....	71
3.1 Phase-Separated Structure of Methylsiloxane Gel in a Long Cylindrical Capillary .....	71
3.2 Interface-Directed Web-to-Pillar Transition in an Open Groove .....	87
CHAPTER 4: STRUCTURES IN A ZERO-DIMENSIONAL MOLD .....	105
CHAPTER 5: APPLICATION TO CAPILLARY HPLC .....	123
SUMMARY .....	139
LIST OF PUBLICATIONS .....	143

ACKNOWLEDGEMENT ..... 146

APPENDIX: ACCURACY OF LSCM OBSERVATION AND OTSU THRESHOLDING ..... 148



## GENERAL INTRODUCTION

Since around 1970s sol-gel method has been drawing a lot of attention for its advantage for low temperature synthesis of glasses and ceramics [1-3]. In recent years, the enthusiasms of most researchers seem to be shifting to porous materials and organic-inorganic hybrids [4]. Porous materials have been utilized in an extended application such as catalysts, sensors, separation media, optical and electronic devices etc. taking advantage of its pore structure, high surface area and transportation behavior inside the pores. Hybridization of inorganic frameworks and organic moieties has also been a foremost strategy of mechanical improvement of brittle ceramics as well as functionalization by reactive organic functional groups.

The first aerogel with extremely high porosity, low density and low refractive index was prepared by supercritical drying (SCD) of waterglass-derived silica gel in 1930s by Kistler [5], and decades later, his sodium silicate-derived aerogels were improved by Teichner et al. as an alkoxysilane-derived sol-gel process together with SCD. Aerogels have been highly important for thermal insulators, Cherenkov detectors and space industry applications etc [6,7]. An ordered mesoporous silica named MCM-41 was firstly prepared by supramolecular templating which was reported by the researchers in Mobil Oil Corp. [8,9]. Highly ordered mesoporous materials have been fascinating the world since then because of their beautiful textures and promising applications. In general procedure of supramolecular templating [8-12], organic compounds such as surfactants, amphiphilic block copolymers and dendrimers etc. are included into the starting solution. The micelle-forming surfactant interplays with growing silica polymers and directs the growing silica into micelle structures resulting in highly ordered mesostructures. In another method called microemulsion templating [13-16], a liquid crystalline mesophase consists of surfactants is pre-formed, and polymerizing species replicate the pre-formed mesophase structure subsequently. This kind of mesoporous materials with various pore

structures is becoming one of the key subjects of recent nanotechnology.

Another novel porous material through sol-gel was invented in 1990s by Nakanishi et al. [17]. Siloxane gels with well-defined bicontinuous macroporous morphology are synthesized by sol-gel accompanied by phase separation. Inducing spinodal decomposition during the network-forming sol-gel reaction of silicon alkoxides and freezing the transient phase-separating structure by gelation yield a unique feature of gel. Macropores with micrometer-range sizes are formed by spinodal decomposition and mesopores with nanometer-range by subsequent hydrothermal aging [18] or even by supramolecular templating [19]. This kind of high-porosity double pore structure finds an application to a separation medium for high performance liquid chromatography (HPLC). Compared with the conventional particle-packed HPLC columns, double pore silica monoliths are highly advantageous in HPLC because macropores contribute the higher permeability and mesopores supply a high surface area which separates the sample solutes effectively. Thus double pore silica monoliths actualize more rapid and efficient separations than any other columns [20].

Monolithic columns with porous structure are usually prepared by polymerization reactions such as sol-gel [17] and (living) radical polymerizations [21-25]. Most polymeric monoliths are directly synthesized in a capillary. The art of these *in situ* polymerizations is undoubtedly an excellent formability. Every kind of column has to be covered by polymers or metals to ensure the high pressure durability in HPLC after the formation of pore structure, whereas a monolithic column can be obtained without cladding; a starting solution is simply introduced in a mold and allowed to polymerize there. However, sol-gel-derived monolithic columns always suffer from a considerable shrinkage during aging and drying because polymerization is a condensation reaction [3]. Thus the “thick” monoliths prepared by sol-gel have to be encapsulated by heat-shrinking poly(ether-ether-ketone) (PEEK) [26] in order to reinforce the column against the high driving pressure. This bothersome process of cladding can be avoided by decreasing the radial thickness of the column because the shrinkage of the sol-gel derived siloxane gel

becomes smaller with decreasing the column radius. Thus the technical interests concerning miniaturization into pressure-driven capillary HPLC, capillary electrochromatography (CEC) and Lab-on-a-Chip with silica monolith have been gathering much attention [27]. Moreover, miniaturization of separation media leads to higher sensitivity and lower environmental load.

Although some successful applications to miniaturized devices are reported [26-28], sol-gel preparation into small confined spaces is often significantly affected by the surface of the mold especially when the size of the mold becomes smaller. The resultant gel morphologies are often deformed and spatially anisotropic whereas polymer-based monoliths are easy for miniaturization [29] due to their different pore-formation mechanism and the non-shrinking polymerization system. Spinodal decomposition, which makes macropores in siloxane sol-gel systems, is an interfacial phenomenon: Only compositional contrast will grow in the initial stage, and the interfaces between separating phases become clear and the characteristic length of the phase-separating structure becomes longer in the middle stage. And finally, after the interfaces become perfectly distinct, only the characteristic length becomes longer and the structure coarsens in a self-similar manner in order to reduce the interfacial area. This kind of sequential interface-forming and hydrodynamic coarsening (especially in siloxane sol-gel) processes make it difficult to prepare an isotropic bicontinuous porous structure in a small confined space. In both low molecular systems and polymer blend systems, the effect of surfaces on phase-separating behavior has been extensively studied. In the early stage of spinodal decomposition, “surface-directed spinodal decomposition” [30-32] has revealed to throw a critical effect by preferential diffusion-induced wetting onto a surface. In the latter hydrodynamic coarsening stage, the wetting is further accelerated by “hydrodynamic pumping” mechanism suggested by Tanaka [33]. In addition to these surface effects, inside mesoporous Vycor glasses [34,35] the critical phenomena is strongly suppressed by random-field and/or wetting effect [36-38]. Thus the importance of phase separation in confined geometry is well recognized because material should be confined in

a container in any experiment and production.

Spinodal decomposition in polymer blends have been well-studied especially by light scattering because of both the slow dynamics resulting from high viscosity and long characteristic length [39-41]. Due to the reciprocal space analysis, however, the obtainable information is strictly limited to overall characters such as characteristic length and compositional contrast etc, and the extraction method of local characteristics such as interfacial curvatures has been unknown. Recently, phase separation in polymer blends or solutions and its dynamics are extensively investigated by using Laser Scanning Confocal Microscopy (LSCM) in real space [42-50]. Jinnai et al. extracted various local geometrical information from a series of obtained 2D sliced LSCM images and subsequent 3D reconstruction, and proved, for the first time, that the time evolution of late stage of spinodal decomposition at a critical composition keeps self-similarity in both global and local structures in a real space [51]. They also demonstrated that LSCM is advantageous in 3D analysis of phase-separated sintered macroporous silica gel [52].

In the present study, the micro-surface effects on the phase formation in siloxane sol-gel are examined in various confined spaces. Especially detailed analysis using LSCM in a two-dimensional (2D) mold is performed and the origin of the deformation is presumed. By examining effects of micro-surfaces in various conditions, a plausible way to prepare isotropic structure in a capillary is suggested by eliminating such an undesirable surface effects and avoiding cracks and voids. The main systems used in this study are one derived from tri-functional methyltrimethoxysilane (MTMS) because of its better formability in confined spaces. A tetra-functional tetramethoxysilane (TMOS)-derived system is also investigated for comparative purposes. The followings are the details of contents in each chapter.

In Chapter 1, fundamental techniques used in this study are collected. Model sol-gel systems, mold preparations, LSCM observations and image analyses are detailed. These are quite important to understand the extensive discussions given in the following

chapters. Also, newly developed methods for LSCM observation of siloxane gels are demonstrated.

In Chapter 2, phase-separated structures in a 2D confined space, i.e. a gap between two parallel plates, are investigated by LSCM. At first the chemical effect of the surfaces is discussed but the hydrodynamic effect is proved to be dominant. A crucial idea for understanding surface effects is described.

In Chapter 3, the structural variations in a 1D capillary and a rectangular-sectioned open groove are described. As mentioned above, structural formation in a 1D capillary is a key technology to prepare isotropic high-efficiency capillary columns. In the open groove, being different from the closed system, the structural formation is dependent on the continuous flow from bulk reservoir and its unique geometrical feature lead to so-called “web-to-pillar transition” in which the inside surfaces of the grooves are bridged by siloxane gel pillars.

In Chapter 4, structures in a 0D mold is studied. A macroporous bicontinuous silica is employed as a 0D mold. An extraordinary behavior of structural formation is observed due to the strict physical confinement.

In Chapter 5, the actual application to the capillary HPLC is described. By tuning the conditions such as compositions of the starting solution and capillary diameters, an isotropic bicontinuous siloxane gels are successfully obtained. These capillaries showed excellent separation ability of low molecular analytes in normal phase. The control of surface polarity is also demonstrated by incorporating a surfactant into a starting solution.

Finally, the whole results and discussions are summarized in the last summary section.

## References

- [1] H. Dislich, *Angew. Chem. Int. Ed. Engl.* **10**, 363 (1969).
- [2] K. S. Mazdiyasi, R. T. Dolloff, J. S. Smith, *J. Amer. Ceram. Soc.* **52**, 523 (1969).
- [3] C. J. Brinker, G. W. Scherer, "Sol-Gel Science: The Physics and Chemistry of Sol-Gel Processing", Academic Press, San Diego, 1990.
- [4] For example, G. J. De A. A. Soler-Illia, C. Sanchez, B. Lebeau, J. Patarin, *Chem. Rev.* **102**, 4093 (2002).
- [5] S. S. Kistler, *Nature*, **127**, 741 (1931).
- [6] J. Fricke, A. Emmerling, *J. Am. Ceram. Soc.* **75**, 2027 (1992).
- [7] J. Fricke, T. Tillotson, *Thin Solid Films*, **297**, 212 (1997).
- [8] C. T. Kresge, M. E. Leonowicz, W. J. Roth, J. C. Vartuli, J. S. Beck, *Nature*, **359**, 710 (1992).
- [9] J. S. Beck, J. C. Vartuli, W. J. Roth, M. E. Leonowicz, C. T. Kresge, K. D. Schmitt, C. T-W. Chu, D. H. Olson, E. W. Sheppard, S. B. McCullen, J. B. Higgins, J. S. Schlenker, *J. Am. Chem. Soc.* **114**, 10834 (1992).
- [10] D. Zhao, Q. Huo, J. Feng, B. F. Chmelka, G. D. Stucky, *J. Am. Chem. Soc.* **120**, 6024 (1998).
- [11] P. F. W. Simon, R. Ulrich, H. W. Spiess, U. Wiesner, *Chem. Mater.* **13**, 3464 (2001).
- [12] S. Inagaki, S. Guan, T. Osuna, O. Terasaki, *Nature*, **416**, 304 (2002).
- [13] K. M. McGrath, D. M. Dabbs, N. Yao, I. A. Aksay, S. M. Gruner, *Science*, **277**, 552 (1997).
- [14] P. Schmidt-Winkel, C. J. Glinka, G. D. Stucky, *Langmuir*, **16**, 356 (2000).
- [15] K. M. McGrath, D. M. Dabbs, N. Yao, K. J. Edler, I. A. Aksay, S. M. Gruner, *Langmuir*, **16**, 398 (2000).
- [16] S. A. El-Safty, T. Hanaoka, *Chem. Mater.* **16**, 384 (2004).
- [17] K. Nakanishi, *J. Porous Mater.* **4**, 67 (1997).
- [18] K. Nakanishi, R. Takahashi, T. Nagakane, K. Kitayama, N. Koheiya, H. Shikata, N. Soga,

*J. Sol-Gel Sci. Tech.* **17**, 191 (2000)

[19] K. Nakanishi, Y. Kobayashi, T. Amatani, T. Kodaira, *Chem. Mater.* in press.

[20] N. Tanaka, H. Kobayashi, N. Ishizuka, H. Minakuchi, K. Nakanishi, K. Hosoya, T. Ikegami, *J. Chromatogr. A*, **965**, 35 (2002).

[21] C. Viklund, E. Pontén, B. Glad, K. Irgum, P. Hörstedt, F. Svec, *Chem. Mater.* **9**, 463 (1997).

[22] C. Viklund, A. Nordstom, K. Irgum, F. Svec, J. M. J. Fréchet, *Macromolecules*, **34**, 4361 (2001).

[23] T. Rohr, S. Knaus, H. Gruber, D. C. Sherrington, *Macromolecules*, **35**, 97 (2002).

[24] B. Buszewski, M. Szumski, S. Sus, *LC·GC Europe*, **12**, 2 (2002).

[25] M. Merhar, A. Podgornik, M. Barut, M. Žigon, A. Štrancar, *J. Sep. Sci.* **26**, 322 (2003).

[26] N. Tanaka, H. Nagayama, H. Kobayashi, T. Ikegami, K. Hosoya, N. Ishizuka, H. Minakuchi, K. Nakanishi, K. Cabrera, D. Lubda, *J. High Resol. Chromatogr.* **23**, 111 (2000).

[27] N. Ishizuka, H. Minakuchi, K. Nakanishi, N. Soga, H. Nagayama, K. Hosoya, N. Tanaka, *Anal. Chem.* **72**, 1275 (2000).

[28] N. Ishizuka, H. Minakuchi, K. Nakanishi, N. Soga, K. Hosoya, N. Tanaka, *J. High. Resol. Chromatogr.* **21**, 477 (1998).

[29] F. Svec, E. C. Peters, D. Sýkora, C. Yu, J. M. J. Fréchet, *J. High, Resol. Chromatogr.* **23**, 3 (2000).

[30] R. A. L. Jones, L. J. Norton, E. J. Kramer, F. S. Bates, P. Wiltzius, *Phys. Rev. Lett.* **66**, 1326 (1991).

[31] G. Krausch, *Mater. Sci. Eng. Rep.* **R14**, 1 (1995).

[32] S. Bastea, S. Puri, J. L. Lebowitz, *Phys. Rev. E*, **63**, 041513 (2001).

[33] H. Tanaka, *J. Phys.: Condens. Matter*, **13**, 4637 (2001).

[34] P. Levitz, G. Ehret, S. K. Sinha, J. M. Drake, *J. Chem. Phys.* **95**, 6151 (1991).

[35] S. G. J. M. Kluijtmans, J. K. G. Dhont, A. P. Philipse, *Langmuir*, **13**, 4976 (1997).

[36] P. G. de Gennes, *J. Phys. Chem.* **88**, 6469 (1984).

[37] M. C. Goh, W. I. Goldberg, C. M. Knobler, *Phys. Rev. Lett.* **58**, 1008 (1987).

- [38] A. J. Liu, D. J. Durian, E. Herbolzheimer, S. A. Safran, *Phys. Rev. Lett.* **65**, 1897 (1990).
- [39] T. Izumitani, T. Hashimoto, *J. Chem. Phys.* **83**, 3694 (1985).
- [40] T. Hashimoto, M. Itakura, H. Hasegawa, *J. Chem. Phys.* **85**, 6118 (1986).
- [41] T. Hashimoto, M. Itakura, N. Shimidzu, *J. Chem. Phys.* **85**, 6773 (1986).
- [42] L. Li, S. Sosnowski, C. E. Chaffey, S. T. Balke, M. A. Winnik, *Langmuir*, **10**, 2495 (1994).
- [43] H. Jinnai, Y. Nishikawa, T. Koga, T. Hashimoto, *Macromolecules*, **28**, 4782 (1995).
- [44] W. R. White, P. Wiltzius, *Phys. Rev. Lett.* **75**, 3012 (1995).
- [45] E. Kumacheva, L. Li, M. A. Winnik, D. M. Shinozaki, P. C. Cheng, *Langmuir*, **13**, 2483 (1997).
- [46] Z. Mitov, E. Kumacheva, *Phys. Rev. Lett.* **81**, 3427 (1998).
- [47] H. Takeno, M. Iwata, M. Takenaka, T. Hashimoto, *Macromolecules*, **33**, 9657 (2000).
- [48] N. Lorén, A. Altskär, A-M. Hermansson, *Macromolecules*, **34**, 8117 (2001).
- [49] M. Moffitt, Y. Rharbi, H. Li, M. A. Winnik, *Macromolecules*, **35**, 3321 (2002).
- [50] N. Lorén, M. Langton, A-M. Hermansson, *J. Chem. Phys.* **116**, 10536 (2002).
- [51] H. Jinnai, Y. Nishikawa, H. Morimoto, T. Koga, T. Hashimoto, *Langmuir*, **16**, 4380 (2000).
- [52] H. Jinnai, K. Nakanishi, Y. Nishikawa, J. Yamanaka, T. Hashimoto, *Langmuir*, **17**, 619 (2001).



# CHAPTER 1: METHODOLOGY

## 1. Introduction

This chapter is devoted to the fundamental methodologies such as gel preparation, mold preparation, Laser Scanning Confocal Microscopy (LSCM) observation and Image analysis. As for model systems, two methyltrimethoxysilane (MTMS)-derived systems yielding bicontinuous structure are mainly discussed. In the two systems, crack-free and almost non-shrinkage gels can be obtained so that these systems are advantageous to prepare miniaturized monolithic devices such as micro-HPLC and lab-on-a-chip.

Laser Scanning Confocal Microscopy (LSCM) [1] has become a powerful tool for a three-dimensional (3D) observation of a sample. This observation tool has been developed by biological and biochemical researchers [2,3] and recently Jinnai et al. applied it to 3D characterization of multi-phase polymer mixtures [4]. They also obtained geometrical and topological parameters such as mean and Gaussian curvatures and euler characteristics etc. directly from “real space” LSCM images by a subsequent 3D image analysis [4,5]. Their outstanding techniques that are used throughout this study are also reviewed in this chapter.

## 2. Structural Formation of MTMS-Derived Sol-Gel Systems

### 2.1. Experimental

Methyltrimethoxysilane (MTMS, Shin-Etsu Chemical Ind. Ltd., Japan), Formamide (FA), Methanol (MeOH) and Nitric acid (Hayashi Pure Chemical, Japan) were used as received.

Appropriate amounts of 1.0 M aqueous Nitric acid and FA or MeOH were mixed in a

glass tube and then MTMS was added under vigorous stirring at 0 °C. After stirring for 5 min, the resultant homogeneous solution was transferred into a polystyrene reaction vessel. Then the solution was allowed to gel at 40 °C in a closed condition. The resultant gel was aged over 24 h at the same temperature and was dried at 40 °C for more than 24 h, then subjected to SEM (S-2600N, Hitachi, Japan) observation.

## 2.2. Results and discussion

We used mainly two systems to prepare methylsiloxane gels; MTMS-FA system and MTMS-MeOH system. In the MTMS-FA system (denoted as MF system), the molar ratio of the components is fixed as MTMS : FA : H<sub>2</sub>O = 1 :  $f$  :  $r_f$ , while in the MTMS-MeOH (denoted as MM system), the molar ratio is MTMS : MeOH : H<sub>2</sub>O = 1 :  $m$  :  $r_m$ . The onset of phase separation ( $t_{ps}$ ) and gelation ( $t_g$ ) are listed in Table 1 for a typical composition in both systems and SEM photographs of obtained bicontinuous gels are exhibited in Figure 1. Structural formation by spinodal decomposition and sol-gel transition are obviously sluggish in the MF system, because the polymerization reaction is conducted under the pH around the isoelectric point (IEP) of MTMS [6]. This means the MF system remains fluidic during the structural formation by spinodal decomposition for longer time. On the other hand, the mobility within the phase separated gel domains is thought to become zero soon after the phase separation in the MM system.

Here we briefly review the structural development in the MF and MM systems. In both systems, phase separation, especially spinodal decomposition, occurs during sol-gel transition, which makes bicontinuous porous siloxane gels. From the Flory-Huggins equation, the miscibility of a polymeric system can be estimated [7]. In a polymeric system, the free energy change of mixing can be described as follows,

$$\Delta G \propto RT \left( \frac{\phi_1}{P_1} \ln \phi_1 + \frac{\phi_2}{P_2} \ln \phi_2 + \chi \phi_1 \phi_2 \right), \quad (1-1)$$

where  $\phi_i$  and  $P_i$  are volume fraction and the degree of polymerization of component  $i$  ( $i=1$  or  $2$ ), respectively. Here we assume component 1 corresponds to the siloxane gel phase,

Table 1 The onsets of gelation  $t_g$  and phase separation  $t_{ps}$ , and phase separation time ( $t_g$   $t_{ps}$ ) for typical compositions of two systems.

	$t_{ps}$ (min)	$t_g$ (min)	$t_g$ $t_{ps}$ (min)
MTMS : MeOH : H <sub>2</sub> O = 1 : 1.0 : 2.0	120	184	64
MTMS : FA : H <sub>2</sub> O = 1 : 2.3 : 2.5	3039	3148	109

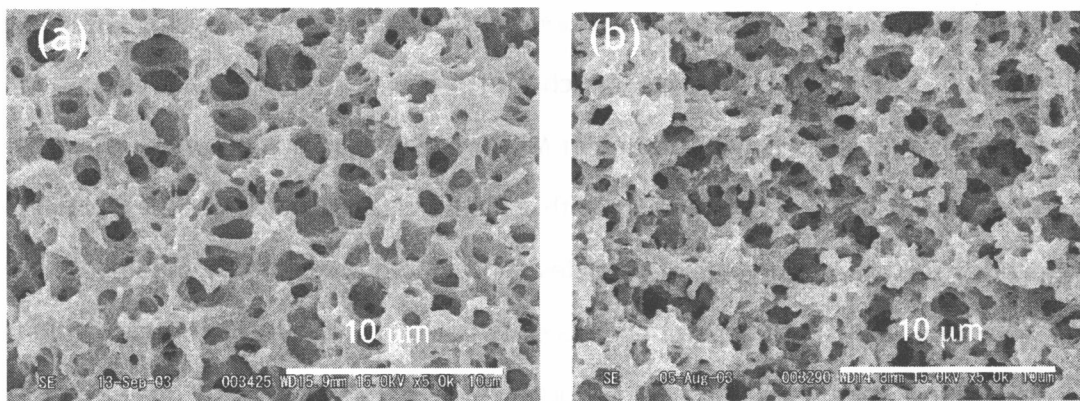


Figure 1 The SEM images of obtained siloxane gels; (a) MTMS : MeOH : H<sub>2</sub>O = 1 : 1.0 : 2.0 and (b) MTMS : FA : H<sub>2</sub>O = 1 : 2.3 : 2.5.

and component 2 to the polar solvent phase (FA or MeOH). The parameter  $\chi$  is the interaction parameter, which relates to the solubility parameter ( $\delta_i$ ) of component  $i$  as

$$\chi \propto \frac{(\delta_1 - \delta_2)^2}{k_B T}. \quad (1-2)$$

Since the solubility parameter is proportional to the cohesive energy density, polar species tend to have a large value of solubility parameter. In the present system, polar silanol groups with high polarity are consumed in the polycondensation reaction, so the polarity of gel phase gradually decreases whereas the polarity of the solvent mixtures remains high (19.2 cal<sup>1/2</sup>·cm<sup>-3/2</sup> for FA, 14.5 cal<sup>1/2</sup>·cm<sup>-3/2</sup> for MeOH, 11-12 cal<sup>1/2</sup>·cm<sup>-3/2</sup> for TMOS-derived polymer, and <10 cal<sup>1/2</sup>·cm<sup>-3/2</sup> for MTMS-derived polymer [8]). As a result, the interaction parameter  $\chi$  increases during sol-gel transition, which makes  $\Delta G$  larger. In addition to that,  $P_1$  in the eq (1) becomes larger, which also makes  $\Delta G$  larger. Thus the system phase-separates during the polymerization of MTMS. When gelation occurs much earlier than phase separation, transparent gels with nanometer-sized pores can be obtained. Bicontinuous structure, aggregates of particles and isolated pores can be obtained if the sol-gel transition and phase separation proceeds nearly concurrently. When gelation takes place much later than phase separation, siloxane gel phase with higher density settles down due to the gravity effect and exhibits macroscopic two phases.

In the MM system, the typical gelation time is around 3 hours, however, in the MF system, it is as long as 60 hours. The difference between these two systems can be explained as follows: Since formamide is hydrolyzed under the presence of a strong acid (1M nitric acid in this case), pH of the solution becomes higher during the sol-gel reaction, namely around the isoelectric point of MTMS [8]. Relation between starting compositions and resultant gel morphology in the both systems are shown in Figure 2. Since the solubility parameter of FA is slightly larger than that of MeOH (19.2 cal<sup>1/2</sup>·cm<sup>-3/2</sup> for FA, and 14.5 cal<sup>1/2</sup>·cm<sup>-3/2</sup> for MeOH), phase separation tendency is higher in the FA system (larger composition areas are recognized representing macroscopic two phases) and bicontinuous structure can be obtained in an extended compositional area in the MM system. The

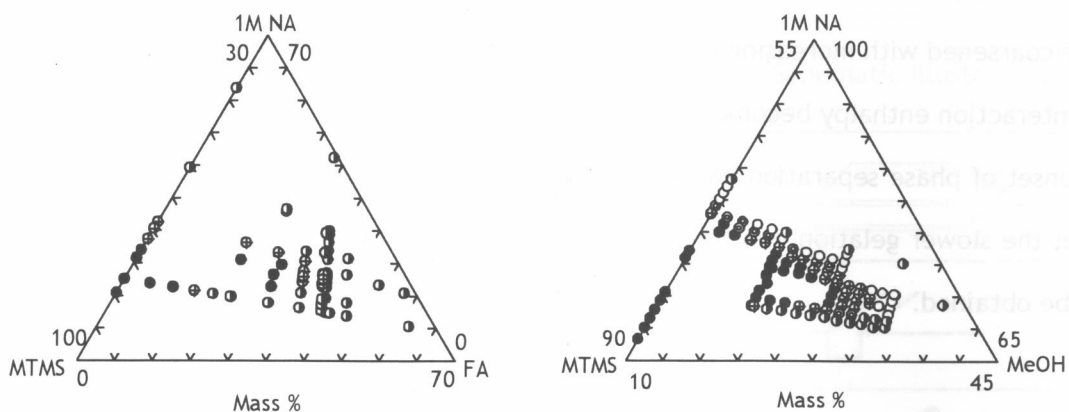


Figure 2 Relationship between starting compositions and resultant gel morphologies in (a) MTMS-FA (MF) system and in (b) MTMS-Methanol (MM) system. Reaction temperature is 40 °C. Symbols are ●: nanoporous, ⊕: bicontinuous structure, ○: particle aggregates, ⊙: isolated pores, and ①: macroscopic two phases.

phase-separated structures which can be obtained from both systems generally tend to be more coarsened with increasing amount of polar solvents (FA or MeOH). In both systems, the interaction enthalpy becomes larger with increasing amount of solvents, which makes the onset of phase separation earlier. Moreover, the increased amount of solvent brings about the slower gelation due to dilution effect, by which the more coarsened structure will be obtained.

### 3. Molds Used in This Study






The purpose of this study is focused on the structural formation in confined geometry. Here “confined” means “where the effect of micro-surfaces is *possibly* emerge”. Basically, when any effects appear, the system is said to be “confined”, however, in some cases there is little influence from the micro-surfaces. Moreover, the term “confined” is not related directly to the size of the space. As described above, the influence of the surfaces is little even when the size of the mold is small. Whereas the resultant gel sometimes is significantly affected in a large space.

The shape of a confining mold is defined according to the dimensionality. A 2D mold is a gap between two parallel plates with a spacer between them; only the thickness direction is confined. A 1D mold is a long cylindrical or rectangular-shaped capillary with only one longitudinal direction is not restricted. A rectangular-sectioned groove with one face is open is also used as a mold which is denoted as “an open groove”. This is regarded as a kind of 1D mold. A 0D mold is short cylindrical maze-like pores inside a bicontinuous porous medium. In fact, a porous silica gel which is also prepared via sol-gel with phase separation is used. Molds used in this study are overviewed in Table 2.

#### 3.1. Preparation of a 2D mold

As a hydrophilic surface, a soda-lime silicate glass slide is used. A glass slide is

Table 2 The overview of the molds used in this study

Dimension	Surface	Example	Schematic Illustration
2D	Flat	A gap between parallel plates	
1D	Flat	A long groove with one side is open	
1D	Curved	A long cylindrical capillary	
1D	Flat	A long rectangular capillary	
0D	Curved	Short cylindrical pores in a porous medium	

subjected to ultrasonic washing in water, and then rinsed off with ethanol followed by drying in air. As a hydrophobic surface, an octadecylsilylated glass slide is used. Amino-substituted octadecyldimethyl-N,N-diethylaminosilane derived from octadecyldimethylchlorosilane is used as a hydrophobic coating agent [9]. A set of two plates are set together to construct a gap with an appropriate spacer between them. For LSCM observation, one plate of the two should be a coverslip with decreased thickness (~150  $\mu\text{m}$ ). Gaps with various thicknesses may be prepared; however, the resultant gel thickness is always suffering from discrepancy with the spacer thickness especially in a gap with thinner spacers (100  $\mu\text{m}$  or less). Possible reasons are slight curve of a coverslip and/or unintended folding of a spacer.

### *3.2. Preparation of a 1D mold*

As a 1D mold, capillaries with circular or rectangular sections are used. As a hydrophilic mold, these capillaries are used without any pretreatments. As a hydrophobic mold, the pretreatment procedure is the same as a 2D hydrophobic mold. In this literature, since the result is almost the same between circular- and rectangular-sectioned capillaries, only the result with cylindrical capillaries is dealt.

An open groove is another type of a 1D mold. The grooves are fabricated on a silica glass chip and used after ultrasonic washing in water, ethanol rinsing and drying in air. The templated silica glass chips are kindly supplied by Techno Quartz Inc. (Tokyo, Japan).

### *3.3. Preparation of a 0D mold*

Porous silica gel with bicontinuous structure as a 0D mold was prepared as follows. First, 0.65 g of poly(ethylene)glycol ( $M_w=10,000$ ) and 0.90 g of urea were dissolved in 10 mL of 0.01 mol/L acetic acid in a glass sample tube. Then 5 mL of tetramethoxysilane, TMOS (Shin-Etsu Chemical Co., Japan), was added under vigorous stirring and ice-cooled condition. After being stirred for 30 min, the resultant homogeneous solution was transferred to an autoclave and allowed to gel at 40°C in a closed condition. The



resultant gel was aged at the same temperature for 24 h followed by a hydrothermal aging at 100°C for 24 h. The aged gel was dried at 40°C for about 24 h, and then sintered at 1000°C for 2 h. Characterization of the pore structure of the mold gel was performed by mercury porosimetry (PORESIZER-9320, Micrometrics, USA) and the average pore size of the mold was determined as approximately 2.74 μm.

## 4. Laser Scanning Confocal Microscopy (LSCM)

### 4.1. Principles

Laser Scanning Confocal Microscopy (LSCM) enables 3D observation by obtaining a number of thin-sliced images of one sample. The focal depth is made to be extremely thin by using a confocal pinhole in front of a detector. In Figure 3 the light path of LSCM is described. The diffraction-limited incident laser beam is focused in the sample via the scanner (not shown) through the objective lens. Emitted fluorescent light from fluorescent agent(s) in the focal plane (solid line) in the sample is focused again at the confocal pinhole via the scanner and dichroic beam splitter. The focused light is directed to the detector (photomultiplier) through the filter in front of it. The filter, typically a long-pass filter, selectively put the fluorescent light through and the reflective light of the incident beam is shut. The fluorescent light from unfocused planes (dotted line) is effectively cut by the confocal pinhole acting as a “spatial filter”. Sequential 2D sliced images are obtained by moving the sample in the direction parallel to the incident beam. Thus the sliced montage images can be obtained as far as the sample can transmit light.

In this literature LSM510 and LSM5 Pascal (Carl Zeiss, Germany) was used. The resolution of these LSCMs is derived by Carl Zeiss as follows:

For the axial resolution,

$$\frac{0.88\lambda_{exc}}{\left(n - \sqrt{n^2 - NA^2}\right)}, \quad (1-3)$$

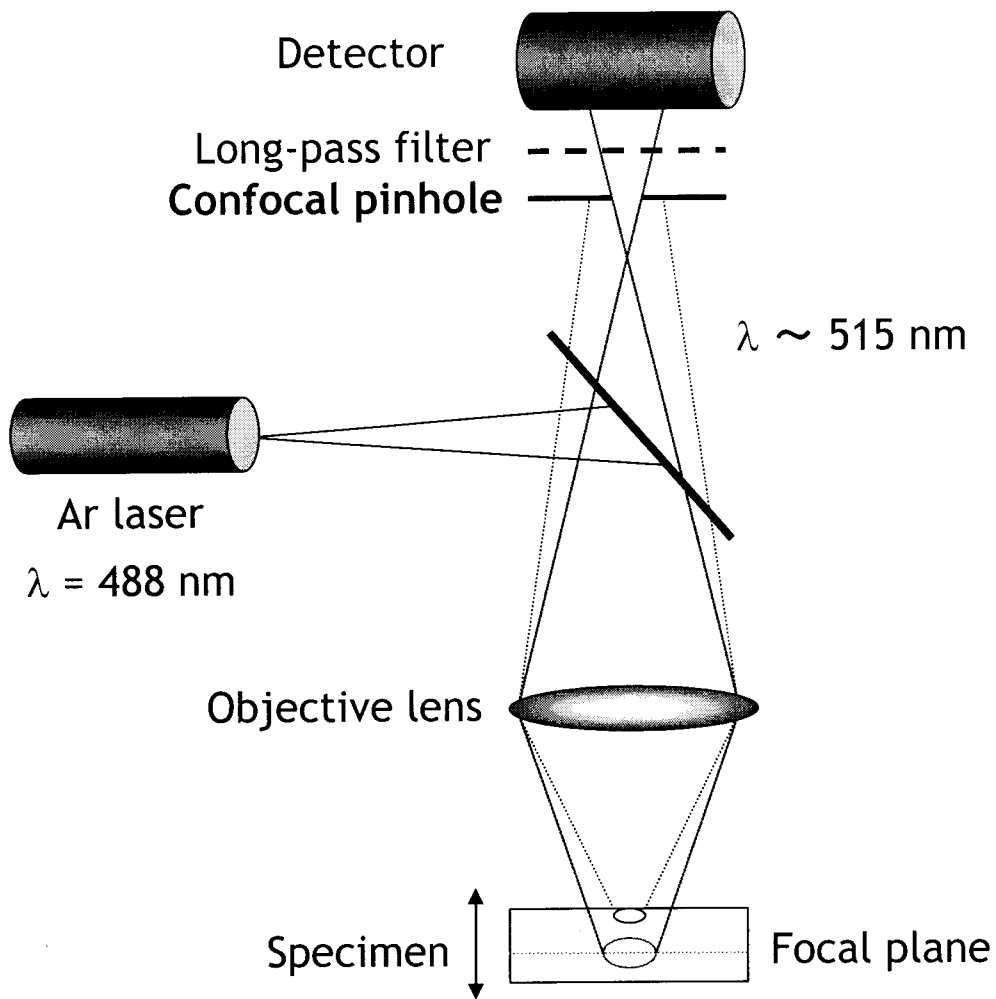


Figure 3 The light path in LSCM. The sample should contain fluorescent agent to enhance the contrast in the images. Fluorescent light from unfocused planes in the sample is effectively cut by confocal pinhole in front of the photomultiplier.

and for the lateral resolution,

$$\frac{0.51\lambda_{exc}}{(NA)}, \quad (1-4)$$

where  $n$  indicates the refractive index of immersion oil of the oil-immersed objective lens. In the standard setting, an Ar laser with wavelength of 488 nm, oil-immersed x63 (NA=1.25) and immersion oil with  $n=1.518$  was used, so the axial and lateral resolutions are 0.553  $\mu\text{m}$  and 0.199  $\mu\text{m}$ , respectively.

#### 4.2. Practical procedure to obtain 3D information by LSCM

As described above principles section, in order to obtain a image with strong contrast by LSCM, observation has to be performed with fluorescence mode and the sample is required to be enough transparent so as for the incident beam and fluorescent light to pass through. In fluorescence mode, the “structure” of the sample is determined by the difference of fluorescent intensity between different regions. In the structural determination of phase separated structure of porous siloxane gel, a fluorescent agent should be introduced either in the siloxane-rich phase or solvent-rich phase. In addition, we have to let the sample be transparent by filling a solvent-rich phase or macropores a liquid which has almost the same refractive index as the gel skeletons. In the following practical examples, it is confirmed that both requirements (transparency and introduction of fluorescent agents) are fulfilled.

##### Case 1. Adding a fluorescent agent in a starting solution

The first is the method by introducing a fluorescent agent in a starting solution. This method is suitable for the observation of an as-prepared structure, however, it is needed that the as-prepared gel is transparent enough. Since the refractive indices of the gel phase and the solvent phase is roughly close in the MF system, this technique can be applied.

In practice, a little amount of fluorescein (Figure 4) is added into a starting solution,

and the observation can be done *in situ*. As fluorescein is distributed in the solvent phase, the solvent phase is detected as a bright region (so the gel phase is as a dark region) in the obtained images (reversed mode).

Although this method is simple and easy, it is not applied to a variety of systems. As for the MF system, though the transparency of the as-prepared gel is relatively high, it is not enough for the observation in the deeper regions. Furthermore, since the minor amount of fluorescein is also distributed in the gel phase, the contrast in the images is not very strong.

#### Case 2. Introducing a fluorescent agent by solvent exchange

This method is applicable to a variety of systems since the introduction of a fluorescent agent and contrast matching is performed after gel preparation. A fluorescent agent is dissolved in an appropriate solvent which has almost the same refractive index as the gel phase, and then this solution is introduced into the solvent phase or macropores. In this case, observation is conducted under a reversed mode as well in which the solvent phase is seen as a bright region.

In the MTMS-derived system, fluorescein is typically dissolved into formamide (FA) or dimethylacetamide (DMA), that have almost the same refractive index as the gel phase (DMA is the closer), and then wet or dried gel sample is immersed in the solution. Note that when using DMA as a solvent, fluorescence intensity of fluorescein is considerably weak, so it is better to use fluorescein sodium salt (uranine, Figure 4) as a dye component. After the complete intrusion of the solution (solvent exchange), the sample is ready to be observed under LSCM.

The solvent is not limited to FA or DMA: It can be substituted by any other solvents as far as they can dissolve fluorescein and have close reflective indices as the gel phase. In the practical observation, since the evaporation of the solvent becomes a significant problem, it is better to use the nonvolatile solvents.

### Case 3. Chemically attaching a fluorescent agent on a sample gel [10-12]

If it is needed that the gel phase has to be observed as a bright region, i.e. in normal mode, we must try this method or the following method, Case 4. In this method the surface of a sample gel is chemically modified by fluorescein-attached silicon alkoxide monomer. More specifically, fluorescein-4-isothiocyanate (FITC isomer I, Figure 4) is covalently attached to the silane coupling agent, 3-aminopropyltrimethoxysilane (APTMS) by an addition reaction between thioisocyanate group and amino group (Figure 5).

The typical procedure is as follows: A small amount of FITC isomer I (approx. 54 mg) and 8.8 mL of APTMS is dissolved in 80 mL of ethanol, and then the solution is allowed to stir overnight (solution A). After the addition reaction, sample gel is immersed in the resultant "solution A" and followed by adding a little amount of saturated aqueous ammonia solution. The amount of saturated ammonia solution is typically 5-10 % in volume. The coupling reaction is allowed to continue for 3-6 hours at 40°C in a light-shielded condition. The resultant gel should be washed with ethanol after the coupling reaction and then solvent-exchanged with appropriate solvent(s) to ensure transparency.

This method is applicable only to the gels with mesoporous skeletons. Since the fluorescent agent is attached just onto the "surfaces", it is impossible for the gels with nonporous skeletons to see the whole regions in the gel phase as bright regions. For this reason, this method can not be applicable to MTMS-derived nonporous gels.

### Case 4. Co-polymerization with a fluorescein-attached alkoxide monomer

As described in Case 3, FITC isomer I-attached silicon alkoxide monomer is obtained by the first addition reaction. This resultant solution can be used as a monomer which may co-polymerize with MTMS monomer in the starting solution. The typical procedure to obtain "solution A" is almost the same as Case 3. An appropriate amount of "solution A" is added into the starting solution and allowed to gel in the normal way.

However, it is difficult to co-polymerize homogeneously probably because of the

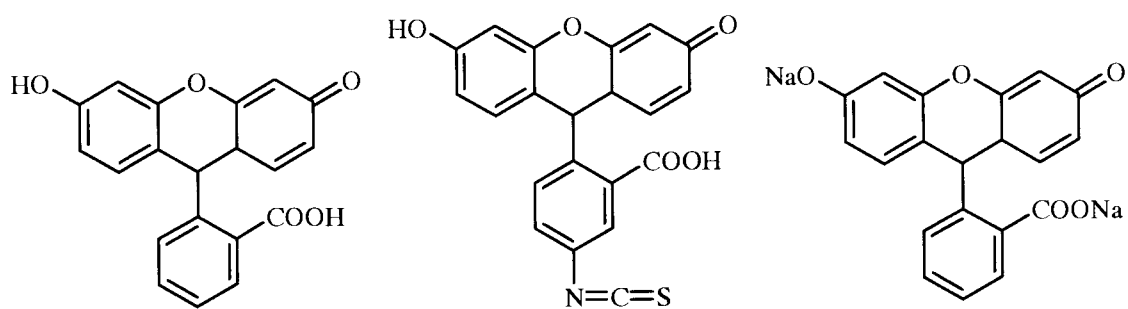


Figure 4 Structural formulae of fluorescein (left), fluorescein-4-isothiocyanate isomer I (FITC isomer I, middle) and fluorescein sodium salt (uranine, right). Isothiocyanate group in FITC isomer I is covalently bonded with amino group by addition reaction.

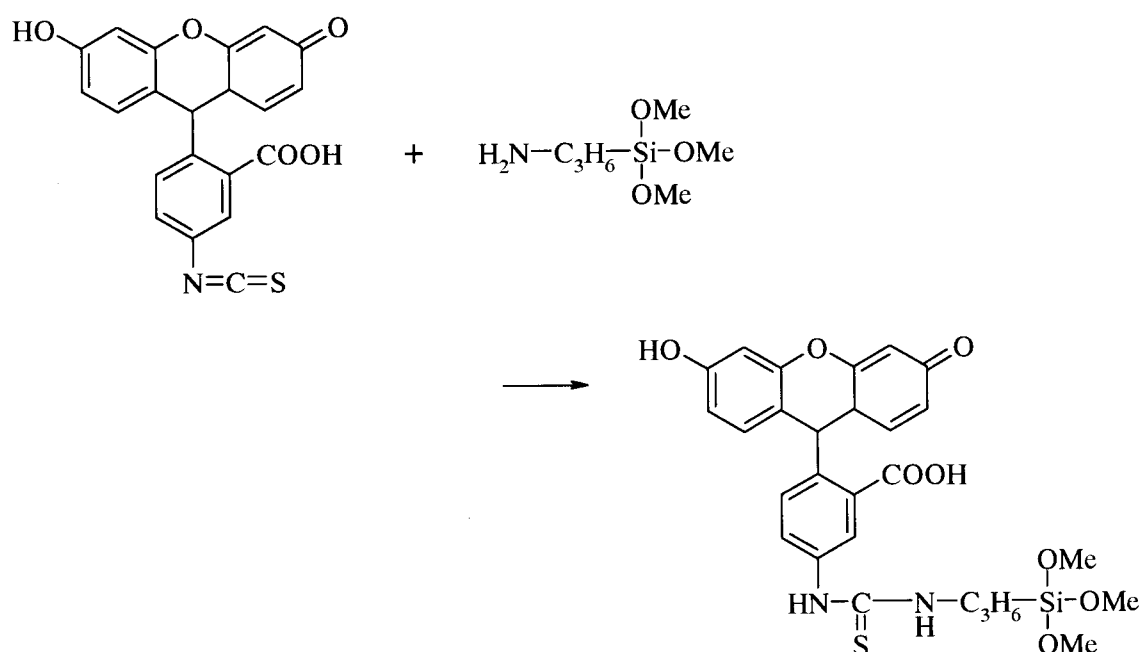


Figure 5 Preparation of dye-attached silane monomer through addition reaction between isothiocyanate and amino groups. The dye-attached monomer reacts with the surface of siloxane gels. Copolymerization between TMOS or MTMS is also possible, but it is difficult to be dispersed homogeneously throughout the gel matrix.

bulky group in FITC isomer I-attached monomer and the difference of reactivity. Still, co-polymerization with tetraethoxysilane (TEOS) seems to result in homogeneously distribution of the dye component throughout the gel skeleton.

## 5. Image Analysis

### 5.1. Definition of a digital image

A 2D digital image is divided by tetragonal lattice and each lattice cell is termed a pixel. Every pixel possesses its own intensity value. In our experiment, LSCM images are obtained by 8 bit gray scale  $512 \times 512$  pixels<sup>2</sup> images. In such images, the tetragonal 2D image possesses total 262,144 pixels and each pixel has a gray value ranging from 0 to 255 (the total number of the value is  $2^8=256$ ).

### 5.2. Image processing

The best-taken LSCM image is still suffering from undesirable high-frequency noises and intensity variations. These uncertainties must be removed by appropriate image processing before stacking into a 3D reconstructed image.

For the purpose of getting rid of local intensity variations, constant variance enhancement (CVE) [13,14] is used. In this process, contrast, which is defined by variance of intensity of an image, and average intensity are calculated in a given size of area, and then convert these values into desirable ones. By changing the size or shape of the mask and continuing the process in a whole image, local intensity and variance are effectively equalized.

Median filter [15] is a widely used filter to get rid of salt and pepper noise. For instance, in  $3 \times 3$  median filtering, the nearest 8 neighbors surrounding a point of interest (POI) are chosen, and then assign the median value  $m$  of the 9 pixels to the POI. The median value  $m$  represents the value that half of the population has smaller values than  $m$ ,

and the other half has larger values than  $m$ . In the practical process, we used 3D median filtering which is extended to 3D. The effect of CVE and 3D median filtering is shown in Figure 6(a) and (b). It is confirmed that the image contrast is successfully enhanced and noises were also reduced after these image processing procedures.

### *5.3. Binarization and reconstruction*

Next the processed sequential images are binarized and reconstructed. The images are binarized into black and white images, and stuck together using marching cubes algorithm [16]. The intensity histograms of the images have to be well-defined bimodal distributions to ensure the accurate interface definition and avoid artificial errors. In other words, taking the best images by LSCM is the most important step in this procedure. The process of binarization and reconstruction is exhibited in Figure 6 (c) and (d), respectively.

Although as much attention as possible should be paid for obtaining the best images with high contrast by preparing samples and manipulating a LSCM device carefully, we can not exclude the arbitrariness during the binarization process. Otsu's method [17] is one way to exclude such artificial effects (see Appendix A). In Otsu's method, thresholds are determined by a mathematical procedure in which a threshold is determined by calculating variances of two classes divided by the threshold so that the variance between two classes becomes largest. This technique gives a unique value of threshold and no arbitrariness is included. In the following chapters, this technique does not be used because the adequacy is not fully checked yet, but this technique should be included in the future because this is an importance process in determining a "unique structure" in a reproducible way.

In the following sections, three kinds of analysis by using processed images are reviewed.



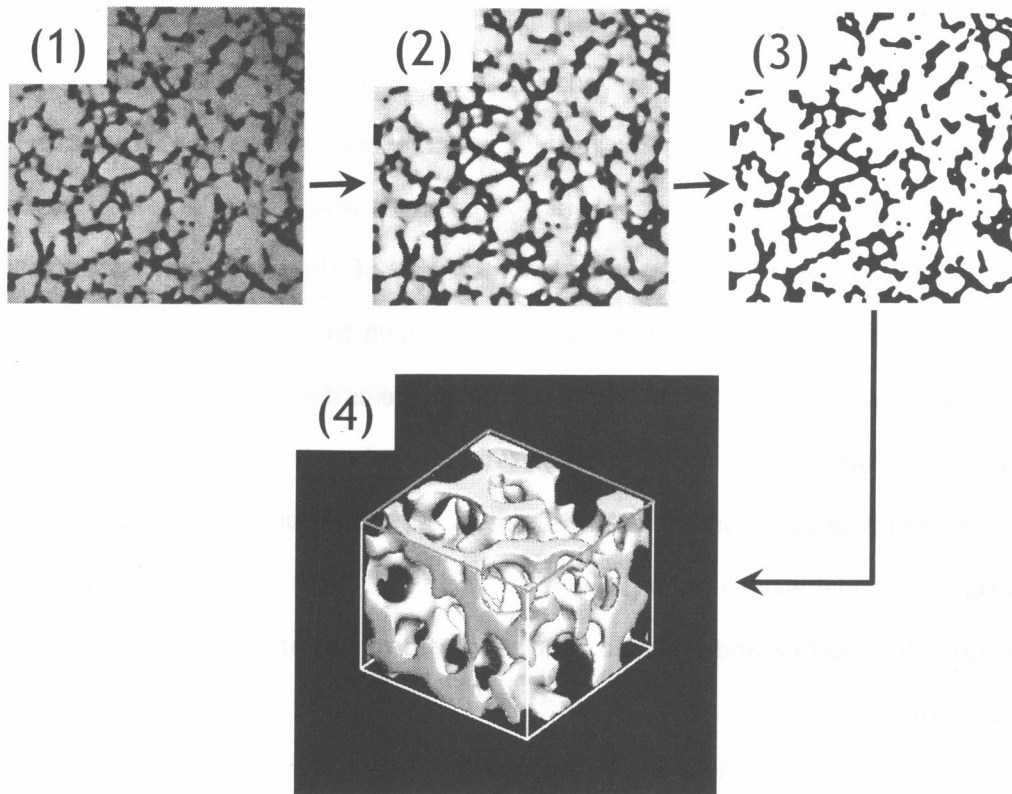


Figure 6 The example of image processing. (a) Raw LSCM sliced image, (b) after CVE and median filtering, (c) after binarization at an appropriate threshold and (d) a reconstructed image.

#### 5.4. 3D Fast Fourier Transformation (FFT)

All the digital images are the superposition of many sine waves with various wavelengths. Each LSCM image contains information about bicontinuous structure, and if there is a periodicity in it, a representative wavelength which contributes to the image most can be regarded as a “characteristic length” of the structure. Bicontinuous structure derived from spinodal decomposition is known to have spatial periodicity and Fourier-space analysis using 2D FFT of a digital image is found to be advantageous to extract such periodicity that the human eye is hardly recognize [18,19]. This is obvious because spinodal decomposition itself is also a superposition of many compositional fluctuations (spinodal waves) in 3D [20].

Fourier transform  $F$  and inversed Fourier transform  $f$  of an image intensity  $f(x, y)$  is defined as follows,

$$\begin{aligned} F(q_x, q_y) &= \iint f(x, y) \exp(-j2\pi(q_x x + q_y y)) dx dy \\ f(x, y) &= \iint F(q_x, q_y) \exp(j2\pi(q_x x + q_y y)) dq_x dq_y \end{aligned} \quad (1-5)$$

where  $q_x$  and  $q_y$  are spatial frequencies or wavenumbers and  $j^2 = -1$ . The power spectrum is defined as

$$|F(q_x, q_y)|^2 = \text{Re}(F(q_x, q_y))^2 + \text{Im}(F(q_x, q_y))^2, \quad (1-6)$$

where Re and Im show the real and imaginary parts, respectively. In the practical process, Fast Fourier Transform (FFT) [15,21] in 3D is used and obtained power spectrum is circularly averaged in the  $q_x$ - $q_y$  plane. Note that both 3D extension and averaging postulate a 3D structural isotropic nature of phase-separated structure. The characteristic length  $\Lambda_m$  of bicontinuous structure can be calculated from the following relation,

$$\Lambda_m = \frac{2\pi}{q_m} \quad (1-7)$$

where  $q_m$  is a wavenumber at the peak intensity.

### 5.5. Area-averaged curvature determination by Parallel Surface Method (PSM)

Since the shape of an interface derived from spinodal decomposition is quite essential to deduce the structural formation, mean and Gaussian curvatures are introduced by which the shape of the interface can be determined quantitatively.

Take a curved interface for example, when the interface is cut by a plane which contains the surface normal at a POI, there are osculating circles at the POI in the plane. The largest and the smallest radii ( $R_1$  and  $R_2$ ) of the osculating circles are defined as principle curvatures ( $\kappa_1 \equiv 1/R_1$  and  $\kappa_2 \equiv 1/R_2$ ), and the signs of curvatures are defined to be opposite between two different sides divided by the interface. Mean and Gaussian curvatures are defined as follows;

$$H \equiv \frac{\kappa_1 + \kappa_2}{2} = \frac{1}{2} \left( \frac{1}{R_1} + \frac{1}{R_2} \right), \quad K \equiv \kappa_1 \cdot \kappa_2 = \frac{1}{R_1 \cdot R_2}. \quad (1-8)$$

The shape around the POI is characterized by the sign of  $K$ . Figure 7 shows an example of a curved interface and the relationships between curvatures and shapes. The sign of mean curvature  $H$  determines the concavity and convexity. For the bicontinuous spinodal decomposition, the most part of the interfaces are recognized to be hyperbolic,  $K < 0$ , since the bicontinuous pattern is a superposition of all sinusoidal compositional waves in 3D. Jinnai et al. revealed that the spinodal interfaces develops with time self-similarly and keeps the minimal interfacial area, i.e.  $K < 0$  and  $H = 0$ , throughout their time resolved observation [4].

In the curvature computing process, a “Parallel Surface Method (PSM)” is used in which area-averaged curvatures can be obtained [22-24]. A parallel surface to an interface is formed by translating the interface along its normal vectors by an equal distance everywhere on the interface. According to the differential geometry, the surface metric of the parallel surface is related to the metric of the interface ( $A(0)$ ) by

$$A(d) = A(0) \left( 1 + 2\langle H \rangle d + \langle K \rangle d^2 \right), \quad (1-9)$$

where  $d$  is the oriented distance along the normal vector and  $A(d)$  is the area of a parallel surface. This equation is reliable when the displacement  $d$  is sufficiently small. The

schematic illustration of a parallel surface and original interface is shown in Figure 8. In this technique we obtain the area-averaged curvatures,

$$\langle H \rangle = \frac{1}{2} \frac{\iint (\kappa_1 + \kappa_2) da}{\iint da}, \quad \langle K \rangle = \frac{\iint (\kappa_1 \cdot \kappa_2) da}{\iint da}, \quad (1-10)$$

where  $da$  is the area element of the interface. Since the curvatures of the interface is varied from point to point, this technique is useful to overview the averaged local structure, however, if we wish to obtain a “real” local structure, we have to obtain the curvatures at each POI and distribution of curvatures by measuring as many points as possible. Nishikawa et al. have developed this kind of technique called “Sectioning Fitting Method (SFM)” [25] but we do not deal details in this literature.

## 6. Future Perspectives

Other recent 3D observation techniques such as Transmission Electron Microtomography (TEMT) [26] or X-ray Computerized Tomography (X-ray CT) [27] have been on a rapid progress and these methods are definitely applicable to our sol-gel derived structures. For example, TEMT will become a powerful tool to visualize meso-structures in macroporous siloxane gels and X-ray CT will be a simpler and easier method compared to LSCM if only the resolution is improved because X-ray CT does not need a fluorescent dye and transparency of a sample.

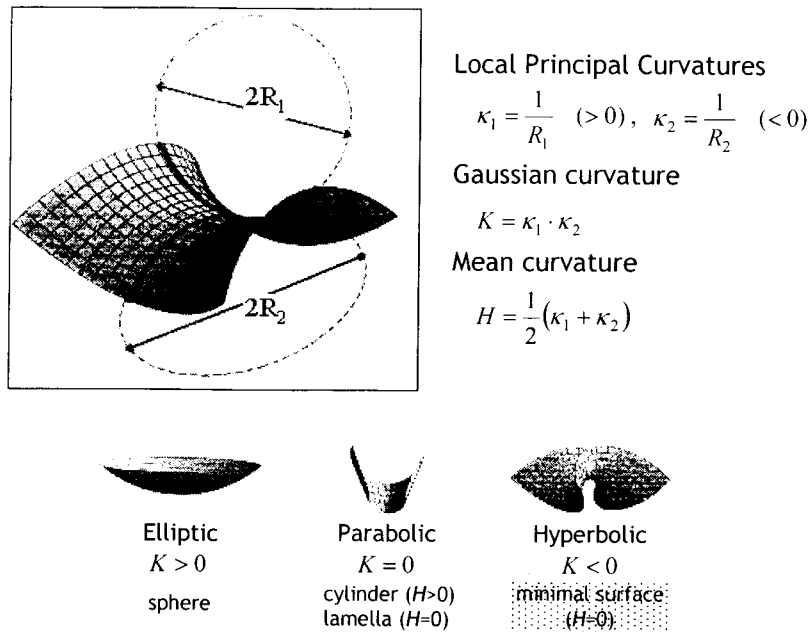


Figure 7 Definition of interfacial curvatures and relationships between curvatures and shapes. Figures are taken from “On swelling and structure of composite materials. Some theory and applications to lyotropic mesophase” by S. T. Hyde [Australia-Japan self-assembly symposium, Fukuoka (1994)].

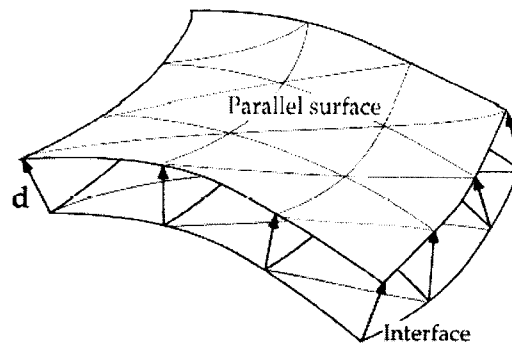


Figure 8 A schematic illustration of a parallel surface (white) at displacement  $d$  from the original interface (grey). This figure is taken from Ref. [18].

## References in Chapter 1

- [1] T. Wilson, "Confocal Microscopy", Academic Press, London (1990).
- [2] S. Paddock, *Science*, **295**, 1319 (2002).
- [3] J. B. Powley, "Handbook of Biological Confocal Microscopy", 2<sup>nd</sup> ed., Plenum, New York and London (1995).
- [4] For example, H. Jinnai, Y. Nishikawa, H. Morimoto, T. Koga, T. Hashimoto, *Langmuir*, **16**, 4380 (2000).
- [5] For example, H. Jinnai, H. Watashiba, T. Kajihara, M. Takahashi, *J. Chem. Phys.* **119**, 7554, (2003).
- [6] C. J. Brinker, G. W. Scherer, "Sol-Gel Science: The Physics and Chemistry of Sol-Gel Processing", Academic Press, New York (1990), pp. 140-141.
- [7] P. J. Flory, "Principles of Polymer Chemistry", Cornell University Press, Ithaca (1971).
- [8] H. Kaji, Kyoto University Doctoral Thesis (1994).
- [9] N. Tanaka, H. Kinoshita, M. Araki, *J. Chromatogr.* **332**, 57 (1985).
- [10] A. van Blaaderen, A. Vrij, *Langmuir*, **8**, 2921 (1992).
- [11] A. van Blaaderen, A. Vrij, *J. Colloid Interface Sci.* **156**, 1 (1993).
- [12] H. Jinnai, K. Nakanishi, Y. Nishikawa, J. Yamanaka, T. Hashimoto, *Langmuir*, **17**, 619 (2001).
- [13] H. C. Andrews, *Appl. Opt.* **15**, 495 (1976).
- [14] J. L. Harris, *Appl. Opt.* **16**, 1268 (1977).
- [15] W. K. Pratt, "Digital Image Processing", Wiley, New York (1978).
- [16] W. E. Lorensen, H. E. Cline, *Computer Graphics SIGGRAPH '87*, **21**, 163 (1987).
- [17] N. Otsu, *IEEE Trans. Sys., Man, and Cybernetics*, **SMC-9**, 62, (1979).
- [18] H. Tanaka, T. Hayashi, T. Nishi, *J. Appl. Phys.* **59**, 653 (1986)
- [19] H. Tanaka, T. Hayashi, T. Nishi, *J. Appl. Phys.* **59**, 3627 (1986)
- [20] J. W. Cahn, *J. Chem. Phys.* **42**, 93 (1965).
- [21] J.W.Cooley, J.W.Tukey, *Math. Comput.* **19**, 297 (1965).

- [22] S. T. Hyde, *J. Phys. Chem.* **93**, 1458 (1989).
- [23] H. Jinnai, T. Koga, Y. Nishikawa, T. Hashimoto, S. T. Hyde, *Phys. Rev. Lett.* **78**, 2248 (1997).
- [24] Y. Nishikawa, H. Jinnai, T. Koga, T. Hashimoto, S. T. Hyde, *Langmuir*, **14**, 1242 (1998).
- [25] Y. Nishikawa, T. Koga, T. Hashimoto, H. Jinnai, *Langmuir*, **17**, 3254 (2001).
- [26] H. Jinnai, Y. Nishikawa, R. J. Spontak, S. D. Smith, D. A. Agard, T. Hashimoto, *Phys. Rev. Lett.* **84**, 518 (2000).
- [27] For example, *MRS Bull.* **29**, No.3 (2004) is a special volume for X-ray microscopy.

## CHAPTER 2: STRUCTURES IN A TWO-DIMENSIONAL MOLD

### Section 2.1 Three-Dimensional Observation of Phase-Separated MTMS-Derived Gels and Comparison with TMOS-Derived Ones: Global Geometry

#### 1. Introduction

It is known that well-defined macroporous silica-based gels with bicontinuous structure can be prepared by inducing spinodal decomposition during the sol-gel transition [1-3]. In a system containing formamide as a polar solvent, tetramethoxysilane (TMOS) or methyltrimethoxysilane (MTMS) as a siloxane source and nitric acid as an acid catalyst, phase separation occurs between the polar solvent and the polymerizing siloxane component [4]. The bicontinuous siloxane gel has found an application as a separation medium for high performance liquid chromatography (HPLC) [5,6] and the miniaturization of the separation medium is of high technical interest [7-12]. In applying such continuous porous material to micro-devices such as capillary columns, thin layer chromatography plates, and chip columns, the surface effect cannot be neglected. Namely, in such a micro-confined space, since the ratio of surface area to total volume of a sample becomes larger, wetting phenomena and shrinkage during aging and drying processes will presumably change the morphogenesis and phase separation tendency.

In the case of phase separating polymer blends in confined geometry, it is demonstrated that preferential wetting of surface(s) by one component strongly influences the phase separation behavior [13-20]; this wetting phenomenon induces the so-called "surface directed spinodal decomposition" and it finally brings the system into a



layered structure stacked perpendicular to the surface [21-33]. The influence of this spinodal decomposition perpendicular to the surface increases with decreasing film thickness because the part of the film that is in close proximity to the surfaces amounts to a significant portion of the total volume of the system. Another effect that becomes significant when thickness of the film decreases, is surface-induced spinodal waves from both sides of the film that interfere with each other, so the intriguing morphology perpendicular to the surfaces appears [34]. These phenomena are of great importance in designing of thin polymer films.

Recently, real space analysis techniques of phase separated polymer mixtures have been developed utilizing Laser Scanning Confocal Microscopy (LSCM) [35-37]. By using LSCM, optically sliced two-dimensional (2D) images along the incident beam can be obtained. The series of sliced images is appropriately digitized and reconstructed to perform the 3D analyses. A bulk sintered silica gel with bicontinuous structure has already been successfully analyzed in 3D by this method; it is revealed that the geometrical features of the bicontinuous silica gel are similar to a phase separating polymer blend at a comparable volume fraction [38].

In this section, siloxane gels with bicontinuous structure derived from the MF system were prepared in 2D confined space such as a gap between two parallel plates, and the structural variety of confined gels was observed in 3D by LSCM. The variety of morphology near a surface, depending on surface character or starting composition is discussed.

## 2. Experimental

### *2.1 Preparation of 2-dimensional Molds*

Glass slides (denoted as G) and octadecylsilylated glass slides (denoted as O) were used, respectively, as hydrophilic and hydrophobic plates to construct 2D confined space.

Each plate was subjected to ultrasonic cleaning in water, followed by rinsing with ethanol and drying in air. Then the plates were brought together into G-G and O-O pairs with various spacers such as 50  $\mu\text{m}$ , 30  $\mu\text{m}$  and 13  $\mu\text{m}$  in thicknesses between them as schematically shown in Figure 1. The actual thickness of each gel, which was determined by LSCM, and corresponding spacer would be described in the following section. For LSCM observation, either plate of each mold was replaced by a coverslip. In the notation of the molds, an initial letter indicates silicon alkoxides (T for TMOS and M for MTMS), the following number indicates the thickness of the sample and the following two letters indicate the set of plates. All the molds were placed in an identical polystyrene vessel (the reaction vessel) to be used as a reaction container.

### *2.2 Preparation of the Starting Solution (MTMS system)*

First, 15.08 g of 1.0 M aqueous solution of nitric acid and 31.58 g of formamide as a polar solvent and 0.04 g of fluorescein as a fluorescence dye for LSCM observation were homogeneously dissolved. Then 40 mL of MTMS were added under vigorous stirring in an ice-cooled condition. That is, the molar ratio of starting solution was; MTMS : FA : H<sub>2</sub>O = 1 : 1.8 : 2.0. After being stirred for 5 min, the resultant homogeneous solution was transferred into the reaction container followed by 1 min of ultrasonic agitation and 5 sec of evacuation with an aspirator to introduce the solution into the molds. The reaction solution was then allowed to gel at 40 °C in a closed condition. The resultant gel was aged at the same temperature for 24 h then the aged gel (wet gel) was subjected to LSCM observation. After observation, the gel was dried at 40 °C and the dried monolithic gel was again observed by LSCM. The dried gels are also observed under SEM (S-510, Hitachi Ltd., Japan). Hereafter, we denote the gel prepared between plates as “confined gel”, and the gels prepared with the same composition and no confinement effects as “bulk gel”.

### *2.3 Preparation of the Starting Solution (TMOS system)*

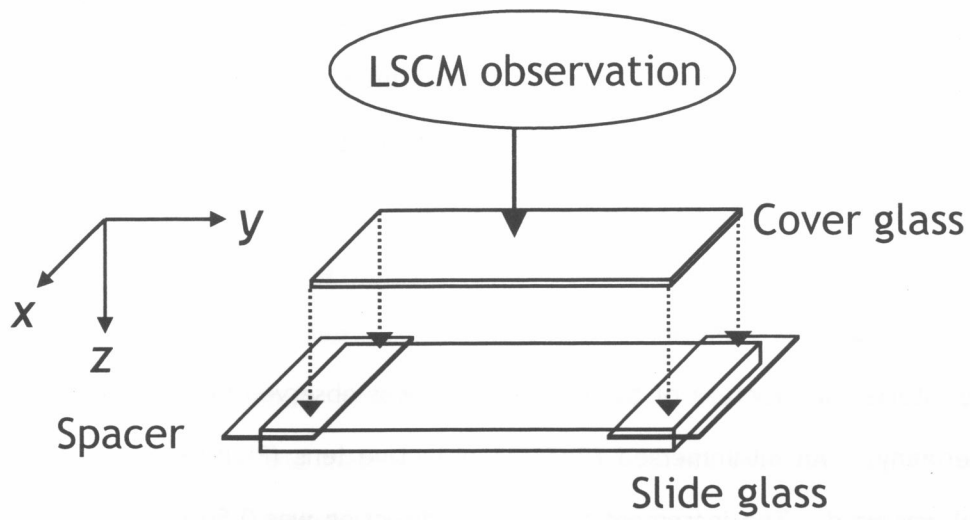


Figure 1 Schematic illustration of the mold for gel preparation, axis definition and the observation directions of LSCM.

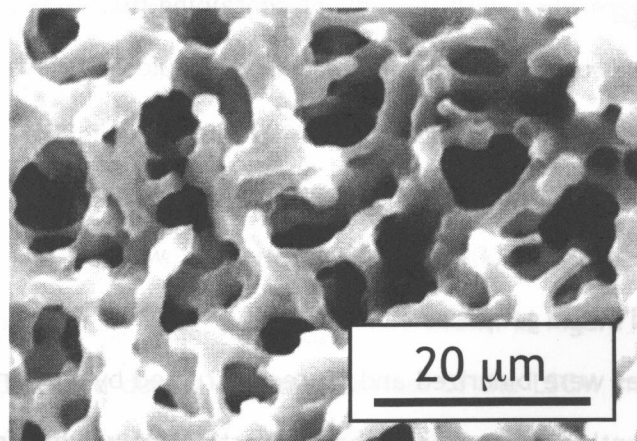


Figure 2 A SEM photograph of dried bulk methylsiloxane gel representing a typical bicontinuous structure. The characteristic length (skeleton thickness plus pore diameter) is 9.6 μm.

The preparation procedure is almost the same as the MTMS system described above. The starting composition is as follows: 9.75 g of 1.0 mol/L nitric acid aqueous solution, 33.53 g of formamide, 0.02 g of fluorescein and 50 mL of TMOS. That is, the molar ratio of starting solution was; TMOS : FA : H<sub>2</sub>O = 1 : 2.2 : 1.5.

#### 2.4 LSCM Observation and Image Processing

The interfacial structure of the resultant gel was observed by LSCM (LSM510, Carl Zeiss, Germany). An oil-immersed 63x/1.25 objective lens (Plan-Neofluar, Carl Zeiss, Germany) was used. The increment along the z-direction was 0.50  $\mu\text{m}$  for all samples. The observation direction is along the z-direction as indicated in Figure 1. The laser was scanned in the plane perpendicular to the z-direction (x-y plane), measuring fluorescent intensity in a 2D optically sliced image composed of 512x512 pixels<sup>2</sup>. In the case of wet confined gel, pores were filled with the solvent containing fluorescein. The Ar laser with 488 nm wavelength was used to excite fluorescein molecules. Dried monolithic gel was observed in almost the same way as reported elsewhere [38]; the dried monolithic gel was immersed in a mixture of toluene and chloroform (17:83) to allow the laser light to transmit through the turbid gel, and a 488 nm Ar laser was used to excite fluorescein molecules distributed in the gel phase.

The LSCM images were binarized and 3D reconstructed by stacking the digitized 2D images [37]. The depth profiles (along the z-direction) of volume fraction of siloxane phase are depicted by summing the pixels representing siloxane phase in the series of binarized images for all confined samples. The characteristic lengths of the phase separated structure are determined by the structure factor  $S(q)$ , which is obtained from Fast Fourier Transformation (FFT) of the series of binarized images and then averaged in the  $q_x$ - $q_y$  plane. The interfacial curvatures of the samples were also computed using the "Parallel Surface Method" (PSM), and obtained curvatures were further scaled with respect to the interfacial area per unit volume. The details of these analyses can be found elsewhere [36-38].

### 3. Results and Discussion

#### 3.1 Structural observation of methylsiloxane gels in near-surface region

Figure 2 shows the SEM photograph of the dried monolithic gel exhibiting the typical morphology of bicontinuous structure; the gel is consisted of the continuous methylsiloxane skeletons and macropores. From the direct measurement of the SEM image, characteristic length (defined as the length of the thickness of the gel skeleton plus the pore diameter) of the dried monolithic gel is estimated to be ca. 9.6  $\mu\text{m}$ . Figure 3 shows the LSCM photographs of the dried sample M92GG (a-c) and M3800 (d-f), exhibiting the depth dependence of the morphology along the z-direction. The thicknesses of the spacers are 50  $\mu\text{m}$  and 13  $\mu\text{m}$ , respectively: The actual thicknesses of the synthesized gels were found to be thicker than the thickness of the spacer. This discrepancy of the thickness is thought to be due to the unintended curve of the coverslips and/or partial folding of the thin spacers. Both samples have layered structure; interface (a,d), methylsiloxane depletion layer (b,e) and continuous bulk-like phase (c,f). The layered structure found near both surfaces is schematically shown in Figure 4. Structure of the interface was not detected due to the low contrast of the LSCM images; however, SEM observation revealed that skin layer had grown on the O surface (part (a) in Figure 4). Since MTMS oligomers are highly hydrophobic, hydrophobic attractive interaction worked between the O surface and MTMS oligomers to develop the skin layer. Conversely, the interaction between the G surface and MTMS oligomers is thought to be less attractive. However, Si-O-Si chemical bond should form between the Si-OH on the G surface and those on MTMS oligomers at the interface (part (b) in Figure 4). Although the methylsiloxane depletion layer was formed both in the M92GG and M3800, the forming mechanism must be different. In the case of M3800, due to the complete wetting of the ODS-modified surface by MTMS oligomers, the methylsiloxane depletion layer had formed.

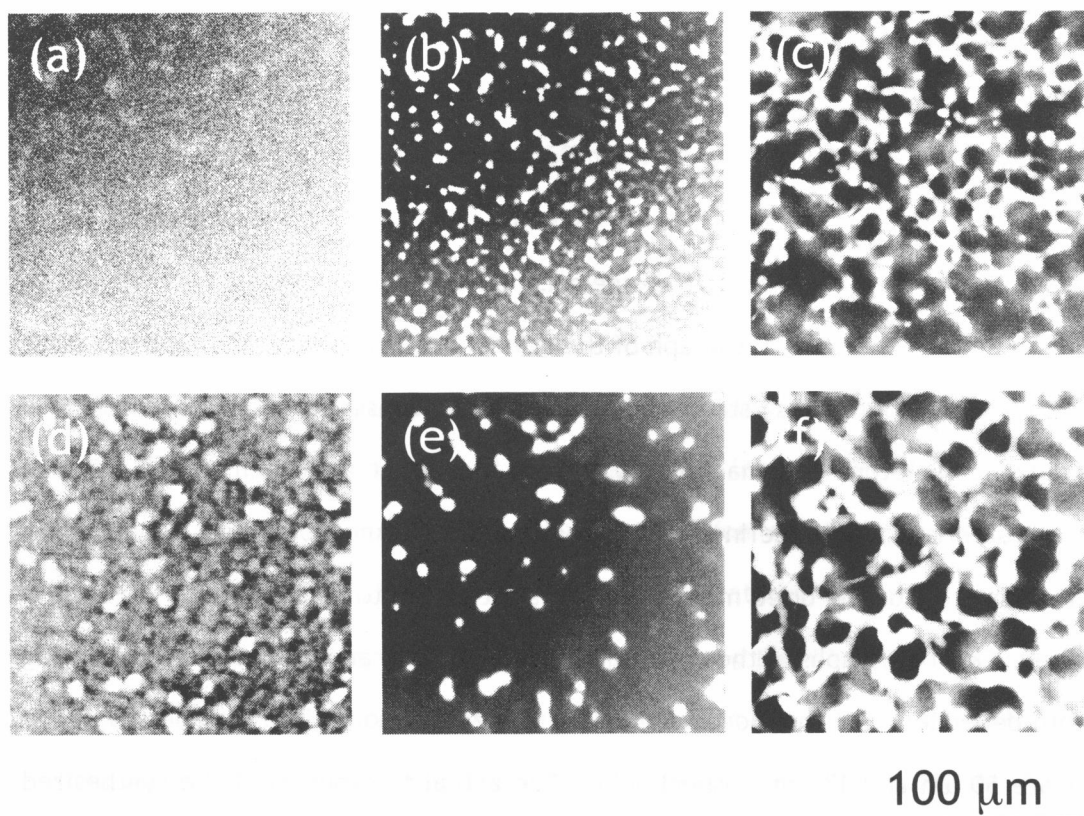


Figure 3 The LSCM images of dried confined gels; upper row is the sample M92GG, lower row is the sample M3800. Each image in a row shows a different altitude along the z-direction; (a) and (d) the surface, (b) and (e) 5  $\mu\text{m}$  beneath the surface showing the methylsiloxane depletion layer, and (c) and (f) 15  $\mu\text{m}$  beneath the surface showing the bulk-like layer. The bright and dark areas correspond to the methylsiloxane phase and the solvent phase, respectively.

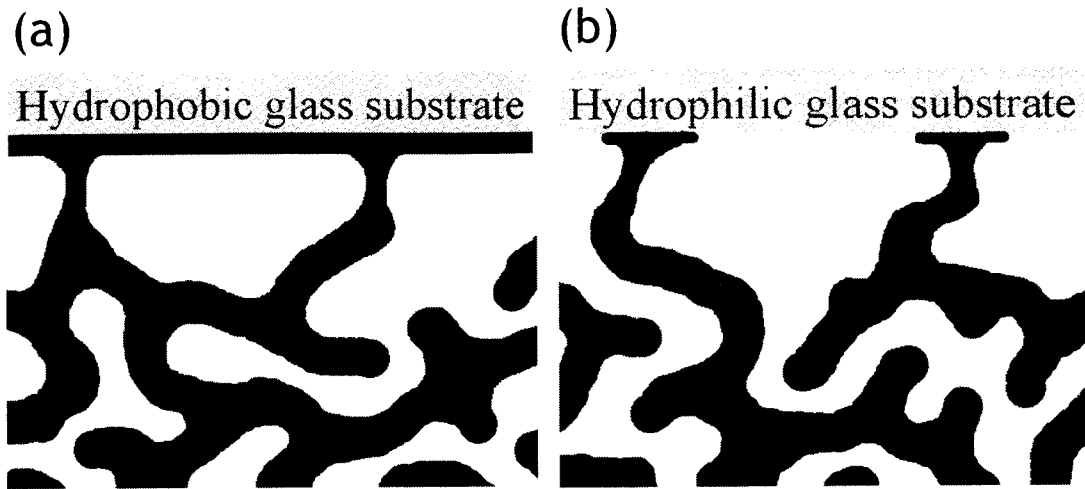


Figure 4 Schematic cross sectional illustrations of layered structure near the surfaces; (a) M3800 and (b) M92GG. The dark area corresponds to the methylsiloxane phase. The most evident difference of the two is the skin layer on the hydrophobic surface.

Once the skin layer formed by hydrophobic interaction, the MTMS monomers or oligomers near the hydrophobic substrate decrease because the most of the MTMS components in this region are distributed to the skin layer. In the case of M92GG, although the attractive interaction between the G surface and MTMS oligomer is not as strong as the case with O surface, MTMS-derived phase will be attracted to the G surface probably because of the low interfacial energy of MTMS-derived phase. The bulk-like phase was formed in the region slight away from the surface. In this region, since the effect of the surface becomes negligible, bicontinuous structure that is similar to the monolithic gel was formed.

The characteristic length of the bulk phase did not change during drying process in all of the confined gels, resulting in the larger domain size than that of the bulk gel. It is also possible that the densification of gel network due to condensation between silanol groups causes some shrinkage during the aging process. In order to examine the shrinkage during aging, the sample of the same composition was prepared and observed under LSCM before and after aging. The LSCM images showed that the confined gels had not shrunk during aging process in contrast with the bulk gel. Namely, no shrinkage occurs in the confined gels during both aging and drying process. The attractive interaction between the gel domains and plate surface, Si-O-Si chemical bonds in the case of G surface and hydrophobic attractive interaction in the case of O surface, was strong enough to inhibit the free shrinkage of the confined gels. From the various thicknesses of the samples, an trend can be seen, that is, the characteristic length of the confined gel generally becomes longer with decreasing the thickness of the samples (for example, part (c) and part (f) in Figure 3).

### *3.2 Structural analysis by 3D reconstruction*

#### *3.2.1. Geometrical properties of the bulk gels*

Figure 5 shows the 3D reconstructed images of the dried bulk gels derived from (a)



the MTMS and (b) TMOS. The characteristic length determined from the structure factor and the volume fraction of methylsiloxane or silica gel and the scaled area-averaged mean and Gaussian curvatures are listed in Table 1. The area-averaged curvatures  $\langle H \rangle$  and  $\langle K \rangle$  are scaled by the interfacial area per unit volume  $\Sigma$ , that is,  $\langle \tilde{H} \rangle = \langle H \rangle / \Sigma$  and  $\langle \tilde{K} \rangle = \langle K \rangle / \Sigma^2$ . The characteristic length of the MTMS-derived gel is much longer than that of the TMOS-derived gel, indicating that the spinodal decomposition is frozen in a later stage. These data are in good agreement with the results previously reported for sintered bicontinuous silica gel: Both the solvent and siloxane phases are bicontinuous exhibiting the 3D periodic isotropic structure; the scaled mean and Gaussian curvatures of the dried bulk gels derived from MTMS and TMOS, respectively, are around zero and negative. This means that most of the interface between the two phases is hyperbolic, which is typical in bicontinuous structures induced by spinodal decomposition [38].

### 3.2.2 Structural variation near a hydrophobic surface

Figure 6 shows the (a) 3D reconstructed image and (b) depth profile of the aged sample M5900, where  $z=0$  indicates the position of the hydrophobic surface. The thickness of the spacer used for M5900 is 30  $\mu\text{m}$ . According to SEM observation, a skin layer has grown at the surface of the methylsiloxane gel film contacting the hydrophobic surface. The skin layer has formed as a result of complete wetting by the methylsiloxane phase on the hydrophobic surface, due to the low polarity of the methylsiloxane phase. Since the thickness of the wetting layer is quite thin (approximately a hundred nanometers), it is far below the resolution of LSCM, so a completely accurate profile of the confined gel-hydrophobic surface interface cannot be depicted. In the case of thin polymer blend films (approximately tens to hundreds of nanometers thick), when one component segregates preferentially to a surface, surface directed spinodal decomposition leads to a layered structure (i.e., lamellar structure) perpendicular to the surface. However, in the present system, layered structure appears only at close

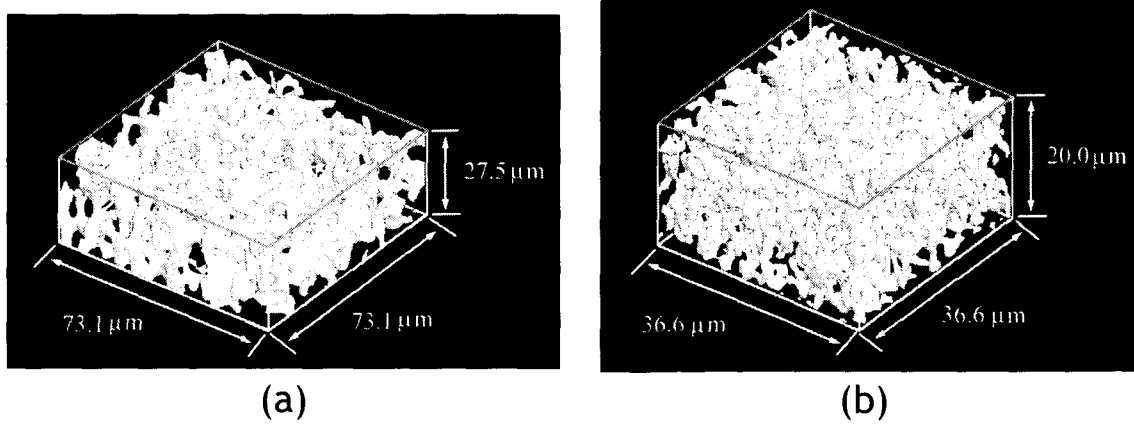


Figure 5 Three-dimensionally reconstructed images of dried bulk gels derived from (a) MTMS-FA system and (b) TMOS-FA system. Each gel exhibits the typical bicontinuous structure derived from spinodal decomposition.

Table 1 The characteristic length, volume fraction of siloxane phase, the scaled mean and Gaussian curvatures of the dried bulk gels

	Characteristic length ( $\mu\text{m}$ )	Volume fraction of siloxane phase	Scaled mean curvature $\langle \tilde{H} \rangle$	Scaled Gaussian curvature $\langle \tilde{K} \rangle$
Dried MTMS bulk	14.1	0.25	-0.535	-1.61
Dried TMOS bulk	3.86	0.22	-0.782	-0.836

proximity to the surface when the sol-gel transition occurs and arrests the phase separation, so it is hard to conclude that the layered structure would develop throughout the film. Nonetheless, due to the complete wetting of the hydrophobic surface, a methylsiloxane depletion layer has formed beneath the skin layer. In the region deeper than the methylsiloxane depletion layer, the bulk-like phase, there exists a bicontinuous structure, which proceeds into the thick film.

The morphology of the methylsiloxane depletion region appears as cylindrical columns perpendicular to the surface, connecting the skin layer and the bulk-like phase. The representative binarized sliced images at various positions in the z-direction are inset in Figure 3 (b); the white and black regions correspond to the solvent and siloxane phases, respectively. The siloxane phase is dispersed in the major solvent phase in the depletion region; in the deeper region, a bicontinuous “bulk-like phase” appears.

Figure 7 shows the (a) 3D reconstructed image and (b) depth profile of the aged sample T7400 (the thickness of the spacer is 13  $\mu\text{m}$ ). From SEM observation, it is revealed that the skin layer has developed at the interface, as seen in the MTMS system. The surface of TMOS oligomer is generally thought to have hydrophilic character, however, the starting composition of this system contains less than the stoichiometric amount of water for complete hydrolysis, so the surface of the alkoxy-containing silica gel can be highly hydrophobic. For this reason, the morphology and the depth profile are similar to the MTMS system. In this case, however, the depletion is shallower than that of the MTMS system (see Figure 6 (b)).

In the depletion layer of the MTMS system, cylindrical columns connecting the skin layer and the bulk phase have formed, but these cannot be found in the TMOS system. This difference can be explained as follows: since unreacted silanols in the gel condense during the aging process, the gel shrinks to some extent. The density of the siloxane network is lower in MTMS-derived gel because each monomer has only three functional groups that can react. Therefore, when the gel shrinks toward the center of the film, MTMS-derived gel skeleton is flexible and can stretch to endure the stress of shrinkage, so the cylindrical

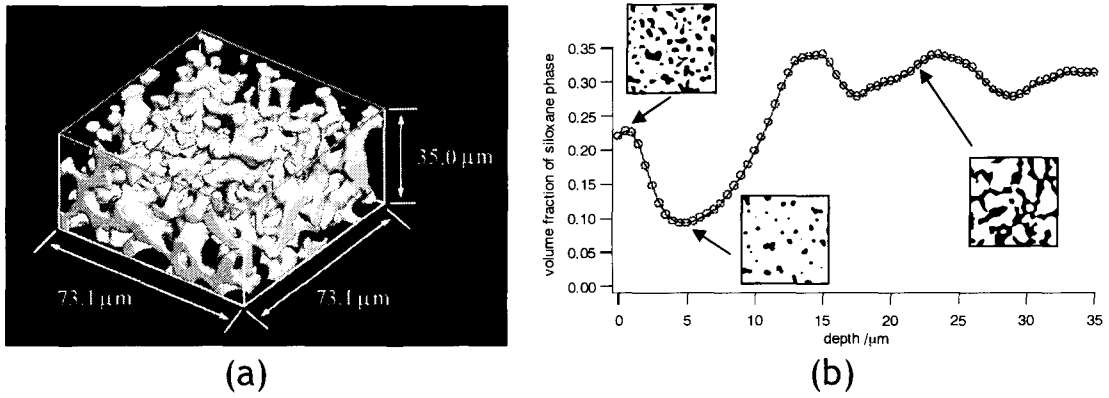


Figure 6 The 3D reconstructed image and the depth vs. volume fraction profile of aged M5900. The uppermost plane of the reconstructed image represents the surface ( $z=0$ ). The column-like structure that connects the interface and the bulk phase can be seen in upper part of the image.

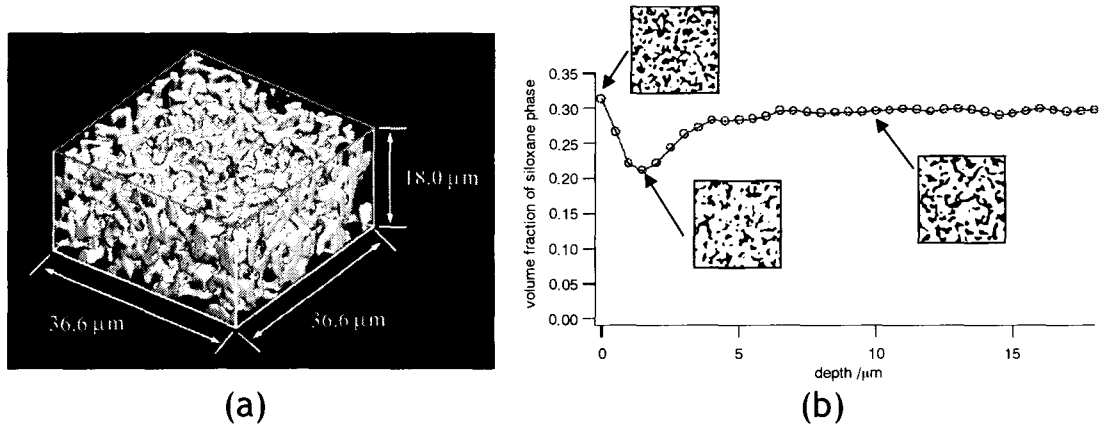


Figure 7 The 3D reconstructed image and the depth vs. volume fraction profile of aged T7400. Unlike the MTMS system, bicontinuous structure is maintained throughout the sample.

columns perpendicular to the surface are formed. On the other hand, the siloxane network of TMOS-derived gel is thought to be more rigid than MTMS-derived gel, so the gel skeleton cannot change its shape during shrinkage. Instead, the gel skeleton broke up in the drying process, in which more shrinkage occurs due to the evaporation of the solvent, while MTMS-derived gel did not crack at all. This fact is also confirmed by the inset images in Figure 7 (b); bicontinuous structure is maintained throughout the sample. Another factor drastically affects the morphology in the proximity of the surface is the characteristic length of the bulk. Since longer characteristic length means longer time between the onset of phase separation and gelation, such deformation becomes more significant when the phase separation time becomes longer. Thus the reasons why TMOS-derived gel did not show significant deformation near the surface are; (1) TMOS-derived gel is hardly deformable because of the rigid network and (2) shorter characteristic length in this case.

### *3.2.3 Structural variation near a hydrophilic surface*

Figure 8 shows the (a) 3D reconstructed image and (b) depth profile of the aged sample M83GG (the thickness of the spacer is 13  $\mu\text{m}$ ). In contrast to the hydrophobic surface, the interaction between the hydrophilic surface and MTMS oligomers is thought to be less attractive; however, the depth profile appears similar to the hydrophobic case (see Figure 6 (b)). The MTMS oligomers with low polarity are thought to exhibit a less attractive interaction with hydrophilic surfaces; however, Si-O-Si chemical bonds can form between the silanol groups on the hydrophilic glass surface and MTMS oligomers or monomers, so a rather attractive interaction between them leads to partial wetting of MTMS phase to the hydrophilic surface. More importantly, the partial wetting forms “footholds” to endure the shrinkage of gel phase that leads to the methylsiloxane depletion layer beneath the surface just as the hydrophobic case. The depth profile looks quite similar to the case of hydrophobic surface. Since the skin layer at the hydrophobic

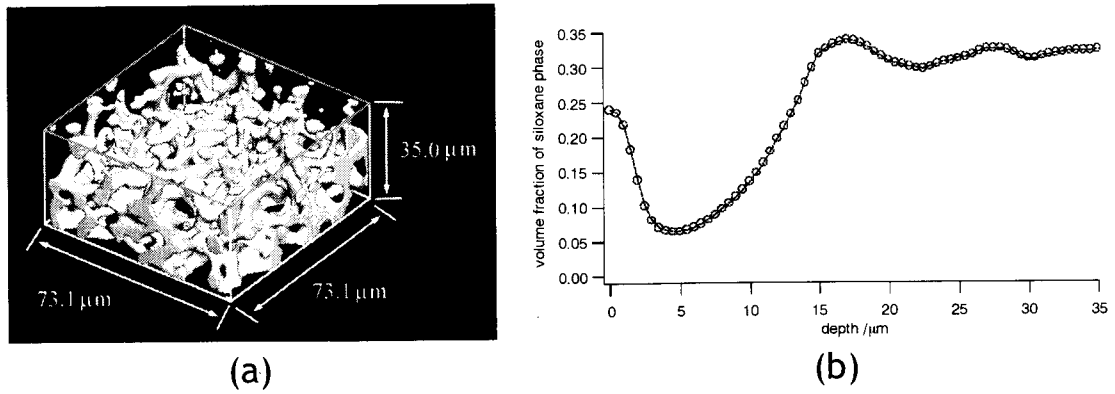


Figure 8 The 3D reconstructed image and the depth vs. volume fraction profile of aged M83GG. There is little difference between this case and hydrophobic case (see Figure 6), though the adsorption mechanism is quite different.

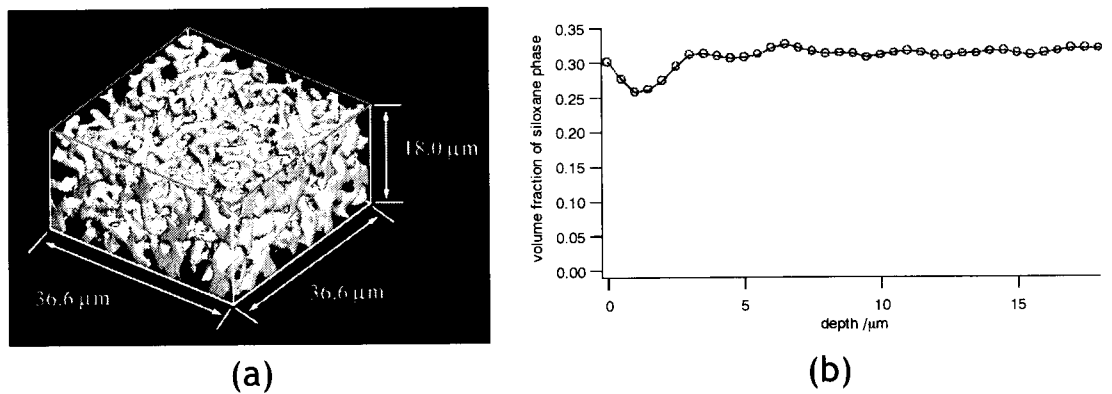


Figure 9 The 3D reconstructed image and the depth vs. volume fraction profile of aged T82GG. Again, though the adsorption mechanism is thought to be quite different, there is little difference between this case and the hydrophobic case (see Figure 7).

surface is quite thin, it has barely influenced the morphology in the deeper region, which resulted in little difference between hydrophobic and hydrophilic cases.

Figure 9 shows the (a) 3D reconstructed image and (b) depth profile of the aged sample T82GG (the thickness of the spacer is 30  $\mu\text{m}$ ). In this case, as is described above, since the surface character of TMOS oligomers is probably highly hydrophobic, partial wetting by TMOS oligomers could have occurred on a hydrophilic surface, which resulted in almost the same behavior as the MTMS system.

In summary, both kinds of affinity between the gel phase and the surface (either hydrophobic interaction or forming a chemical bond) lead to the gel depletion layer in both MTMS and TMOS systems. The surface segregation tendency is thought to be stronger for the hydrophobic interaction, which resulted in complete wetting of the gel phase on the surface. The shape of the gel depletion layer is quite different between the two alkoxide systems due to the difference in crosslinking density and phase separation time.

The characteristic lengths of the bicontinuous structures of the confined gels are longer than for the bulk gels. Although we cannot give an explicit account for this phenomenon at the present stage, it is probable that the shrinkage during the condensation reaction of silanols is restricted due to the geometrical confinement.

## 4. Conclusion

Bicontinuous siloxane-based gels were synthesized in 2D confined spaces and 3D observation was performed by LSCM. The volume fraction of the confined gels oscillates with depth near the surface. The structural variances of the thick samples near a hydrophobic surface and a hydrophilic surface are similar to each other; however, SEM observation revealed that a skin layer has formed at the interface of a hydrophobic substrate. In the case of the MTMS system, a cylindrical columnar gel skeleton formed in the methylsiloxane depletion region, which reflects the flexibility of the 3-functional gel.

Conversely, since the TMOS-derived gel has a more rigid siloxane network and shorter characteristic length which exhibits the shorter phase separation time, such deformation could not occur.

In the following section, more detailed discussion about the relationship between structural deformation and phase separation time is given. Since deformation occurs during phase separation (more precisely, during the systems remain fluidic after the occurrence of phase separation), this dynamic factor will be found more effective than the static chemical factor which was discussed in this section.



## References in Section 2.1

- [1] K. Nakanishi, *J. Porous Mater.* **4**, 67 (1997).
- [2] K. Nakanishi, R. Takahashi, T. Nagakane, K. Kitayama, N. Koheiya, H. Shikata, N. Soga, *J. Sol-Gel Sci. Tech.* **17**, 191 (2000).
- [3] K. Nakanishi, *J. Sol-Gel Sci. Tech.* **19**, 65 (2000).
- [4] H. Kaji, K. Nakanishi, N. Soga, *J. Sol-Gel Sci. Tech.* **1**, 35 (1993).
- [5] N. Tanaka, H. Kobayashi, K. Nakanishi, H. Minakuchi, N. Ishizuka, *Anal. Chem.* **73**, 420A (2001)
- [6] N. Tanaka, H. Kobayashi, N. Ishizuka, H. Minakuchi, K. Nakanishi, K. Hosoya, T. Ikegami, *J. Chromatogr. A*, **965**, 35 (2002).
- [7] N. Ishizuka, H. Minakuchi, K. Nakanishi, N. Soga, K. Hosoya, N. Tanaka, *J. High Resol. Chromatogr.* **21**, 477 (1998).
- [8] N. Tanaka, H. Nagayama, H. Kobayashi, T. Ikegami, K. Hosoya, N. Ishizuka, H. Minakuchi, K. Nakanishi, K. Cabrera, D. Lubda, *J. High Resol. Chromatogr.* **23**, 111 (2000).
- [9] N. Ishizuka, H. Minakuchi, K. Nakanishi, N. Soga, H. Nagayama, K. Hosoya, N. Tanaka, *Anal. Chem.* **72**, 1275 (2000).
- [10] N. Ishizuka, H. Minakuchi, K. Nakanishi, K. Hirao, N. Tanaka, *J. Sol-Gel Sci. Tech.* **19**, 371 (2000).
- [11] S. Kumon, K. Nakanishi, K. Hirao, *J. Sol-Gel Sci. Tech.* **19**, 553 (2000).
- [12] K. Nakanishi, S. Kumon, K. Hirao, H. Jinnai, *Mat. Res. Soc. Symp. Proc.* **628**, CC7.6.1 (2000).
- [13] U. Steiner, J. Klein, E. Eiser, A. Budkowski, L. J. Fetters, *Science*, **258**, 1126 (1992).
- [14] H. Tanaka, *Phys. Rev. Lett.* **70**, 53 (1993).
- [15] H. Tanaka, *Phys. Rev. Lett.* **70**, 2770 (1993).
- [16] H. Tanaka, *Europhys. Lett.* **24**, 665 (1993).
- [17] S. Puri, K. Binder, *Phys. Rev. E*, **49**, 5359 (1994).
- [18] H. Tanaka, T. Sigehuzi, *Phys. Rev. Lett.* **52**, 829 (1995).

- [19] J. Rysz, A. Budkowski, A. Bernasik, J. Klein, K. Kowalski, J. Jedliński, L. J. Fetters, *Europhys. Lett.* **50**, 35 (2000).
- [20] H. Tanaka, *J. Phys.: Condens. Matter*, **13**, 4637 (2001).
- [21] R. A. L. Jones, L. J. Norton, E. J. Kramer, F. S. Bates, P. Wiltzius, *Phys. Rev. Lett.* **66**, 1326 (1991).
- [22] F. Bruder, R. Brenn, *Phys. Rev. Lett.* **69**, 624 (1992).
- [23] A. Budkowski, U. Steiner, J. Klein, *J. Chem. Phys.* **97**, 5229 (1992).
- [24] A. Hariharan, S. K. Kumar, M. H. Rafailovich, J. Sokolov, X. Zheng, D. Duong, S. A. Schwarz, T. P. Russell, *J. Chem. Phys.* **99**, 656 (1993).
- [25] G. Krausch, C. Dai, E. J. Kramer, F. S. Bates, *Phys. Rev. Lett.* **71**, 3669 (1993).
- [26] J. F. Marko, *Phys. Rev. E*, **48**, 2861 (1993).
- [27] G. Krausch, *Mater. Sci. Eng. Rep.* **R14**, 1 (1995).
- [28] M. Geoghegan, R. A. L. Jones, A. S. Clough, *J. Chem. Phys.* **103**, 2719 (1995).
- [29] J. Rysz, A. Bernasik, H. Ermer, A. Budkowski, R. Brenn, T. Hashimoto, J. Jedliński, *Europhys. Lett.* **40**, 503 (1997).
- [30] R. Cherrabi, A. Saout-Elhak, M. Benhamou, *J. Chem. Phys.* **111**, 8174 (1999).
- [31] J. Rysz, H. Ermer, A. Budkowski, M. Lekka, A. Bernasik, S. Wróbel, R. Brenn, J. Lekki, J. Jedliński, *Vacuum*, **54**, 303 (1999).
- [32] A. Bernasik, J. Rysz, A. Budkowski, K. Kowalski, J. Camra, J. Jedliński, *Macromol. Rapid Commun.* **22**, 829 (2001).
- [33] H. Morita, T. Kawakatsu, M. Doi, *Macromolecules*, **34**, 8777 (2001).
- [34] G. Krausch, C. Dai, E. J. Kramer, J. F. Marko, F. S. Bates, *Macromolecules* **26**, 5566 (1993).
- [35] H. Jinnai, Y. Nishikawa, T. Koga, T. Hashimoto, *Macromolecules*, **28**, 4782 (1995).
- [36] H. Jinnai, T. Koga, Y. Nishikawa, T. Hashimoto, S. T. Hyde, *Phys. Rev. Lett.* **78**, 2248 (1997).
- [37] H. Jinnai, Y. Nishikawa, H. Morimoto, T. Koga, T. Hashimoto, *Langmuir*, **16**, 4380 (2000).

[38] H. Jinnai, K. Nakanishi, Y. Nishikawa, J. Yamanaka, T. Hashimoto, *Langmuir*, 17, 619 (2001).

## Section 2.2 Local Geometrical Analysis of Structural Deformation in MTMS-Derived Phase-Separating Gels: Effect of Wetting, Gravity, and Viscoelasticity

### 1. Introduction

In the previous section, near-surface structure of phase-separated siloxane gels confined between two parallel substrates is observed under LSCM, and the origin of deformation was discussed from the viewpoint of chemical characters of the surfaces.

Compositional oscillation due to the preferential wetting in thin polymer blend film had been reported as “surface-directed spinodal decomposition” [1]. In this mechanism, the more wettable phase with lower interfacial energy segregates onto existing surface(s) by van der Waals interaction in a diffusive manner and the oscillating wave perpendicular to the surface propagates into the film internally with time [1,2]. Surface-directed spinodal decomposition, however, is a characteristic phenomenon only in the early stage of SD, and in the later stage of spinodal decomposition, the dynamic interplay between phase separation and wetting in polymer blends or solutions confined in 2 or 1 dimensional spaces has been studied by Tanaka et al [3]. They found that hydrodynamic flow derived from wetting in a polymer mixture plays an important role during the morphological evolution via spinodal decomposition. Namely, more wettable phase wets on a surface through bicontinuous channels, which are originally formed by spinodal decomposition and transform to a columnar structure in the later stage. More recently, Jinnai et al. performed the real-space analysis of phase-separating deuterated polybutadiene (DPB)/polybutadiene (PB) polymer blend sandwiched between two parallel coverslips by LSCM [4]. When the characteristic length,  $\Lambda_m$ , of the blend exceeds the separation,  $D$ , between the coverslips, i.e.  $D/\Lambda_m < 1$ , the isotropy of bicontinuous structure break up significantly and sequential transition to columnar structure connecting thick wetting

layers has been observed. In the case of 2D confined methylsiloxane gels, it was found that the more elongated columnar structure was formed nearby glass substrates in relatively thick samples as described in Section 2.1. Also, the oscillating wave of volume fraction of siloxane phase had been revealed in the depth direction. The oscillating wave seems to be similar to that of surface-directed spinodal decomposition, however, the formation mechanism is thought to be totally different as is described above. Obviously, it is important to examine how wetting effects impose the structural deformation when considering precise structural control of phase-separated siloxane gels in confined geometry.

In this chapter, phase-separated structure of methylsiloxane gel has been synthesized in a variety of confining molds and structural deformation due to preferential wetting has been observed. In particular, LSCM observation and curvature determination by Parallel Surface Method (PSM) [5,6] have been performed in a thinner gap between parallel plates (a 2D space) than what is reported in Section 2.1. Interfacial curvatures are the most fundamental local properties in the course of late-stage spinodal decomposition, because the morphological development is mainly driven by interfacial energy. Hence the shape of the spinodal interfaces normally keeps minimal surface area in the case of 3D isotropic spinodal decomposition.

## 2. Experimental

A gap between two glass plates was used as a 2D mold. A pair of polyethylene film spacers was used to adjust separation between the plates, ca. 25-50  $\mu\text{m}$ . Glass plates were cleansed in water using an ultrasonic washer, and one of the glass plates is replaced by a coverslip for the purpose of LSCM observation. As a scaled spacing of the molds, we also introduce  $D/\Lambda_m$  in this study [4]. Here,  $D$  is defined as separation between the substrates for the 2D mold, and  $\Lambda_m$  shows characteristic length of 3D isotropic bulk gel.

Methyltrimethoxysilane (MTMS, Shin-Etsu, Japan) and formamide (FA), methanol (MeOH) and nitric acid (Hayashi Pure Chemical Industries, Japan) were used as source materials without further purification. The molar ratio of the starting solution is MTMS : FA : H<sub>2</sub>O = 1 :  $f$  : 2.5, for the MF system, and MTMS : MeOH : H<sub>2</sub>O = 1 :  $m$  : 2.0 for the MM system. The molar ratios  $f$  and  $m$  was varied from 2.0 to 2.3 and 0.9 to 1.1, respectively. Appropriate amounts of 1.0 M aqueous Nitric acid and FA or MeOH were mixed in a glass tube and then MTMS was added under vigorous stirring at 0°C. After stirring for 5 min, the resultant homogeneous solution was transferred into the polystyrene reaction vessel in which the molds were placed, followed by an ultrasonic agitation for 1 min and vacuum deaeration. Then the solution was allowed to gel at 40°C in a closed condition. The resultant gel was aged over 24 h at the same temperature. Then some of the 2D and 3D samples were solvent exchanged with Fluorescein-dissolved FA or DMA solution in order to enhance the contrast in LSCM images. Thus, LSCM observation was conducted in reversed phase; solvent phase (pores in dried state) and siloxane phase are seen as bright and dark areas, respectively. The other samples were dried at 40°C more than 24 h, and then subjected to SEM observation.

Laser Scanning Confocal Microscope (LSM 510, Carl Zeiss, Germany) and SEM (S-2600N, Hitachi, Japan) were employed for observation of the gel morphologies. In LSCM observation, sufficiently thin focal depth can be obtained by shutting emitted light from unfocused planes in a sample by a confocal pinhole, and hence series of 2D sliced images in the depth direction can be obtained by moving the motorized observation stage along the light axis. An Ar ( $\lambda=488$  nm) laser was used to excite Fluorescein molecules, and an oil immersed 63×/1.25 objective lens (Plan-Neofluar, Carl Zeiss) was used. Intensity of fluorescence from a particular point in a focal plane ( $x$ - $y$  or lateral plane) at a given depth  $z$ ,  $I(x,y,z)$ , was recorded by the detector behind the long-pass filter (over 505 nm) into 512×512 pixels<sup>2</sup>, 8 bit gray scale images.

From digitized LSCM images, the area-averaged mean ( $\langle H \rangle$   $\mu\text{m}^{-1}$ ) and Gaussian ( $\langle K \rangle$   $\mu\text{m}^{-2}$ ) curvatures determination of the spinodal interfaces was performed on the basis of

PSM [5,6], in which variation of surface area is measured by parallel displacement of an original interface. The area of the parallel surface,  $A(d)$ , and that of the original interface,  $A(0)$ , depend on the interfacial curvatures, thus

$$A(d) = A(0)\left(1 + 2\langle H \rangle d + \langle K \rangle d^2\right), \quad \langle H \rangle = \frac{\kappa_1 + \kappa_2}{2}, \quad \langle K \rangle = \kappa_1 \kappa_2, \quad (2-1)$$

where  $d$  presents a displacement of the parallel surface from the original interface,  $\kappa_1$  and  $\kappa_2$  are the principal curvatures of an interface. This equation is valid when the displacement  $d$  is sufficiently small. Since the values of  $\langle H \rangle$  and  $\langle K \rangle$  are slightly affected by the size and portion of the obtained structure, we introduce the dimensionless scaled curvatures,  $\langle \tilde{H} \rangle$ ,  $\langle \tilde{K} \rangle$  as

$$\langle \tilde{H} \rangle = \langle H \rangle / \Sigma, \quad \langle \tilde{K} \rangle = \langle K \rangle / \Sigma^2 \quad (2-2)$$

where  $\Sigma$  is interfacial area per unit volume ( $\mu\text{m}^{-1}$ ) of the spinodal interface, which is directly obtained from LSCM observation. Hereafter, we discuss the interfacial curvature using these scaled values.

### 3. Results and Discussion

#### 3.1 The MF system

In Figure 1, reconstructed LSCM images are shown ( $f=2.3$  for part (a)-(c),  $f=2.4$  for part (d)-(e)). The feature of the bulk prepared far from any surfaces, we denote it as 3D bulk, clearly exhibits isotropic bicontinuous structure where both the siloxane skeleton and macropores are interconnected as shown in part (a). The geometrical properties are listed in Table 1, which shows the scaled mean and Gaussian curvatures,  $\langle \tilde{H} \rangle$  and  $\langle \tilde{K} \rangle$ , were calculated as  $-0.446$  and  $-1.78$  respectively, indicating most of the spinodal interfaces consist of saddle-like hyperbolic ones [7] and are slightly concave to the siloxane phase [8]. The periodic length of the structure,  $\Lambda_m$ , which is another characteristic parameter in the course of spinodal decomposition, was computed by 3D

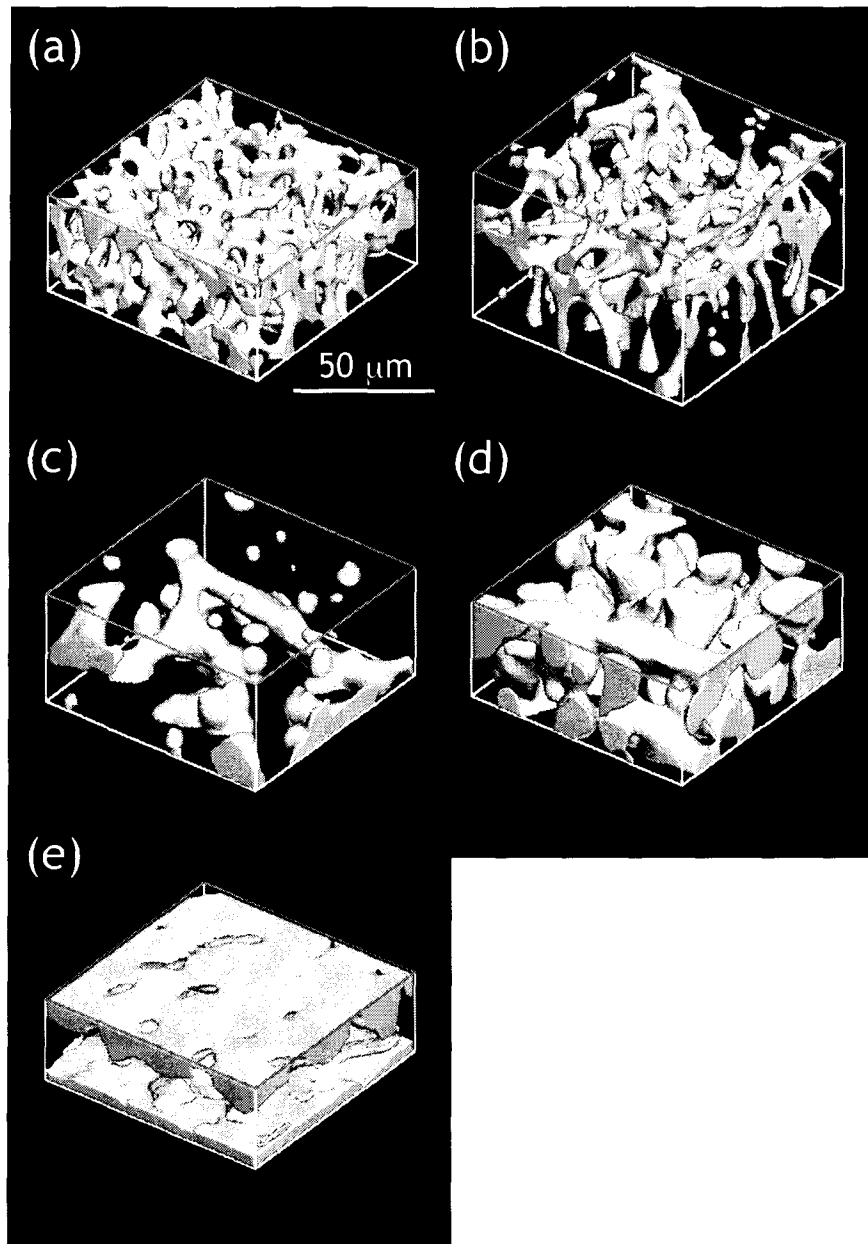


Figure 1 Three-dimensional reconstructed images obtained from LSCM; (a) 3D bulk gel prepared in free space far from any surfaces ( $f=2.3$ ), (b) and (c) confined gel (identical composition with part (a) prepared between parallel plates separated by 47.0 and 34.5  $\mu\text{m}$ , respectively and (d) confined gel prepared between parallel plates separated by 25.3  $\mu\text{m}$  ( $f=2.4$ ). The values of  $D/\Lambda_m$  in part (b), (c) and (d) are 2.9, 2.1 and 0.67, respectively. The significantly elongated columnar structure in part (b) and (c), and wetting transition in part (d) can be easily confirmed.



FFT of the each binarized sliced images then the structure factor is circular averaged in the  $q_x$ - $q_y$  plane. The wavenumber at a maximum intensity,  $q_m$ , has the relation with  $\Lambda_m$  as  $\Lambda_m=2\pi/q_m$  and  $\Lambda_m$  of the 3D bulk is found to be 16.3  $\mu\text{m}$ .

The gel features in a 2D confined mold are considerably affected by the parallel surfaces. Part (b) in Figure 1 exhibits the identical MTMS-derived gels confined between parallel glass plates separated by 47.0  $\mu\text{m}$  and hence  $D/\Lambda_m=2.9$ . The uppermost and lowermost planes are corresponding to the glass surfaces of the mold. Differently from previously reported DPB/PB polymer blend system [4], drastic structural deformation near the surfaces occurs even in a relatively large value of scaled thickness  $D/\Lambda_m$  in the present methylsiloxane system. This is partly because the high wettability of MTMS-rich phase in the present case allows phase-separated components to move more rapidly than polymer blend system. That is, separated phases can “feel” the existing surface even in the far inside portion of the 2D sample. Here, “wettability” is characterized by the asymmetry of interfacial energies of different phases, and is the driving force that causes preferential transport of one of the phases. Its dynamical behavior is naturally related with the viscosity. That is, in the present case, MTMS-derived phase is thought to have the lower interfacial energy compared to the solvent phase which mainly consists of FA and MeOH because MTMS oligomers do not have a strong effective intermolecular interaction at the onset of phase separation compared to methanol and FA, which are tend to form hydrogen bond.

Actually, the confined gel seems to have wetting layers in the proximity of the surfaces, however, we could not capture them obviously because the wetting layers are very thin and are to be observed in negative phase as described in the experimental section. The existence of the wetting layers is deduced from the fact that  $\phi_{sil}$  of the shown volume of the sample is only 0.156, which is less than  $\phi_{sil}$  of 3D bulk (=0.290).

In Figure 2(a), the partitioned figures of the same image are shown. The image is cut by the border depicted in Figure 2 (b), which indicates the volume fraction profile of the identical sample in the depth direction. Drastic depletion regions are confirmed nearby

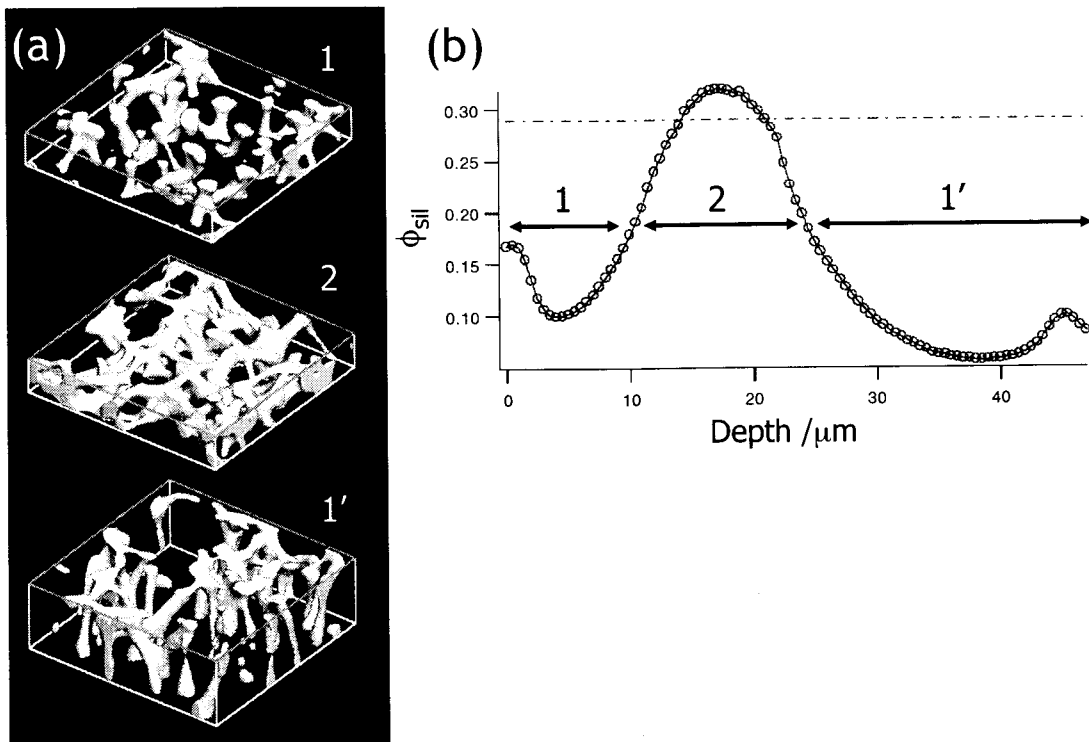


Figure 2 (a) Montage images of 2D confined gel shown in Figure 1(b). Partition borders are depicted in part (b). In the regions 1 and 1', which are nearby the surfaces, elongated columnar structure perpendicular to the surfaces can be corroborated, and in the region 2, rather transversal bicontinuous structure is left at nearly midst of the sample. (b) The depth profile of volume fraction of siloxane phase,  $\phi_{sil}$ , which oscillates significantly between the surfaces. In particular, the drastic depletion region near both the surfaces reflects the columnar structure resulted from wetting. The broken line corresponds to the  $\phi_{sil}$  of the 3D bulk gel.

both the surfaces, which correspond to the columnar structure. The upper and lower parts of the montage image clearly show that most of the gel skeleton is elongated and perpendicular to the surface and middle part of it shows that there is transversal bicontinuous structure in nearly the midst of the sample. The characteristic length in the bicontinuous part is longer than that in 3D bulk gel (see Table 1), but the reason is still unclear<sup>\*1</sup>. The elongated skeletons perpendicular to the surface are thought to act as material transfer channels [3] through which the more wettable MTMS-derived phase is brought onto the surfaces. Comparison of the curvatures between these three parts and 3D bulk are listed in Table 1. The Gaussian curvature  $\langle \tilde{K} \rangle$  of the various portion of the sample is almost unchanged, however, the mean curvature  $\langle \tilde{H} \rangle$  changed considerably between columnar gel skeleton and bicontinuous portion. This reflects the geometrical difference between these structures. Since the principal curvature whose center locates in the solvent-rich phase is defined positive, deviation to a large absolute value with signed negative means the developed columnar structure as illustrated in Figure 3. Columnar gel skeleton still mostly has a hyperbolic surface, i.e.  $\langle \tilde{K} \rangle < 0$ , however, from Figure 2(a), its surface is found to be more straight than bicontinuous one. This is indeed related to the depletion of siloxane phase in the columnar region (upper and lower part in Figure 2 (a)). The large value of the mean curvature is unfavorable from the view point of interfacial energy. According to Laplace equation, when different phases are separated by an interface with mean curvature  $H$ , pressure difference generates between the phases following the equation

$$\Delta p = \gamma(\kappa_1 + \kappa_2) = 2\gamma H, \quad (2-3)$$

where  $\Delta p$  and  $\gamma$  are the pressure difference and interfacial energy, respectively. That is, wetting is dominated by the pressure difference between wetting layer and elongated skeleton, not by interfacial energy [3,4].

In the sample which has more decreased thickness,  $D=34.5 \mu\text{m}$ , i.e.  $D/\Lambda_m=2.1$ , the typical bicontinuous structure has disappeared and observed were only the columnar gel skeletons connecting between two surfaces as is shown in part (c) of Figure 1. These

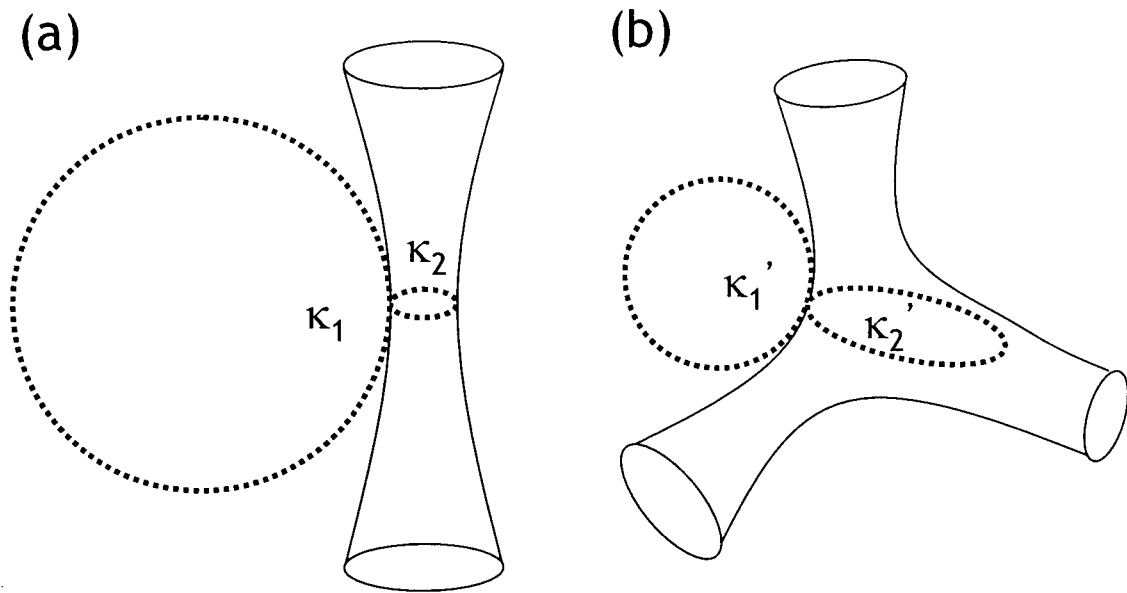


Figure 3 Schematic illustration of the relationship between the shape of siloxane gel skeleton and curvatures; (a) columnar skeleton often observed near the surfaces and (b) saddle-like skeleton in the bicontinuous portion. Since  $\kappa_1 > 0$  and  $\kappa_2 < 0$ , mean curvature  $H = (\kappa_1 + \kappa_2)/2$  becomes smaller in columnar skeleton where  $|\kappa_1|$  and  $|\kappa_2|$  becomes smaller and larger, respectively. Whereas hyperbolic saddle-like points in the bicontinuous pattern shows  $|\kappa_1| \approx |\kappa_2|$  thus  $H \approx 0$ . Gaussian curvature  $K = \kappa_1 \kappa_2$  is not apparently varied between these two.

significantly deformed structures do not resemble the case of DPB/PB polymer blend film [4], in which the columnar structure easily breaks up due to the low viscosity asymmetry. Indeed, the present case is somewhat related with the “viscoelastic phase separation” [9] where if the separated phases had intrinsic dynamic asymmetry, phase separation behavior would be dominated by the difference in viscosities of the phases in a certain time regime. Since the present system separates into the solvent-rich phase with no elasticity and highly viscoelastic network-forming siloxane gel phase, significantly elongated columnar skeletons appeared owing to the “viscoelastic phase separation”. Shrinkage during aging and drying process due to condensation of residual silanols [10] is also responsible for the elongated columnar structure as seen in these two samples. According to the listed values of curvatures in Table 1, this structure seems to have an elliptic interface, but these values are significantly affected by the elliptic portions of the siloxane phase as shown in Figure 1(c). Since the elongated gel skeletons are to be broken up in the course of wetting, these parts are thought to be the result of breakup and adsorption to the surfaces.

The sample with more increased value of  $f$  ( $=2.4$ ), where  $D/\Lambda_m$  became less than unity, showed “wetting transition” in the 2D mold. The characteristic length of 3D bulk gel is  $37.8 \mu\text{m}$ , which is shown in Figure 1 (d) and Table 1. In the sample with  $D=25.3 \mu\text{m}$ , (thus  $D/\Lambda_m=0.67$ ), the siloxane component completely wets the surfaces forming thick wetting layers, and no structure is left between them as is shown in Figure 1 (e) and Table 1. When spinodal wavelength exceeds the dimension of the mold, there will be no way to develop the wave in the confining mold, and transition to complete wetting will be promoted. What is noteworthy is the congruency of  $\phi_{sil}$  in 3D bulk and 2D confined gel as is shown in Table 1, and both the curvatures become closer to zero, indicating the mostly planer interfaces.

### 3.2 The MM system

As described in Chapter 1, phase separation and gelation behavior is substantially

Table 1 Geometrical parameters of phase-separated methylsiloxane gels.

	$\Lambda_m$ ( $\mu\text{m}$ )	$\phi_{sit}$	$\Sigma^*$ ( $\mu\text{m}^{-1}$ )	$\langle \tilde{H} \rangle$	$\langle \tilde{K} \rangle$
Bulk gel in Figure 1(a)	16.3	0.290	0.407	-0.446	-1.78
Region 1 in Figure 2(a)	-**	0.128	0.205	-1.71	-2.16
Region 2 in Figure 2(a)	24.7	0.283	0.355	-0.469	-1.95
Region 1' in Figure 2(a)	-**	0.105	0.171	-2.19	-3.46
Confined gel in Figure 1(c)	29.0	0.104	0.0996	-2.90	9.21
Bulk gel in Figure 1(d)	37.8	0.429	0.264	-0.317	-0.795
Confined gel in Figure 1(e)	-**	0.415	0.206	-0.112	1.66

\* $\Sigma$ : Area of spinodal interface per unit volume

\*\* : It is hard to define characteristic length because the power spectrum does not have a sharp peak (no periodic structure).

 Table 2 The geometrical parameters of siloxane gels obtained from the MM system ( $m=1.0$ ).

	$D/\Lambda_m$	$\langle \tilde{H} \rangle$	$\langle \tilde{K} \rangle$
Bulk	-	-0.27	-1.79
Thin GG	2.60	-0.47	-2.05
Thin OO	4.80	-0.42	-2.31
Thick GG	18.2*	-0.72	-1.88
Thick OO	18.2*	-1.05	-2.52

\*The actual thickness can not be determined by LSCM. Sample thickness  $D$  is deduced as 200  $\mu\text{m}$  which is a thickness of the spacer.

different between the MF and the MM systems. If the hypothesis of the origin of deformation, that is, preferential wetting by hydrodynamic flow during the phase separation, is correct, a significant variation in the dynamic deformation should appear. Since the deformation due to preferential wetting occurs in between the onset of phase separation and that of gelation, the effect of wetting will be insignificant in the MM system with shorter phase separation time.

In Figure 4 phase-separated siloxane gels derived from the MM system ( $m=1.0$ ) are exhibited, and the geometrical parameters are listed in Table 2. Part (a) represents the bulk gel with  $\Lambda_m=11.0 \mu\text{m}$  and it is confirmed that the volume fraction profile is flat ( $\phi_{sil}=0.31$ ). Part (b) and (c) shows the identical gel confined between hydrophilic and hydrophobic plates, respectively. Although the volume fraction profile oscillates in both cases, the structural deformation is much less than the case of the MF system. The inset images on the volume fraction profiles indicate that there remains a somewhat transversal gel connection, which is a brilliant contrast to the MF system (see Figure 6 (b) in Section 2.1).

On the contrary, when the identical gels are confined between much thicker 2D spaces, deformation became more significant. Figure 5 shows the samples confined in  $D=200 \mu\text{m}$  spaces. Much elongated gel skeletons beneath the surfaces are confirmed in both (a) hydrophilic and (b) hydrophobic cases. Since the bulk gels prepared from the MM system is susceptible to the gravity because the system phase-separates into heavier viscoelastic siloxane-rich phase and lighter solvent-rich phase with no elasticity (siloxane skeleton density is ca. 1.44 g/cc from Hg porosimetry, and that of methanol, which is the main constituent of solvent-rich phase, is 0.79 g/cc), this unexpected phenomenon in confined geometry is also considered as the gravity effect [11]. That is, when surface/volume ratio becomes smaller, the upper surface must endure the weight of larger volume of gel. During the phase formation after the onset of phase separation, the

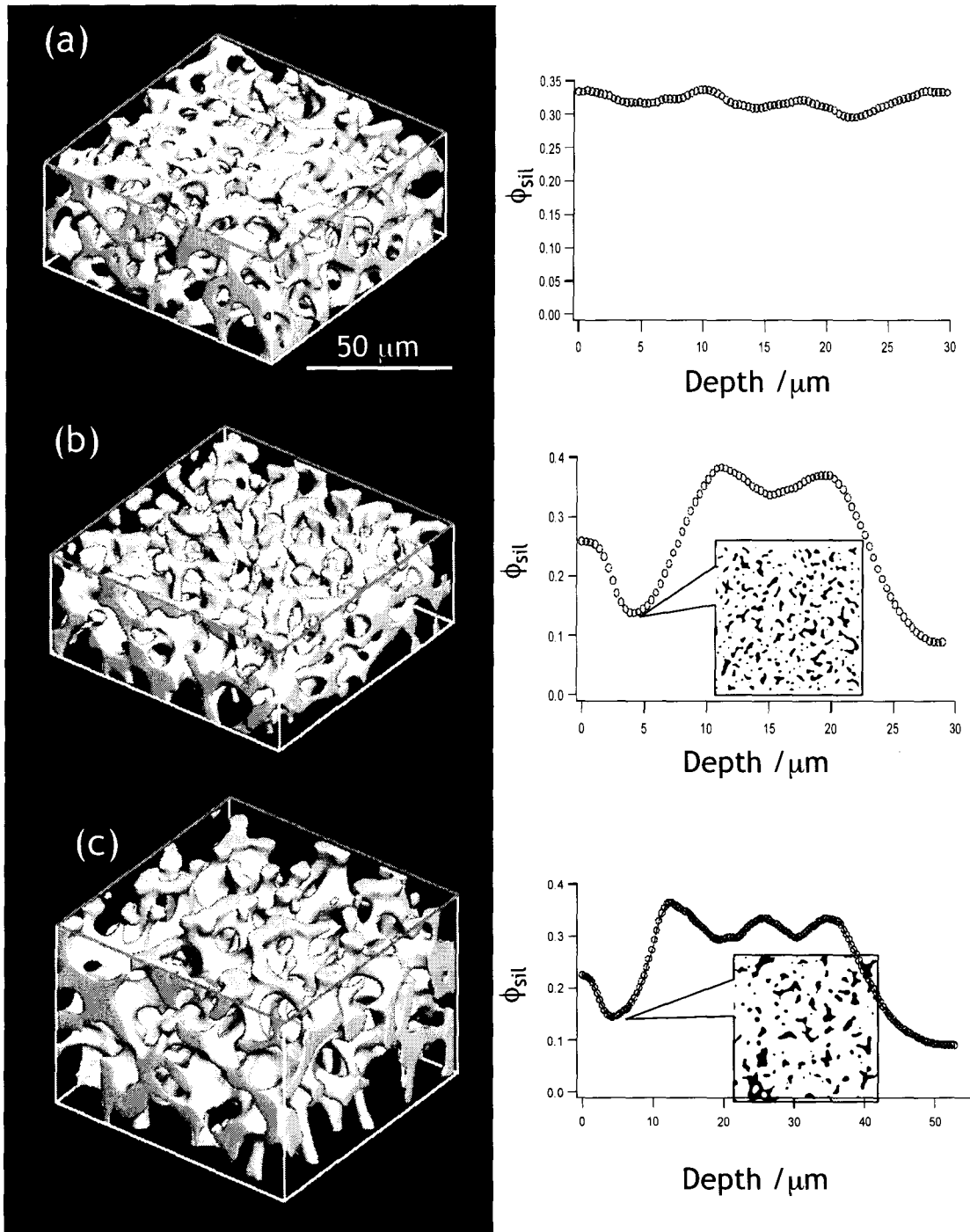


Figure 4 Three-dimensional reconstructed images of phase-separated siloxane gels derived from the MM system ( $m=1.0$ ). (a) Bulk gel ( $\phi_{sil}=0.31$ ), (b) gel confined between hydrophilic plates ( $D=29.1 \mu\text{m}$  and  $D/\Lambda_m=2.6$ ) and (c) gel confined between hydrophobic plates ( $D=52.9 \mu\text{m}$  and  $D/\Lambda_m=4.8$ ).



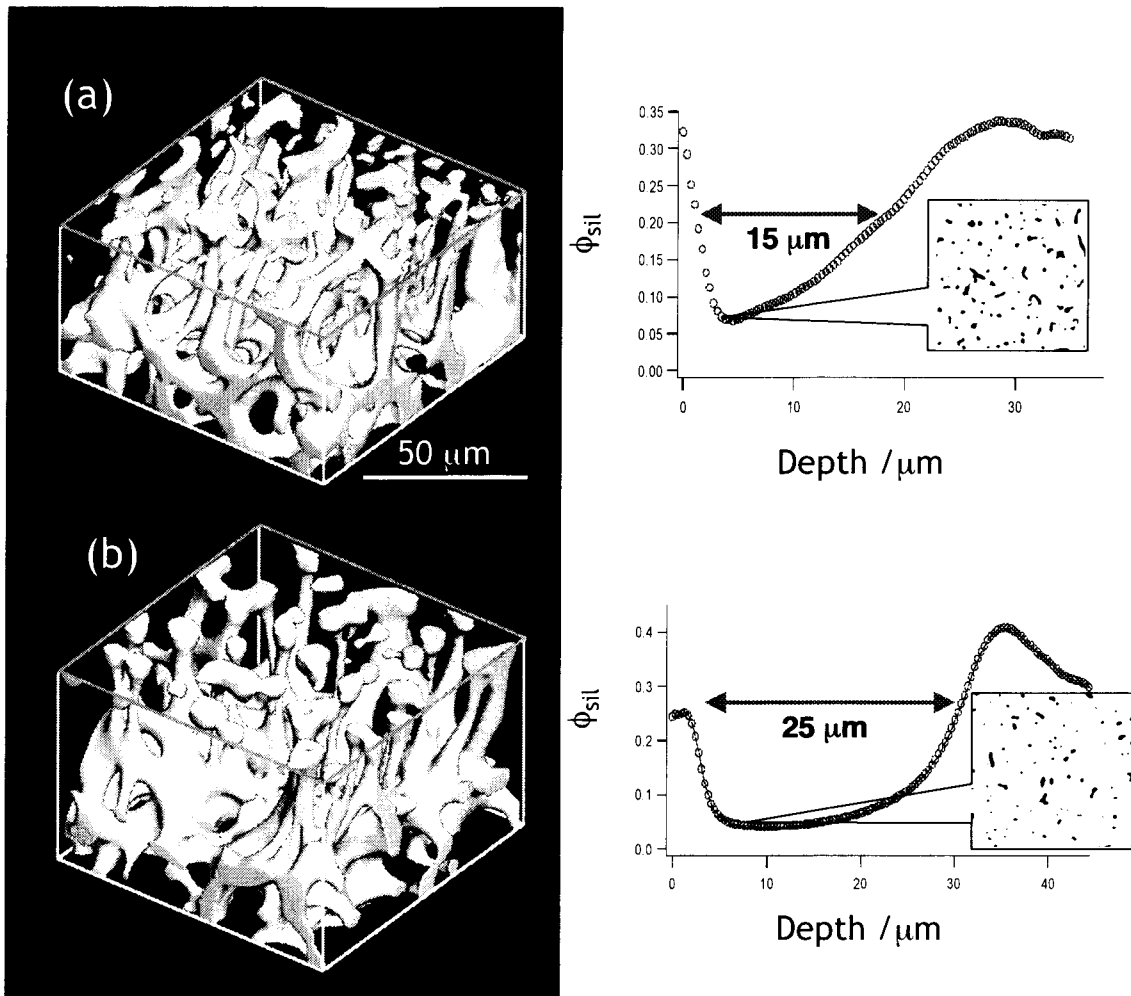


Figure 5 Phase-separated siloxane gels derived from the MM systems confined between thick 2D spaces fabricated by (a) hydrophilic substrates and (b) hydrophobic substrates. The thicknesses of the both samples are 200  $\mu m$ . The starting composition is the same as in Figure 3.

near-surface structure is slightly deformed into columnar gel skeletons perpendicular to the surface, and then the deformed skeletons are elongated by the larger volume of a gel which is settling down by the gravity. The absolute values of mean curvature, which is the indication of deformation, become larger due to the significantly deformed columnar gel skeletons as listed in Table 1. Since the siloxane gel phase tends to wet more significantly onto the hydrophobic substrate because of the hydrophobic interaction, the columnar deformation is slightly larger in the case of hydrophobic substrates.

As described above, these deformation phenomena are considered to be related to “viscoelastic phase separation” [9], that is, the system phase-separates into very viscoelastic siloxane-rich phase and solvent-rich phase with no elasticity. From this point of view, if the viscosity of solvent-rich phase becomes higher by adding water-soluble polymers etc., the deformation will be restricted. As is confirmed in DPB/PB polymer mixture system [4], the lack of difference in viscosity should avoid the deformation. Poly(ethylene glycol)-block-poly(propylene glycol)-block-poly(ethylene glycol) (EO<sub>108</sub>PO<sub>70</sub>EO<sub>108</sub>,  $M_w=12,600$ ) (denoted simply as EOPOEO) was added to the starting solution instead of MeOH, and it was confirmed that all of the EOPOEO block copolymer molecules were distributed in the solvent-rich phase by TG-DTA measurement. Figure 6 represents the gels obtained from this block copolymer-included system. The 2D substrate is hydrophobic substrate with  $D=200\ \mu\text{m}$  in which the deformation becomes most significant in the MM system as shown in Figures 4 and 5. Although small depletion can be seen at around  $6\ \mu\text{m}$  in depth, the deformation is highly suppressed: In Figure 5 (b) we can confirm the well-developed columnar skeletons (as long as  $25\ \mu\text{m}$ ) and siloxane phase fraction in the depletion region settles down to 0.04. However, in the same 2D substrate the depletion is much smaller ( $\phi_{sil}=ca. 0.19$ ) and transversal connections of siloxane gel skeletons are confirmed. For the purpose of investigating the effect of phase separation time within the MM system, a phase-separated gel was prepared using dilute 0.4M NA as a catalyst. By using a dilute acid, hydrolysis will slow down due to the decreased concentration of the catalyst [10,12], and polycondensation reaction will also be retarded

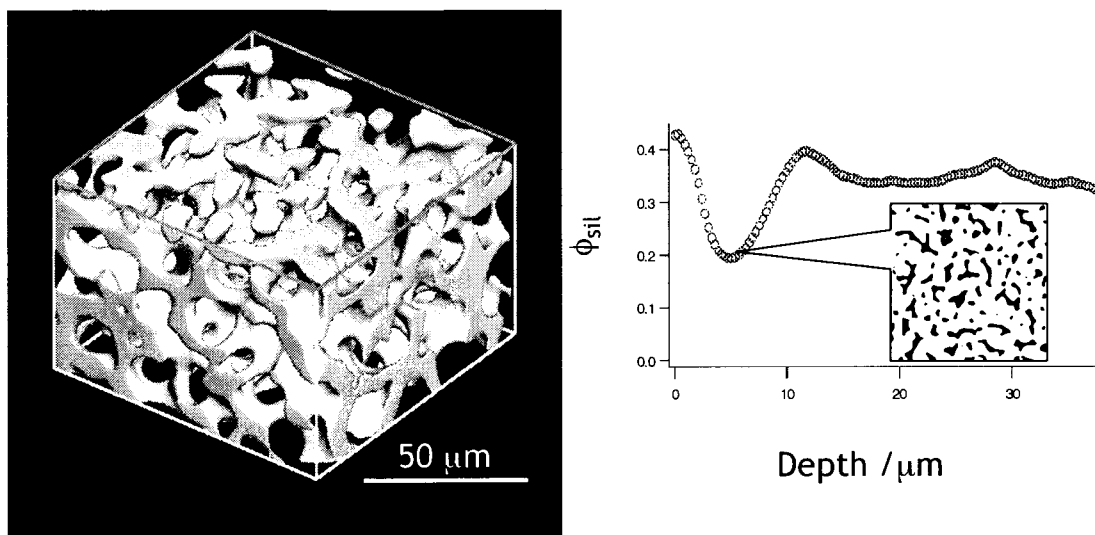


Figure 6 Phase-separated siloxane gels derived from MTMS-EOPOEO-1M NA system confined between thick 2D spaces fabricated by hydrophobic plates. The thickness of the sample is 200 μm. The striking deformation seen in Figure 4 (b) is effectively suppressed by incorporating viscous EOPOEO in the solvent-rich phase.

since the pH in the reacting solution becomes closer to the IEP of MTMS [10]. In the MTMS-MeOH-0.4M NA system, both the gelation and phase separation times become over three times those of the MM system where 1M NA is used. In the hydrophilic substrates with  $D=200\ \mu\text{m}$ , the thickness of the siloxane wetting layer is confirmed to be  $0.8\ \mu\text{m}$  and  $4.0\ \mu\text{m}$  in the 1M NA and the 0.4M NA systems, respectively. This fact implies that the dynamic factor such as the phase separation time affects the wetting behavior of siloxane gel.

#### 4. Conclusion

The effect of wetting, gravity, and viscoelastic factors on the phase separation in 2D molds is intensively studied.

In a phase-separated gel derived from MTMS-FA-1M NA system (MF system) in a thinner 2D mold, columnar deformation near a surface is much notable compared to the case of thick samples shown in Section 2.1. The relationship between wetting effect is discussed using Tanaka's hypothesis and Laplace law. According to the curvatures in the deformed regions, "hydrodynamic pumping" mechanism is suggested to be predominant.

For the purpose of confirming the "hydrodynamic pumping" hypothesis, where the dynamic parameters such as phase separation time will be influential, the MM system with a much faster reaction rate is studied. In the MTMS-MeOH-1M NA system (MM system), as is anticipated, the deformation is effectively suppressed compared to the MF system. However, when the thickness of the 2D substrate becomes as thick as to be affected by the gravity, extraordinary deformation appears. In avoiding such deformation induced by the gravity, a water-soluble polymer such as EOPOEO which is mostly distributed to the solvent-rich phase plays a crucial role by reducing the difference in viscosity in the both siloxane-rich and solvent-rich phases. The effect of reaction time is also confirmed by using the similar system with diluted catalyst.

In this chapter, a prehistory of the consideration of siloxane deformation in a 2D mold was demonstrated. The dynamic effect was found to be more significant than the chemical one, contrary to the tentative conclusion given in the previous part. But the author thinks the truth is not certified unless the time-evolution is observed *in real space*; scattering method such as light scattering does not give an insight. Time-resolved real-space analysis of the phenomena is strongly needed to further approach the truth in these results.

**Footnote**

\*1: Coarsening acceleration was observed by experimentally [13], and it was confirmed by numerical simulation [14] that the hydrodynamic wetting accelerates the coarsening “near” surfaces.

## References in Section 2.2

- [1] R. A. L. Jones, L. J. Norton, E. J. Kramer, F. S. Bates, P. Wiltzius, *Phys. Rev. Lett.* **66**, 1326 (1991).
- [2] G. Krausch, *Mater. Sci. Eng. Rep.* **R14**, 1 (1995).
- [3] H. Tanaka, *J. Phys.: Condens. Matter*, **13**, 4637 (2001).
- [4] H. Jinnai, H. Kitagishi, K. Hamano, Y. Nishikawa, M. Takahashi, *Phys. Rev. E*, **67**, 021801 (2003).
- [5] H. Jinnai, T. Koga, Y. Nishikawa, T. Hashimoto, S. T. Hyde, *Phys. Rev. Lett.* **78**, 2248 (1997).
- [6] Y. Nishikawa, H. Jinnai, T. Koga, T. Hashimoto, S. T. Hyde, *Langmuir*, **14**, 1242 (1998).
- [7] H. Jinnai, Y. Nishikawa, H. Morimoto, T. Koga, T. Hashimoto, *Langmuir*, **16**, 4380 (2000).
- [8] H. Jinnai, K. Nakanishi, Y. Nishikawa, J. Yamanaka, T. Hashimoto, *Langmuir* **17** (2001) 619.
- [9] H. Tanaka, *J. Phys.: Condens. Matter*, **12**, R207 (2000).
- [10] C. J. Brinker, G. W. Scherer, "Sol-Gel Science: The Physics and Chemistry of Sol-Gel Processing", Academic Press, New York, 1990.
- [11] D. Beysens, P. Guenoun, F. Perrot, *Phys Rev. A*, **38**, 4173 (1988).
- [12] K. J. McNeill, J. A. DiCaprio, D. A. Walsh, R. F. Pratt, *J. Am. Chem. Soc.* **102**, 1859 (1980).
- [13] P. Wiltzius, A. Cumming, *Phys. Rev. Lett.* **66**, 3000 (1991).
- [14] H. Tanaka, T. Araki, *Europhys. Lett.* **51**, 154 (2000).

## CHAPTER 3: STRUCTURES IN A ONE-DIMENSIONAL MOLD

### Section 3.1 Phase-Separated Structure of Methylsiloxane Gel in a Long Cylindrical Capillary

#### 1. Introduction

In the previous chapter, phase-separated structure of methylsiloxane gels derived from both MF and MM systems in a 2D mold was investigated especially by LSCM. The 2D confined gels derived from the MM system are revealed to be less deformed compared to those from the MF system. This means the MM derived gels are advantageous for applying to a HPLC separation medium which is required to have isotropic homogeneous structure. Preparing such an isotropic structure in a 1D capillary is of high technical and practical concerns for capillary HPLC and capillary electrochromatography (CEC) [1-6]. Also, phase separation and wetting of mixtures of low molecules and/or polymers in a 1D capillary holds rich physics.

In this section, structures of MF- and MM-derived methylsiloxane gels in a long cylindrical capillary are studied. Owing to the technical difficulty of LSCM observation of a capillary, the structural observations are performed only by SEM. The practical application to capillary HPLC is detailed in Chapter 5.

#### 2. Experimental

Molds used in this chapter are detailed in Chapter 1. A long cylindrical capillary (Polymicro, Phoenix, USA, denoted simply as capillary) are used as received (hydrophilic)

or after octadecylsilylation (hydrophobic). The internal diameters (ID) of capillaries are 10, 50 and 100  $\mu\text{m}$ . In this case the scaled spacing of a mold  $D/\Lambda_m$  is also defined. Here,  $D$  in a capillary represents ID.

The experimental procedure is the same as in the previous chapter. Two systems yielding methylsiloxane gels, the MF and MM systems are examined. The molar ratio in the MF system is MTMS : FA : H<sub>2</sub>O = 1 :  $f$  : 2.5 and that in the MM system is MTMS : MeOH : H<sub>2</sub>O = 1 :  $m$  : 2.0. Characterization of obtained gels was performed by SEM (S-2600N, Hitachi, Japan).

### 3. Results and Discussion

#### 3.1 Gels derived from the MF system in a capillary

In the sample with  $f=2.2$ , 3D bulk and gels confined in hydrophilic capillaries are shown in Figure 1. Periodic length of the 3D bulk (see part (a)) is found to be  $\Lambda_m=1.06 \mu\text{m}$ , which was directly measured from the enlarged SEM micrograph. In the capillaries with larger internal diameters ( $D=100$  and  $50 \mu\text{m}$ , shown in part (b) and (c), respectively), homogeneous bicontinuous structure was formed. Since the smaller  $\Lambda_m$  corresponds to shorter time-lag between the onset of phase separation and the complete structural freezing point, wetting effect has not been become significant yet at that stage. This is because the hydrodynamic wetting effect starts to play right after the phase separation takes place [21]. On the other hand, thinner capillary with  $D=10 \mu\text{m}$ , an intriguing transition to the columnar structure has occurred even if it has the larger value of  $D/\Lambda_m$  ( $=9.4$ ), which is shown part (d). In a thinner capillary, there is not enough space for the development of bicontinuous structure, only columnar structure was left inside, which is similar to the 2D case shown in Figure 1(c) in Section 2.2.

In Figure 2, results of the system with increased phase-separation tendency with  $f=2.3$  are shown, where periodic length of the 3D bulk (part (a)) is  $\Lambda_m=25.9 \mu\text{m}$ , gels with



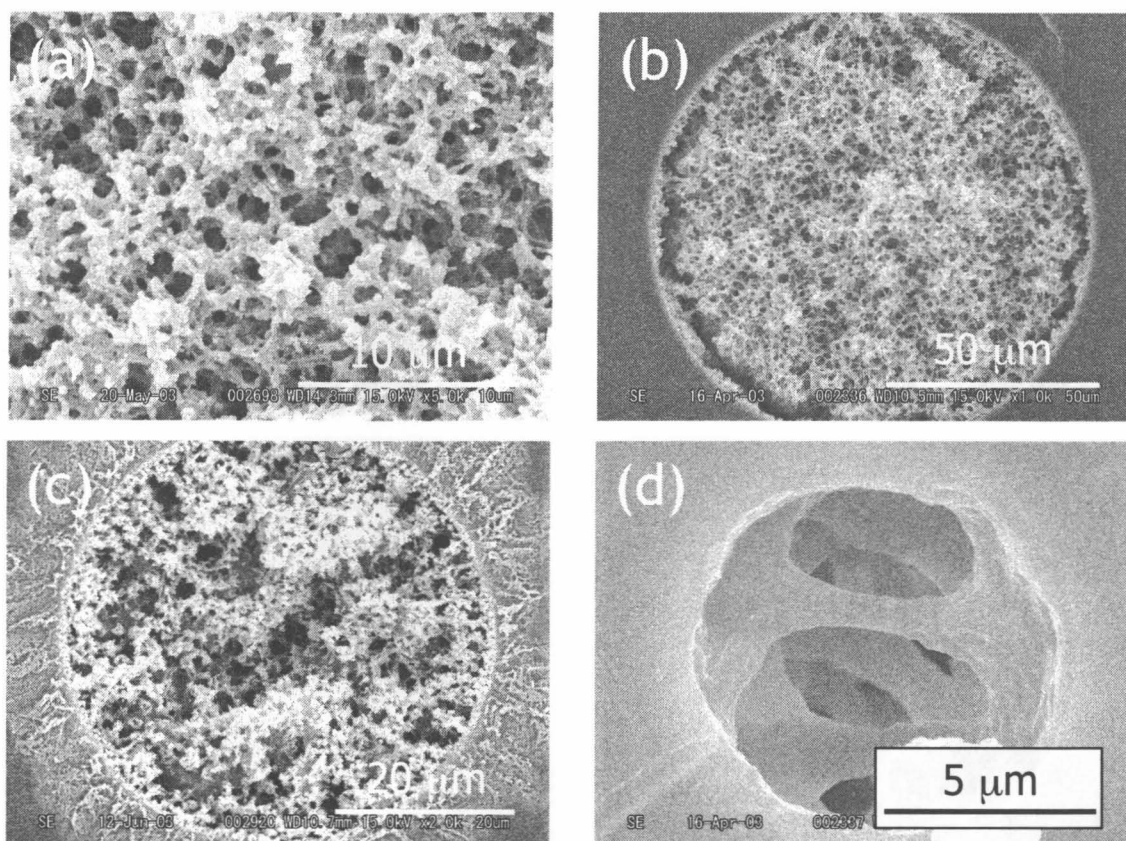


Figure 1 Scanning electron microscope images of 1D confined gels derived from the MF system ( $f=2.2$ ). (a) 3D bulk gel ( $\Lambda_m=1.06 \mu\text{m}$ ) and (b)-(d) the corresponding confined gel in 1D hydrophilic molds with internal diameters of 100, 50 and  $10 \mu\text{m}$ , respectively. The values of  $D/\Lambda_m$  are (b) 94, (c) 47 and (d) 9.4.

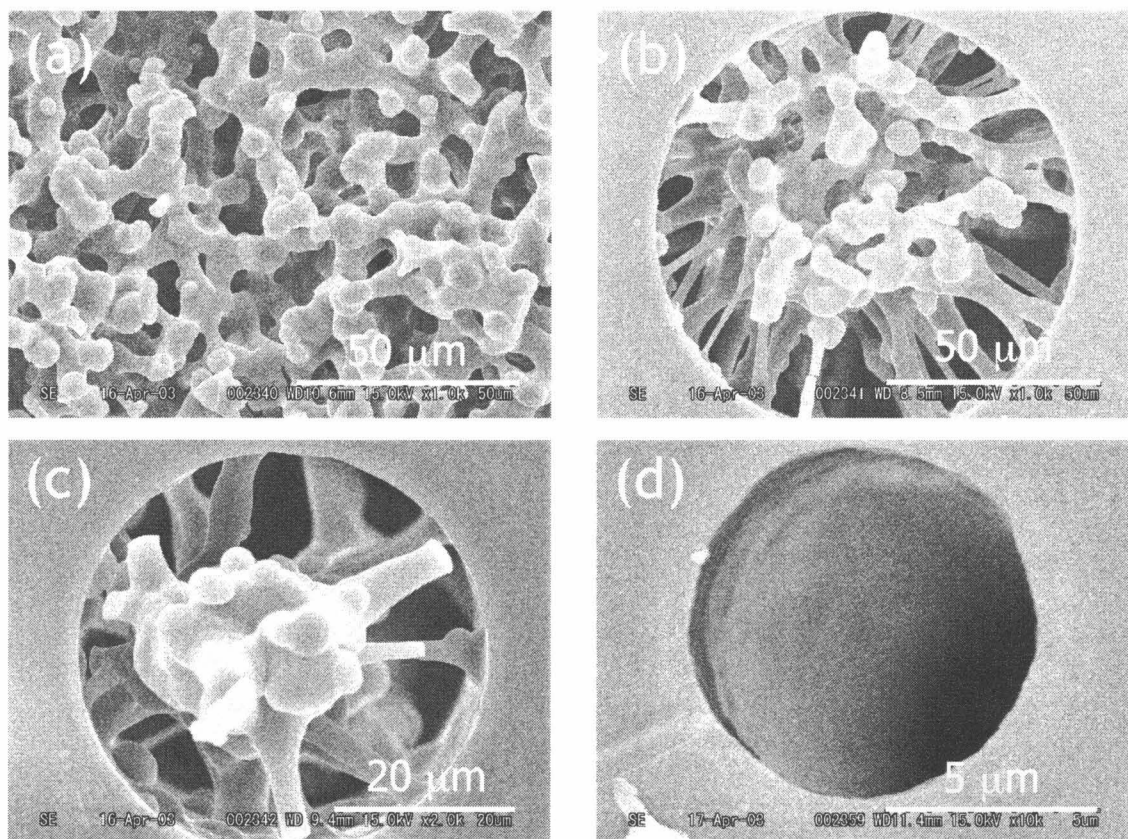


Figure 2 Scanning electron microscope images of gels confined in hydrophilic capillaries with more increased value of  $f$  ( $=2.3$ ). The placement of the figures is the same with in Figure 2. The values of  $D/\Lambda_m$  are (b) 3.9, (c) 1.9 and (d) 0.4.

columnar skeleton near the surfaces and core structure was obtained in the hydrophilic capillaries with  $D=100$  and  $50\ \mu\text{m}$  ( $D/\Lambda_m=3.9$  and  $1.9$ , respectively) in part (b) and (c), respectively. These behaviors are thought to be similar to the 2D case, however, formation of the columnar gel skeleton seems to start at the larger  $D/\Lambda_m$  value probably due to the larger surface area per unit volume in 1D geometry. In the capillary with  $D=10\ \mu\text{m}$ , no phase-separated domains were left inside the space, showing the wetting transition has occurred. The value  $D/\Lambda_m=0.4$  is less than unity which is also similar to the case of 2D mold.

### 3.2 Gels derived from the MM system in a capillary

In the previous chapter 2D confined gels derived from the MF system tend to be more deformed compared to those from the MM system. In a 1D capillary, it is also revealed that the MF-derived gels deform significantly when  $D/\Lambda_m$  becomes closer to unity, and wetting transition is found to occur when  $D/\Lambda_m$  becomes less than unity. Here the structures of MM-derived gels are discussed.

Figure 3 represents the MM-derived gels with  $m=0.9$  and  $\Lambda_m$  of the bulk (a) is  $6.27\ \mu\text{m}$ . Parts (b) to (d) exhibit the gels inside hydrophilic capillaries, and very homogeneous structure is confirmed in all capillaries. Especially even in  $10\text{-}\mu\text{m}$ -capillary allows an isotropic structure with no deformation, which is a good contrast to the case of the MF system. The MF-derived gel in  $10\text{-}\mu\text{m}$ -capillary is significantly deformed into columnar structure at  $D/\Lambda_m=9.4$  (see Figure 1 (d)), whereas the MM-derived gel in the same ID of capillary does not exhibit the deformation at  $D/\Lambda_m=1.6$ . Here, again, difference in the phase separation time may affect the extent of the deformation. In a hydrophobic capillary, more unambiguous difference appears. Figure 4 exhibits the gels in octadecylsilylated hydrophobic capillaries. The bulk gel is identical with one in Figure 3 (a). For all samples, a thick skin layer is developed on the interface of the capillary. This is the result of hydrophobic interaction and since there are few chemical bonds between siloxane-rich phase and the octadecylsilylated surface, the gels are stripped off

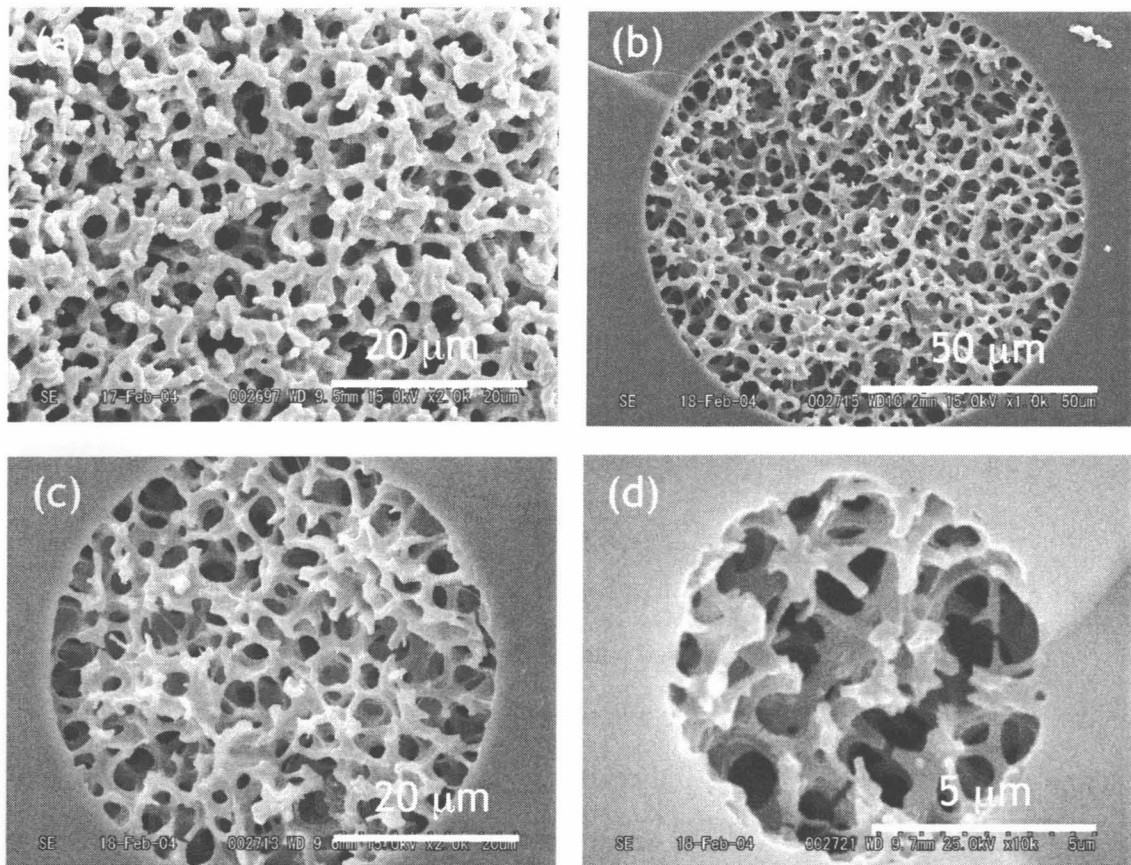


Figure 3 Scanning electron microscope images of 1D confined gels derived from the MM system ( $m=0.9$ ). (a) 3D bulk gel ( $\Lambda_m=6.27 \mu\text{m}$ ) and (b)-(d) the corresponding confined gel in 1D hydrophilic molds with internal diameters of 100, 50 and 10  $\mu\text{m}$ , respectively. The values of  $D/\Lambda_m$  are (b) 16, (c) 8.0 and (d) 1.6.

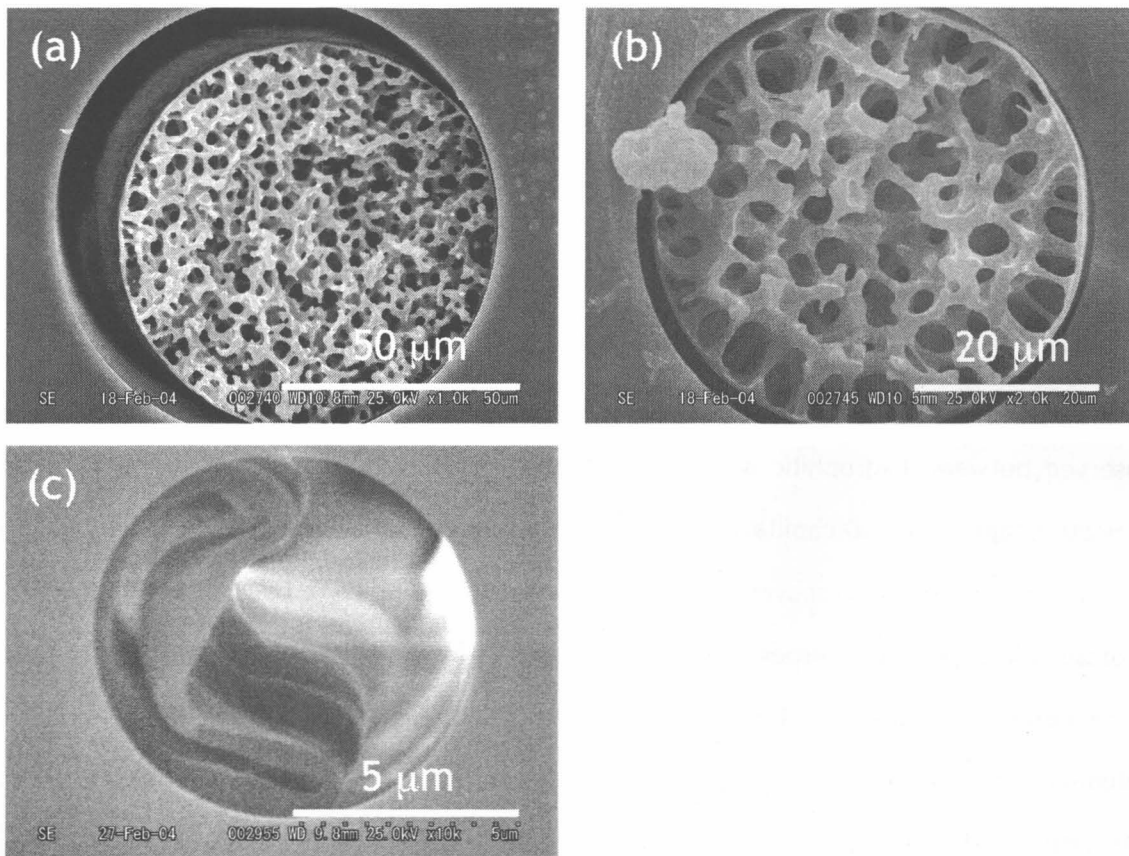


Figure 4 Scanning electron microscope images of confined gels derived from the MM system ( $m=0.9$ ) in hydrophobic capillaries. The 3D bulk gel is Figure 4 (a). Capillary IDs are (a) 100  $\mu\text{m}$ , (b) 50  $\mu\text{m}$  and (c) 10  $\mu\text{m}$ . The values of  $D/\Lambda_m$  are (a) 16, (b) 8.0 and (c) 1.6.

from the surface and shrink during aging and drying. Although bicontinuous structure is almost homogeneous in a capillary with 100  $\mu\text{m}$  ID, columnar structure appears near the surface in a 50  $\mu\text{m}$  ID capillary. Part (c) shows the wetting transition and the gel skin is stripped off as well. Thus structural deformation is much proceeded in a hydrophobic capillary. As the driving force of hydrodynamic wetting emerged from interfacial energy is the same in both hydrophilic and hydrophobic capillaries, these drastic differences must have been induced by hydrophobic interaction. Although an effective difference is not observed between hydrophilic and hydrophobic surfaces in a 2D mold described in the previous chapter, in a 1D capillary the drastic difference is confirmed.

Figures 5 and 6 also show the phase-separated structure at  $m=1.0$  in hydrophilic and hydrophobic capillaries, respectively. Again, gels in hydrophobic capillaries tend to be more deformed which can be obviously understood by comparing two figures. The columnar structure which is similar to the MF system ( $D/\Lambda_m=9.6$ ) is also appeared in the MM system. However, the value of  $D/\Lambda_m$  is 0.91 where the wetting transition occurs in the MF system. Figure 7 and 8 are the more coarsened gels with  $m=1.1$ . The similar tendency is also corroborated in these figures. Part (d) shows the hydrophilic capillary with 10  $\mu\text{m}$ , and the transition to complete wetting is recognized to be under proceeding. Here again, gels in hydrophobic capillaries are more deformed.

Characteristic length in the cross-sectional direction, that is, within the paper plane, tends to become shorter than the corresponding bulk. On the contrary, in a 2D mold, it becomes longer in the x-y plane as described in the previous chapter. From this discrepancy, it can be deduced that the characteristic length in the confined direction becomes shorter and that in the non-confined direction becomes longer than bulk. For instance, from Figure 6 in Section 2.1 clearly shows the characteristic length in z-direction, i.e. the confined direction is shorter than the bulk (14.1  $\mu\text{m}$  for the bulk and ca. 10  $\mu\text{m}$  for the confined sample). An LSCM image of phase-separated structure of MF-derived gel in a rectangular-sectioned capillary is shown in Figure 9, and it can be confirmed that the most



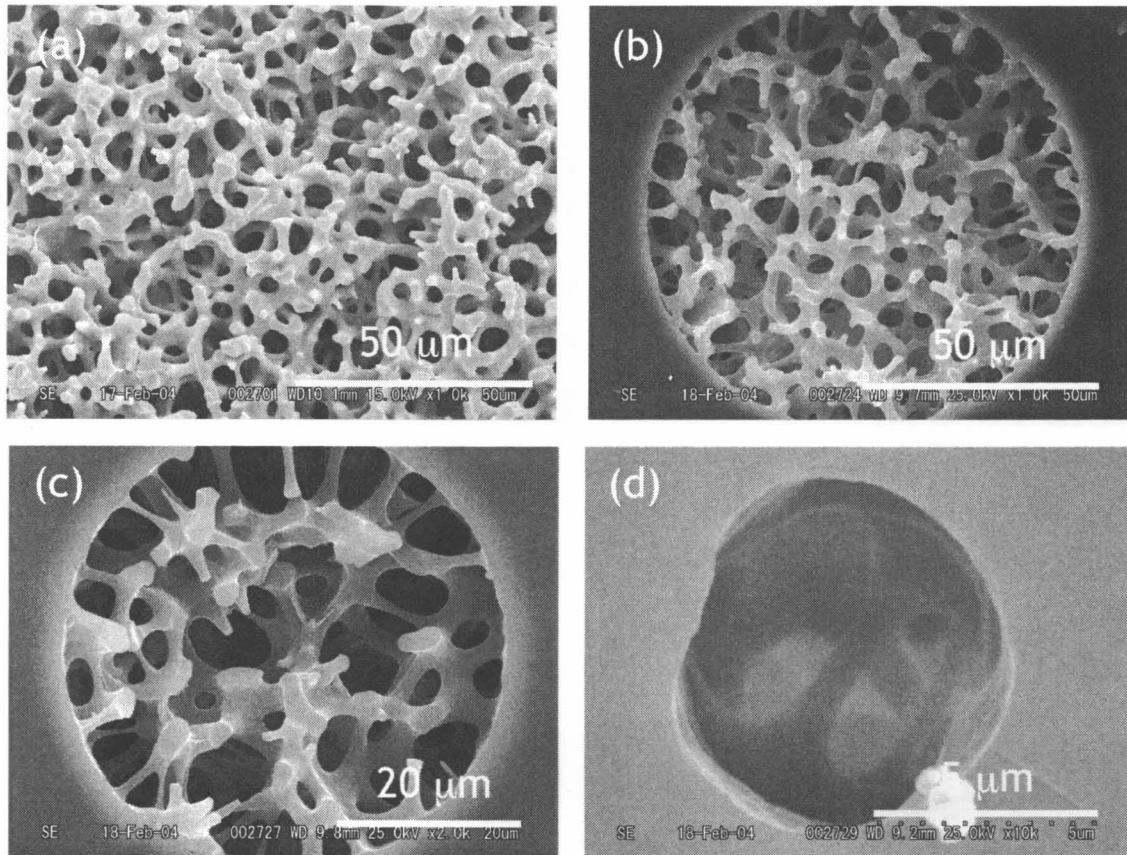


Figure 5 Scanning electron microscope images of 1D confined gels derived from the MM system ( $m=1.0$ ). (a) 3D bulk gel ( $\Lambda_m=11.0 \mu\text{m}$ ) and (b)-(d) the corresponding confined gel in 1D hydrophilic molds with internal diameters of 100, 50 and 10  $\mu\text{m}$ , respectively. The values of  $D/\Lambda_m$  are (b) 9.1, (c) 4.5 and (d) 0.91.

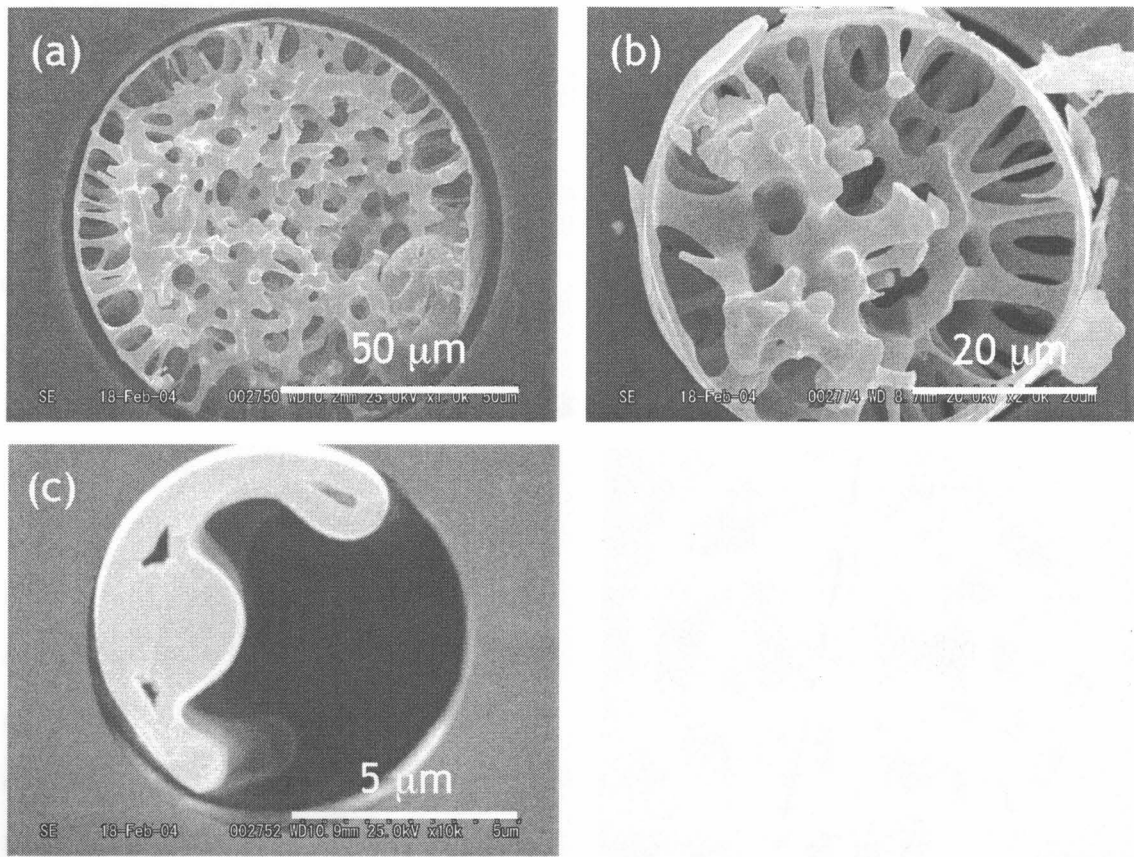


Figure 6 Scanning electron microscope images of confined gels derived from the MM system ( $m=1.0$ ) in hydrophobic capillaries. The 3D bulk gel is Figure 6 (a). Capillary IDs are (a) 100  $\mu\text{m}$ , (b) 50  $\mu\text{m}$  and (c) 10  $\mu\text{m}$ . The values of  $D/\Lambda_m$  are (a) 9.1, (b) 4.5 and (c) 0.91.



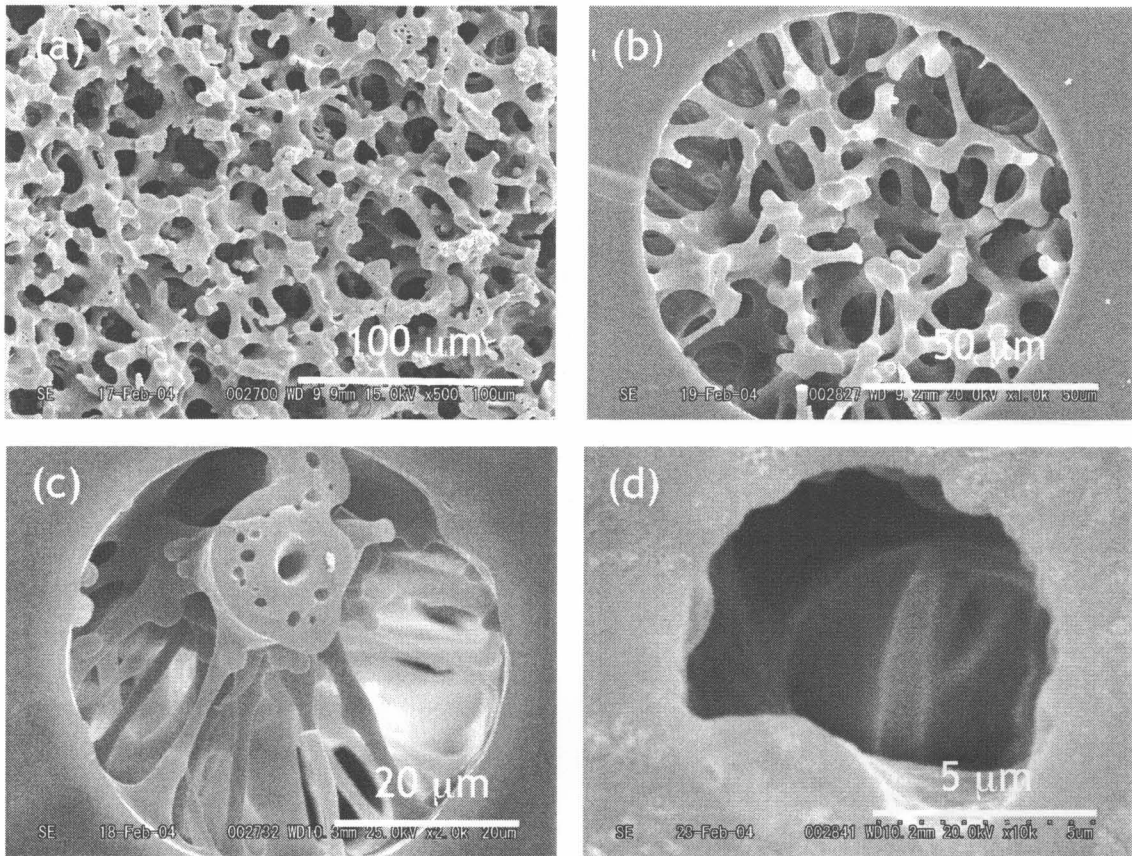


Figure 7 Scanning electron microscope images of 1D confined gels derived from the MM system ( $m=1.1$ ). (a) 3D bulk gel ( $\Lambda_m=29.7 \mu\text{m}$ ) and (b)-(d) the corresponding confined gel in 1D hydrophilic molds with internal diameters of 100, 50 and 10  $\mu\text{m}$ , respectively. The values of  $D/\Lambda_m$  are (b) 3.4, (c) 1.7 and (d) 0.34.

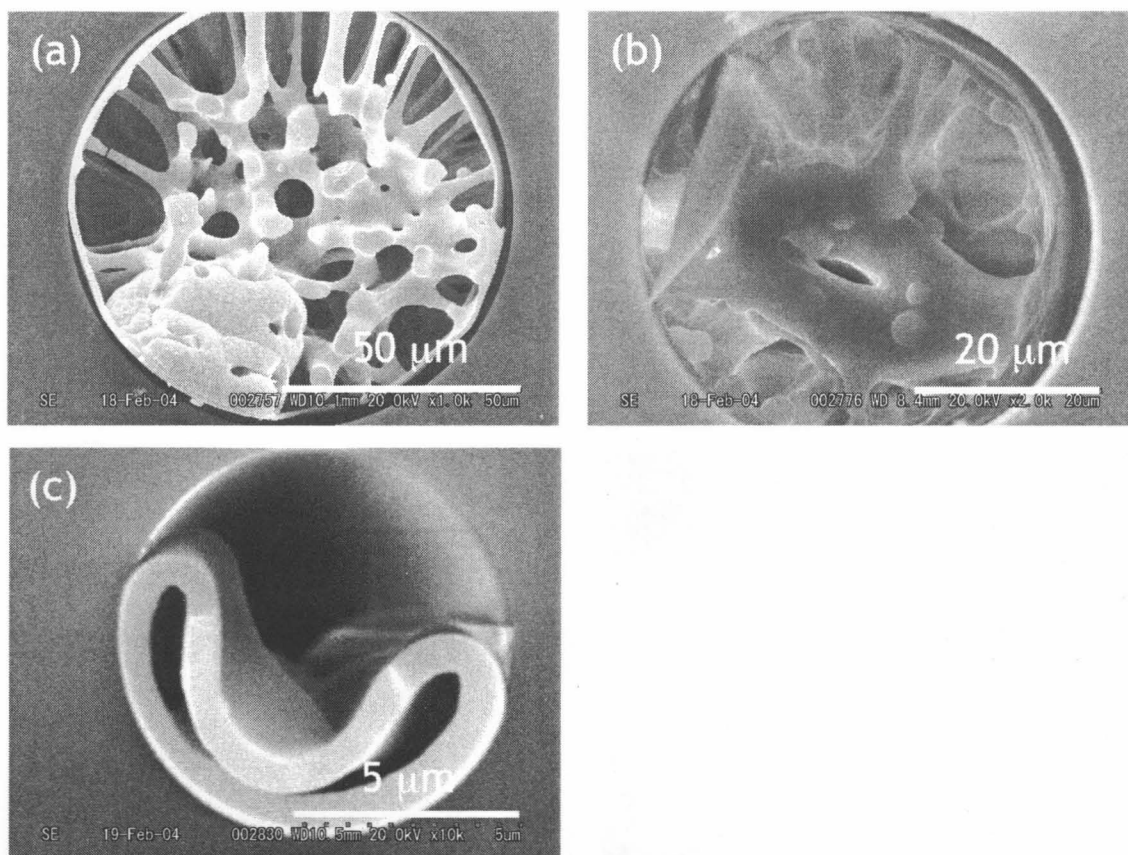


Figure 8 Scanning electron microscope images of confined gels derived from the MM system ( $m=1.1$ ) in hydrophobic capillaries. The 3D bulk gel is Figure 8 (a). Capillary IDs are (a) 100  $\mu\text{m}$ , (b) 50  $\mu\text{m}$  and (c) 10  $\mu\text{m}$ . The values of  $D/\Lambda_m$  are (a) 3.4, (b) 1.7 and (c) 0.34.

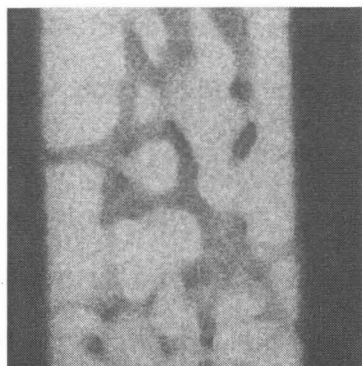


Figure 9 An LSCM image of phase-separated siloxane gel structure derived from the MF system in rectangular-shaped capillary. The bright and dark regions are corresponding to the solvent-rich and siloxane-rich phases, respectively. The dark regions on both right and left sides are capillary walls.

gel networks are directed to the non-confined direction. Thus phase-separating structure coarsens preferentially in the non-confined direction, while that in the confined direction can not coarsen rapidly. Since the coarsening behavior also has a complex relation with wetting and its derivative structure, note that this is not the only case determining the characteristic length. Cumming et al. found a fast-mode domain growth in addition to the normal growth by light scattering in a thick polymer blend film [9,10] and concluded that the fast-mode kinetics are resulted from a surface-mediated wetting. Although their conclusion is derived from 2D light scattering and lack of evidence, both wetting and confined geometry should affect the coarsening dynamics.

#### 4. Conclusion

From SEM observations, the structural deformation in a long cylindrical capillary was discussed. In the MF system the overall features of deformation was found to be similar to the 2D cases that were already discussed in Chapter 2. Gels derived from the MM system showed a drastic difference from the MF system. In a hydrophilic capillary, the extent of deformation is much smaller than the MF system and transition to the columnar structure was observed when  $D/\Lambda_m$  became less than unity. Wetting transition took place when  $D/\Lambda_m$  became much smaller. In a hydrophobic capillary, much deformed gel with thick skin layer was obtained, and wetting transition occurred when  $D/\Lambda_m$  became less than unity. This is the same result as the MF system. The reason of the fast deformation is thought to be hydrophobic interaction. Although we have suffered from experimental difficulty to prepare a sample with intended thickness in a 2D mold, a 1D capillary gave us the more detailed information on structural variation and tendency. Characteristic length in the confined direction is usually found to become shorter whereas that in the non-confined direction tends to become longer. A complex relationship between characteristic length and wetting-induced deformed structure is also responsible for the

coarsening behavior.

## References in Section 3.1

- [1] M. M. Dittmann, G. P. Rozing, *J. Chromatogr. A*, **744**, 63 (1996).
- [2] S. Lüdtke, T. Adam. K. Unger, *J. Chromatogr. A*, **786**, 229 (1997).
- [3] R. Dadoo, R. N. Zare, C. Yan, D. S. Anex, *Anal. Chem.* **70**, 4787 (1998).
- [4] F. Svec, E. C. Peters, D. Sýkora, C. Yu, J. M. J. Fréchet, *J. High Resol. Chromatogr.* **23**, 3 (2000).
- [5] N. Ishizuka, H. Minakuchi, K. Nakanishi, N. Soga, H. Nagayama, K. Hosoya, N. Tanaka, *Anal. Chem.* **72**, 1275 (2000).
- [6] B. Buszewski, M. Szumski, S. Sus, *LC-GC Eur. DEC* **1**, 2 (2002).
- [7] H. Tanaka, *Phys. Rev. Lett.* **70**, 53 (1993).
- [8] H. Tanaka, *Phys. Rev. Lett.* **70**, 2770 (1993).
- [9] P. Wiltzius, A. Cumming, *Phys. Rev. Lett.* **66**, 3000 (1991).
- [10] B. Q. Shi, C. Harrison, A. Cumming, *Phys. Rev. Lett.* **70**, 206 (1993).

## Section 3.2 Interface-Directed Web-to-Pillar Transition in an Open Groove

### 1. Introduction

Silica gels with bicontinuous structure have been applied to analytical devices such as high performance liquid chromatography (HPLC) [1] and solid phase extraction (SPE) [2] etc in recent days. This type of monolithic column is synthesized via sol-gel accompanied by spinodal decomposition [3]. In siloxane sol-gel systems, phase separation can be induced by the growth of siloxane polymer in the presence of water soluble polymers or low molecular weight polar solvents. Another important process is mesopore formation inside the silica skeletons [4] developed by phase separation. The mesopore formation is achieved by aging-treatment with a basic aqueous solution or incorporating surfactants in the starting solution.

Methylsiloxane gel derived from 3-functional methyltrimethoxysilane (MTMS) etc is another promising material for various applications because 3-functional gel prepared with small amount of water in an acidic condition does not tend to shrink and crack during aging and drying, which allows better formability than 4-functional silica gel. Miniaturized monolithic separation devices such as capillary columns or those prepared in flow channels in Lab-on-a-chip devices are drawing a lot of attention because fewer amount of sample is required and very high efficiency of mixing, synthesis, separation and purification is expected. For this purpose, much effort has been made for tailoring micro-structures using inorganic sol-gel [5], molded polymerization [6] and deep reaction ion etching [7].

In this section, we show the general tendency of development of pillar structure in micro-fabricated open grooves and propose a phenomenological model of the growth of it.

## 2. Experimental

An optical microscope image of the grooved glass chip is shown in Figure 1. The widths of the grooves are 1, 3, 5, 7, 10, 15 and 20  $\mu\text{m}$ . In this case the scaled spacing of a mold  $D/\lambda_m$  is also defined. Here,  $D$  represents the width of a groove.

The experimental procedure is the same as in the previous section. The schematic illustration of the preparation in open grooves is exhibited in Figure 1 (b). Note that the groove inside and the starting solution is continuous throughout the process. Characterization of obtained gels was performed by SEM and LSCM.

For the sample subjected to LSCM, in order to obtain the normal phase images, i.e. siloxane-rich phase is recognized as a bright region, co-polymerization with dye-attached monomer is tried using the MF system. The preparation of dye-monomer is given in Chapter 1. Molar ratio of starting solution is MTMS : FA : H<sub>2</sub>O = 1 : 2.9 : 2.5 and 1 mL of dye-monomer solution was dissolved just before MTMS was added. All the other procedures and conditions are the same as those described in the previous chapter.

## 3. Results

### 3.1 *The difference between two systems*

As described above, two different systems are investigated in this study. In the MF system, since the hydrolysis and polycondensation reactions are significantly slow because the pH in the starting solution rises to 4-5 when the condensation reaction proceeds. This is because formamide is hydrolyzed by a strong acid and water. Thus the MF system is thought to be allowed an efficient period of time for the competitive structural formation between spinodal decomposition and wetting and the frozen structure reflects the well-developed one. While in the MM system, as the reaction rate is about 20 times higher than the MF system, the obtained structure does not represent the well-developed



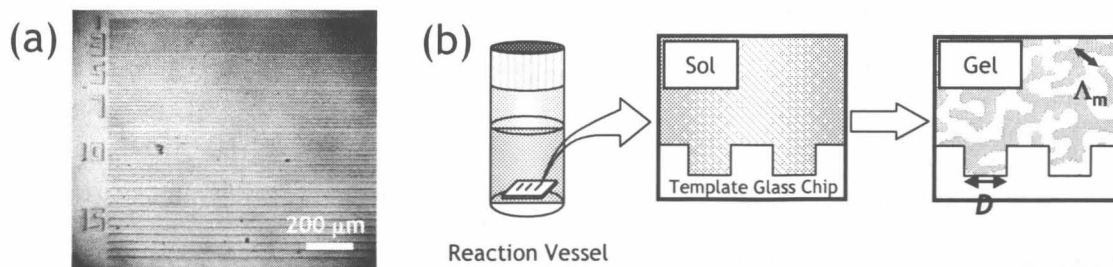


Figure 1 (a) Optical microscope image of the surface of the glass chip on which micro-grooves are fabricated. (b) Schematic cartoon of the procedure. The template glass chip is soaked in a starting sol, and then it turns to gel with forming web-like bicontinuous structure. Inside the grooves and outer bulk solution or gel is continuous throughout the process.

one. Other detailed features in both systems have been already described in Chapter 1.

### 3.2 The MF system

As described above, the MF system is thought to exhibit the well-developed structure during wetting, so we start with the results of the MF system. Figure 2 shows the MTMS-derived bicontinuous structure with  $f=2.3$ ; (a) bulk, (b) in 20-, (c) in 15- and (d) in 10- $\mu\text{m}$  wide grooves. The bulk characteristic length is estimated to be 8.3  $\mu\text{m}$  from LSCM images. Therefore these grooves are wider than bulk characteristic length; i.e.  $D/\Lambda_m > 1$ . Web-like phase-separated structure which is characteristic feature of spinodal decomposition can be confirmed in these figures. Especially, the similar structure as bulk can be seen in the micro-fabricated grooves. On the other hand, in the narrower grooves than bulk characteristic length, that is  $D/\Lambda_m < 1$ , a sharp transition to pillar structure can be seen in Figure 3. This is what we call “web-to-pillar transition”. The pillar structure is somehow disordered in 7- $\mu\text{m}$ -wide grooves as shown in part (a), however, more orderly aligned in 5- and 3- $\mu\text{m}$  grooves which are shown in part (b) and (c), respectively. In 1- $\mu\text{m}$ -wide grooves (part (d)), even though an overall morphology is a little varied, the pillar structure remains.

### 3.3 The MM system

The MM system allows much shorter time until gelation, which makes the wetting tendency smaller than the MF system. As a consequence, the web-to-pillar transition does not occur until  $D/\Lambda_m$  becomes much smaller, i.e. phase separation is more progressed. Figure 4 exhibits the structural transition in (a) 7-, (b) 5-, (c) 3 and (d) 1- $\mu\text{m}$ -wide grooves with  $m=1.0$ . The bulk characteristic length is 7.4  $\mu\text{m}$ . Obvious pillar structure can be seen only in 1- $\mu\text{m}$ -wide grooves ( $D/\Lambda_m=0.14$ ); the others are more or less remaining “branched” network structure. This is a remarkable difference from the MF system.

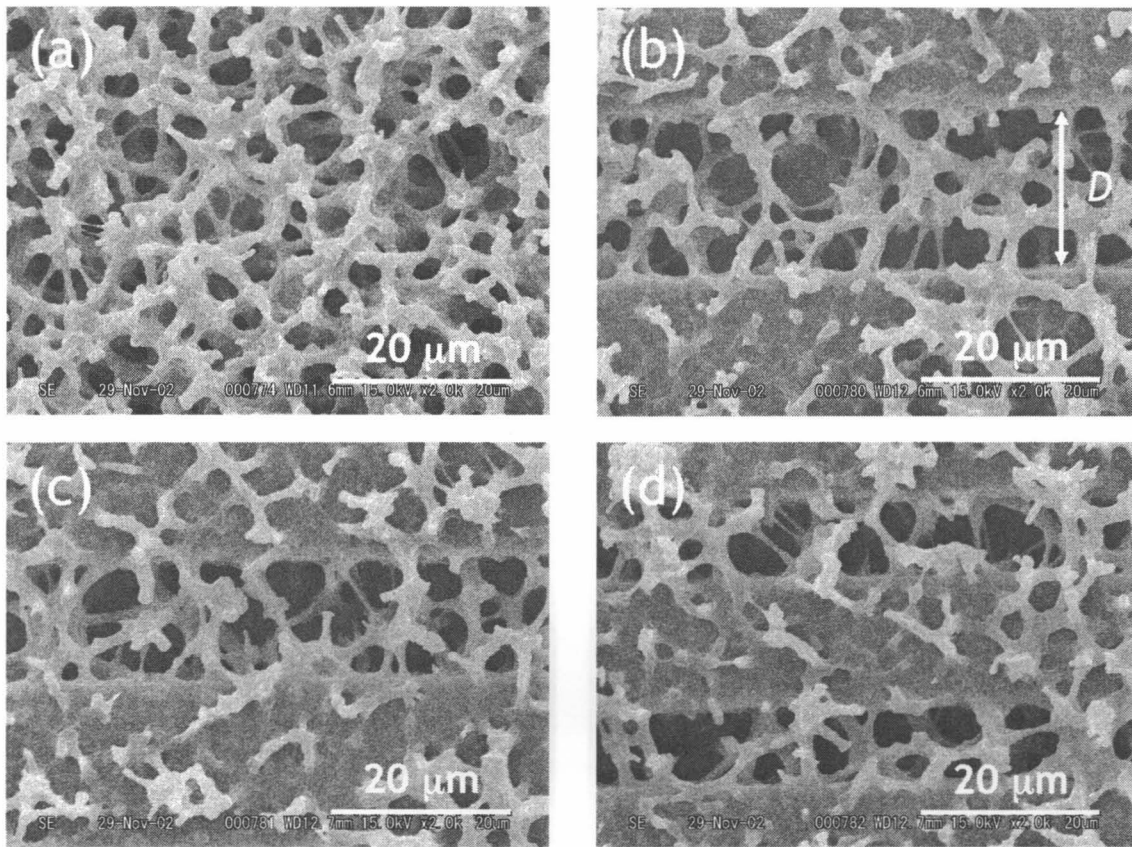


Figure 2 Phase-separated structures of the MF system; (a) bulk, (b) inside a 20- $\mu\text{m}$ -width groove, (c) inside a 15- $\mu\text{m}$ -groove and (d) inside a 10- $\mu\text{m}$ -width groove. The width of the groove is indicated in part (b). These grooves are wider than the characteristic length of bulk 8.3  $\mu\text{m}$ , and spatially homogeneous web-like bicontinuous structure can be confirmed. The values of  $D/\Lambda_m$  are (b) 2.4, (c) 1.8 and (d) 1.2.

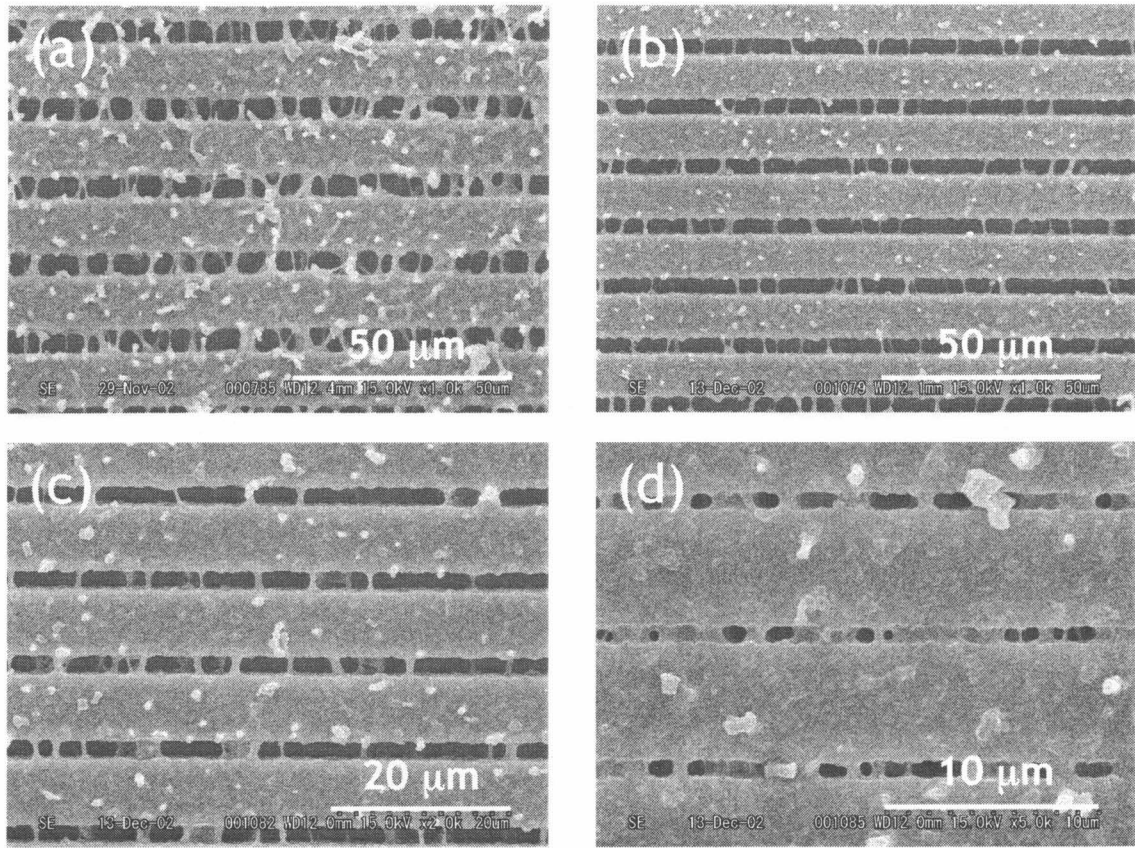


Figure 3 Gel structures derived from the MF system showing “web-to-pillar transition”. The widths of the grooves are (a) 7, (b) 5, (c) 3 and (d) 1  $\mu\text{m}$ , those are narrower than the characteristic length of the bulk. The values of  $D/\Lambda_m$  are (a) 0.84, (b) 0.60, (c) 0.36 and (d) 0.12. The pillar structure is more aligned in the narrower grooves.

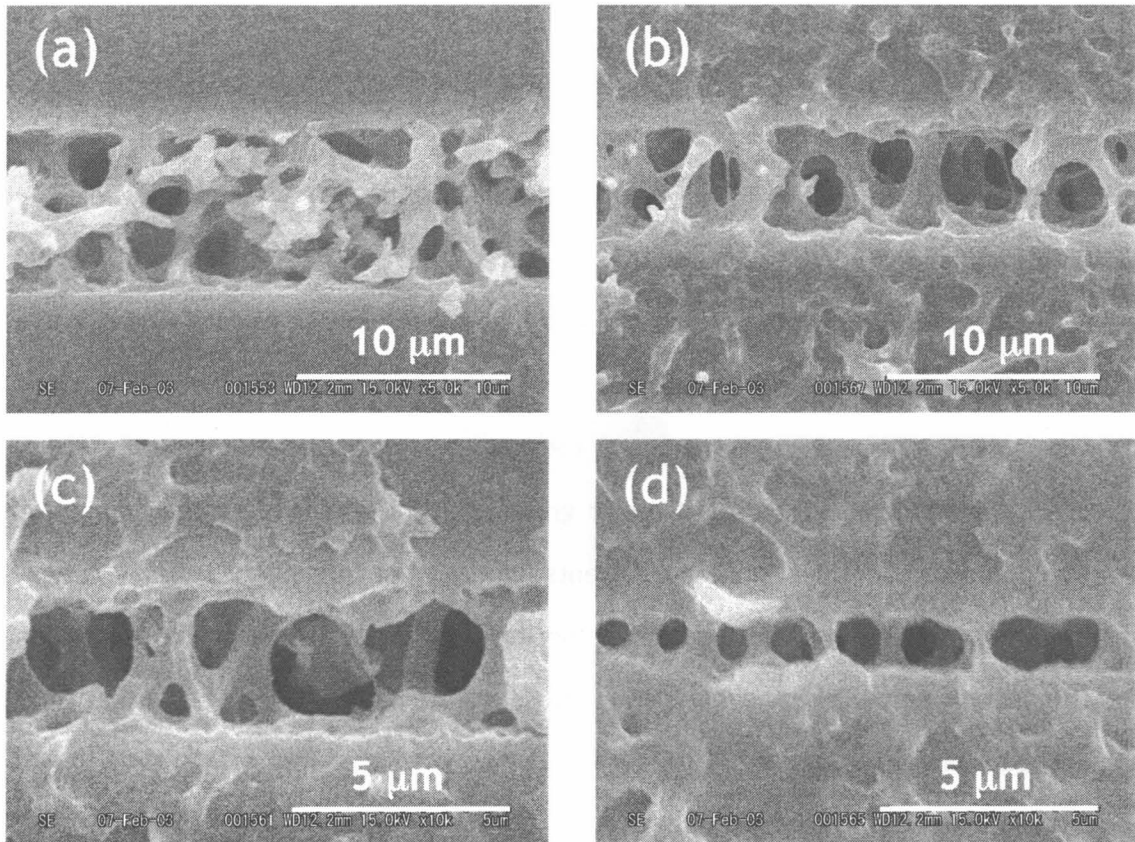


Figure 4 Gel structures derived from the MM system showing “web-to-pillar transition”. The widths of the grooves are (a) 7, (b) 5, (c) 3 and (d) 1  $\mu\text{m}$ . The values of  $D/\Lambda_m$  are (a) 0.95, (b) 0.68, (c) 0.41 and (d) 0.14. Although these are narrower than the characteristic length of the bulk, there are a lot of connections of the gel skeletons in the longitudinal direction; only part (d) shows the intact pillar structure.

## 4. Discussion

### 4.1 *Wetting phenomena in phase-separating fluids*

Wetting behavior of a phase-separating polymer liquid mixture was closely studied by Tanaka [8] and experimentally studied by Jinnai et al. using LSCM [9]. Here, we briefly review the wetting behavior in a closed mold such as a gap between parallel plates. In a closed confined space, one phase which has lower interfacial energy must wet the surface after the onset of phase separation. In the present methylsiloxane sol-gel system, siloxane gel phase gradually loses its polar groups (silanol groups) as polycondensation reaction proceeds. Besides, since the solvents (methanol or formamide and water) have high polarity, MTMS-derived gel phase has the lowest interfacial energy in the system. For this reason methylsiloxane gel phase moves to the surface preferentially. After homogeneous phase separation, MTMS-derived components near the surface start to wet and spread on the surface, resulting in the formation of material transfer channels perpendicular to the surface. Thus siloxane phase flows to the surface not by diffusion but by hydrodynamic flow; the components move cooperatively with forming smaller area of interfaces. Once the channels form, wetting will be accelerated by pressure difference between inside the wetting layer and the channels. The schematic illustration is depicted in Figure 5 (a). According to the Laplace law, pressures of the components separated by an interface are dependent on their mean curvatures (arithmetic average of two principal curvatures) of the interface: When two components are divided by a curved interface, pressure inside the interface is always higher than outside. In this case, pressure inside the channels are supposed to be higher than inside the wetting layer because the channels have larger mean curvature than the planar wetting layer ( $\sim 0$ ). This pressure-assisted acceleration of material flow to the surface is called “hydrodynamic pumping” [8]. This effect continues until both surfaces of a gap are connected by pillars developed from the channels (Figure 5 (b)). The pillar structure will either decay or grow depending on the radius of the pillars and separation of the gap. In Figure 6, a schematic

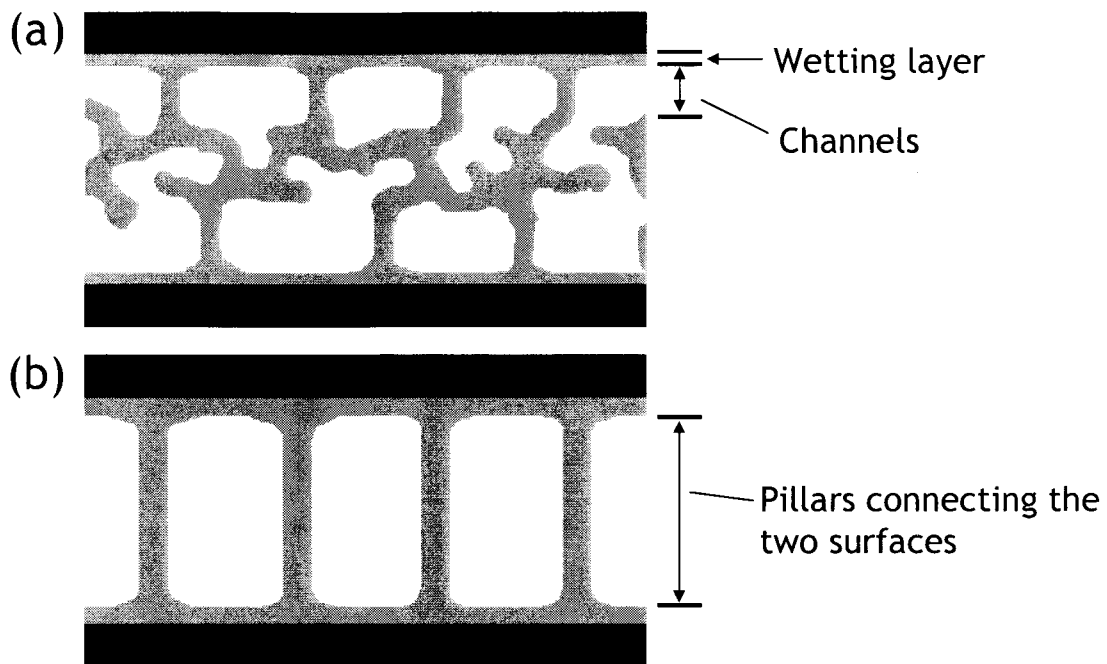


Figure 5 Schematic illustrations of “hydrodynamic pumping” process. As shown in part (a), the flow channels form if one phase (gray phase in this case) is preferentially wetted on the surfaces shown in black. Since this channel part has a larger mean curvature than the bicontinuous part located in the center of the mold, pressure in the channels will become large compared to the wetting layer. Thus the flow to the surfaces is accelerated by hydrodynamic pumping as a result (see also Figure 6). The accelerated wetting leads to the pillar structure connecting the two surfaces as shown in part (b).

illustration which exhibits the pillars with different diameters is shown. The thinner pillar “A” has smaller diameter  $a_A$  compared to the thicker pillar “B”,  $a_B$ . In this situation, the mean curvature is defined as follows;

$$H = \frac{1}{2} \left( \frac{2}{a_i} - \frac{2}{D'} \right) = \left( \frac{1}{a_i} - \frac{1}{D'} \right), \quad (3-1)$$

where  $a_i$  means the radius of pillar “i” ( $i=A$  or  $B$ ). Note that  $D'$  is the diameter of one of the osculating circles and supposing that the two principal curvatures have opposite signs. In the present example, the sign of a curvature is defined as positive if the center of an osculating circle exists inside the pillar. The pressure difference can be written as

$$\Delta p = 2\gamma H = 2\gamma \left( \frac{1}{a_i} - \frac{1}{D'} \right), \quad (3-2)$$

where  $\gamma$  shows interfacial energy between two phases and  $\Delta p$  is the pressure difference between inside a pillar and wetting layer. Since  $\gamma$  and  $D'$  are constant now,  $\Delta p$  becomes positive when  $a_i < D'$ . In this situation pressure inside the pillar becomes higher, resulting in flow into the wetting layer. Thus the pillar will disappear. Conversely, when  $a_i > D'$ , the pressure inside the pillar becomes smaller than the wetting layer, the pillar will be fattened by the flow from the wetting layer.

Although there are some differences between polymer fluid mixture system and gelling siloxane system, we have observed the similar phenomenon in siloxane-based sol-gel systems. In “closed” confined spaces such as a gap between parallel plates and long cylindrical capillary etc, the “transient” pillar structure has been observed. This type of pillar structure will turn to complete wetting, in which all of the gel phase is spread on the surfaces of the mold (wetting transition). In other words, pillar structure is formed just before the wetting transition occurs in a closed system, and it will disappear when phase separation tendency becomes larger or  $D/\Lambda_m$  becomes smaller. The wetting transition takes place when  $D/\Lambda_m$  becomes less than unity in the MF system, while in the MM system, it does not take place until  $D/\Lambda_m$  becomes much smaller compared to the MF system. This fact reflects the difference in the reaction rate between two systems as



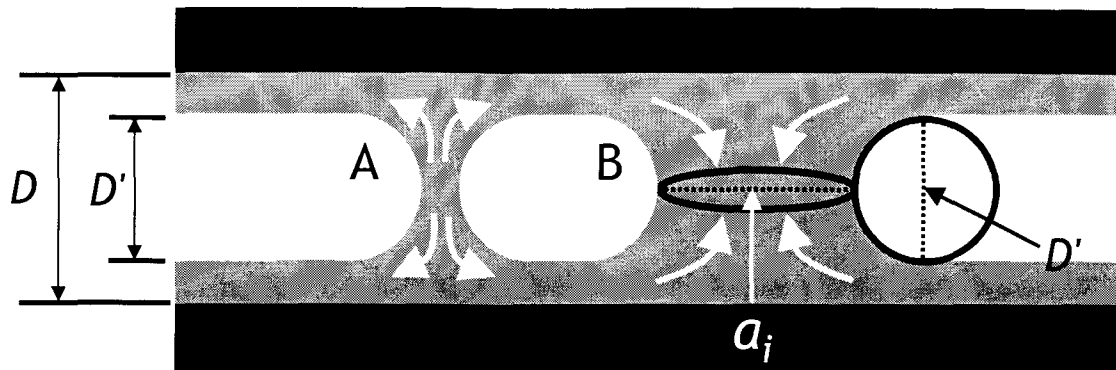


Figure 6 A schematic illustration of the pillar formation/deformation processes. The pillar “A” is thinner than  $D'$ , the thickness of the mold  $D$  minus thicknesses of the wetting layers. In this case, since the mean curvature of pillar “A” becomes larger than that of the wetting layer, pressure inside the pillar becomes larger. Thus flow from the pillar to the wetting layer induced, and the pillar will diminish. In the case of pillar “B”, a completely converse phenomenon happens, and the pillar will be fattened.

already described above.

#### 4.2 A reasonable model which elucidates the formation mechanism

As the siloxane sol-gel system is fluidic between the onset of phase separation and gelation, Tanaka's theory about liquid polymer mixtures becomes a good guide in considering the present case. In Figure 7, a schematic illustration exhibits the case of the closed system. Columnar-shaped gel skeletons are formed perpendicular to the surfaces in the proximity of them due to the wetting flow when  $D/\Lambda_m$  is relatively large. Then all of the gel structure is deformed into complete wetting because gel portion inside the confined space is equally strained by the surface wetting layer. The same is true for different-shaped closed space such as 2D gap between parallel plates and 1D cylindrical capillary etc. While in the open grooves, the stabilization of pillars is related with the characteristic triple-face surfaces and a unique structure that emerges before the web-to-pillar transition. Figure 8 shows the possible formation mechanism of the pillar structure in an open groove. There are two routes to the transition of the structure; one is when the lateral pillar is thicker than the vertical pillar ( $a_l > a_v$ ), and the other is the reverse ( $a_l < a_v$ ). The lateral pillar is connecting two surfaces and the vertical pillar is bonded between the lateral pillar and the basal plane. At first, spatially homogeneous spinodal fluctuation develops inside the groove as shown in the left figure in Figure 8. When the lateral pillar happens to be thicker than the vertical pillar in a certain portion of the sample, the vertical pillar will disappear by the flow indicated as arrows (the upper route). This flow supplies MTMS-derived gel components to the lateral pillar and makes it a stable structure. On the contrary, when the lateral pillar is thinner than the vertical pillar (the lower route), the lateral pillar will disappear owing to the flow in the indicated direction. The remained blob on the basal plane will also disappear in order to reduce the interfacial energy. Thus some portions will remain as the pillars but the other portion will transform into the complete wetting making whole part into the pillar structure as shown in Figures 3 and 4.

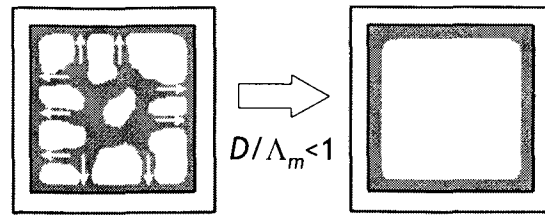


Figure 7 A schematic illustration of phase separation progress in a closed space. After the onset of phase separation, more wettable gray phase flows onto the surrounding surfaces, and then turns to complete wetting in which all of the gray phase segregates onto the surface, leaves no structure inside the space.

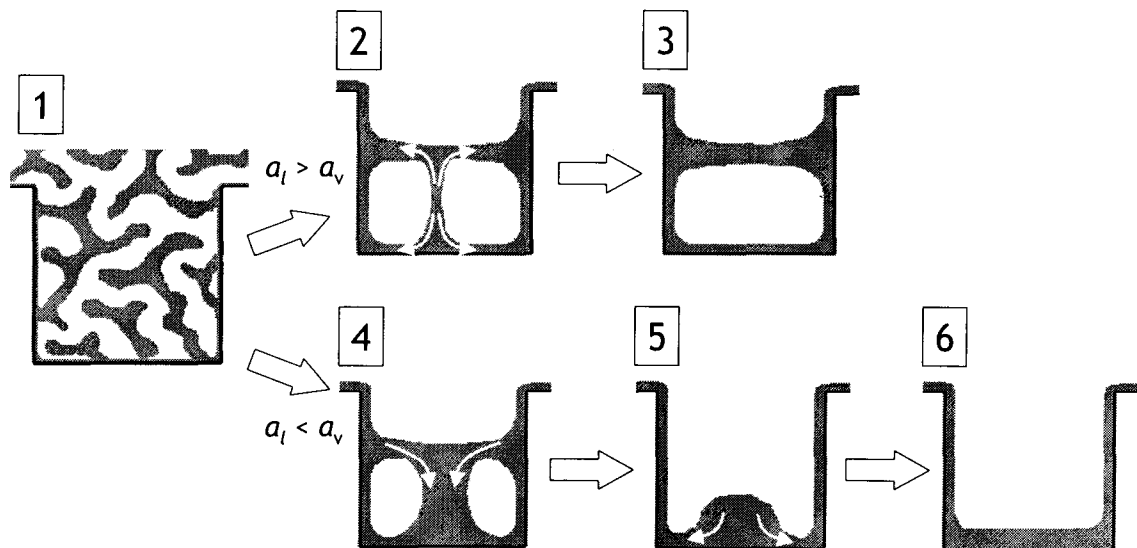


Figure 8 A schematic illustration of phase separation progress in an open groove. After the homogeneous phase separation, trifurcate structure, which is a characteristic structure in the present case, appears inside the groove (2 and 4). If the vertical pillar is thinner than the lateral one (2), the lateral pillar tends to remain (3), and if the vertical pillar is thicker than the lateral one (4), the lateral pillar disappears (5) and flattened by the requirement of interfacial energy (6).

Although the proposed mechanism has not been checked yet because real-time observation is technically difficult, 3D observations of resultant gel structure using LSCM has been additionally performed and the transient structures such as part (2), (4) and (5) in Figure 8 have found practically (shown in Figure 9). We are expecting this kind of analysis will clarify the formation mechanism and lead to a thorough control of the structural characters such as pillar diameter and density etc.

#### 4.3 Difference between MF and MM systems

The reaction rate is significantly different between MF and MM systems as described above. Since sol-gel reaction is quite sluggish in the MF system, the system remains fluidic for longer time during phase separation. This fact surely affects the wetting behavior in both systems. From Figures 2 and 3 the web-to-pillar transition in the MF system is recognized at  $D/\Lambda_m=1$ , while it occurs when  $D/\Lambda_m$  becomes smaller in the MM system. This means that in the MF system the obtained structure reflects the most stable form in the course of phase separation and wetting, however, the transient structure is frozen in an unstable form in the MM system because of the rapid gelation. For this reason the occurrence of the web-to-pillar transition shifts to the smaller value of  $D/\Lambda_m$ .

This difference in reaction rate also affects the obtained structure in a closed mold. As described in Chapter 2 and Section 3.1, the MM system is less affected by the surfaces and less deformed, homogeneous structure can be obtained in the very narrow space. Thus the MM system has the edge in the application to micro-devices such as capillary chromatography or lab-on-a-chip.

## 5. Conclusion

The pillar structure can be tailored in micro-fabricated open grooves on a silica glass chip by methylsiloxane sol-gel accompanying phase separation. In a closed mold, wetting

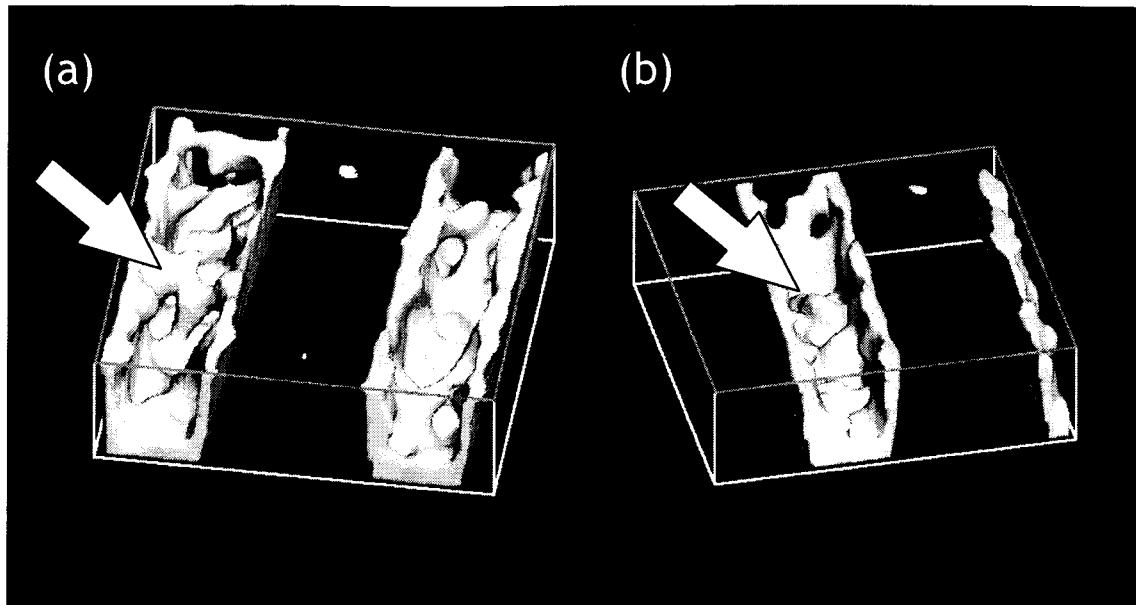


Figure 9 The reconstructed LSCM images of gels derived from dye-incorporated MF system in open grooves. The width of the groove is  $15\ \mu\text{m}$ . Bulk characteristic length is  $14.7\ \mu\text{m}$ . The portions indicated by arrows show (a) the trifurcate structure which corresponds to part (2) and (4) in Figure 8, and (b) the remaining blob which corresponds to part (5) in Figure 8. The trifurcate structure can also be found in the right groove in part (a).

transition occurs when bulk characteristic length exceeds the size of the mold; however, pillar structure remains in an open groove. This discrepancy is derived from the characteristic shape of the mold. As the confined space is surrounded by three faces, the transient structure during web-to-pillar transition is trifurcate and directed to each surface. This unique transient structure yields a pressure difference among lateral and vertical pillars and the wetting layer, leading to the pillar structure.

Although both MF and MM systems show web-to-pillar transition, values of  $D/\Lambda_m$  when the transition occurs are different; this reflects the reaction rate difference, in particular, phase separation time.

The author is expecting many unknown interesting phenomena will be found in the field of phase separation in confined geometry, and they will be effective and useful in the application to porous flow channels such as micro-HPLC. One example is double phase separation induced by rapid structural coarsening by wetting coupled with relatively slow compositional diffusion [10,11]. In Figure 10 SEM and FE-SEM photographs are shown, in which secondary phase separation appears in the solvent phase (macropores in dried state). Structuring new kinds of porous morphology is currently underway.

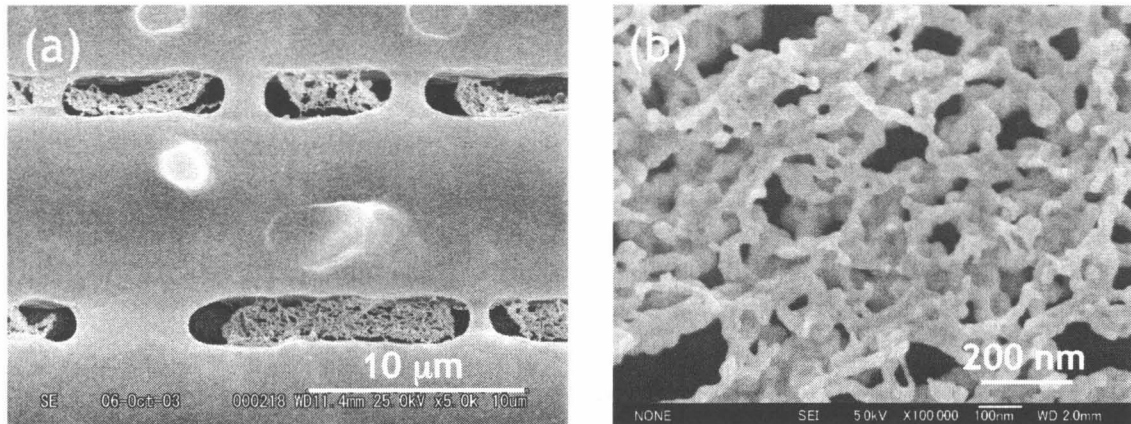


Figure 10 An intriguing double phase separation observed in the MM system: (a) a SEM image and (b) an FE-SEM image with higher magnification. The width of the groove is 3 μm. The origin of this phenomenon is deduced from the fact that compositional diffusion can not keep up with the fast coarsening accelerated by wetting, making nano-scaled bicontinuous structure derived from secondary phase separation in the solvent-rich phase.

## References in Section 3.2

- [1] N. Tanaka, H. Kobayashi, N. Ishizuka, H. Minakuchi, K. Nakanishi, K. Hosoya, T. Ikegami, *J. Chromatogr. A*, **965**, 35 (2002).
- [2] S. Miyazaki, K. Morisato, N. Ishizuka, H. Minakuchi, Y. Shintani, M. Furuno, K. Nakanishi, *J. Chromatogr. A*, **1043**, 19 (2004).
- [3] K. Nakanishi, *J. Porous Mater.* **4**, 67 (1997).
- [4] K. Nakanishi, R. Takahashi, T. Nagakane, K. Kitayama, N. Koheiya, H. Shikata, N. Soga, *J. Sol-Gel Sci. Tech.* **17**, 191 (2000).
- [5] N. Tanaka, H. Nagayama, H. Kobayashi, T. Ikegami, K. Hosoya, N. Ishizuka, H. Minakuchi, K. Nakanishi, K. Cabrera, D. Lubda, *J. High Resol. Chromatogr.* **23**, 111 (2000).
- [6] F. Svec, E. C. Peters, D. Sýkora, C. Yu, J. M. J. Fréchet, *J. High Resol. Chromatogr.* **23**, 3 (2000).
- [7] F. E. Regnier, *J. High Resol. Chromatogr.* **23**, 19 (2000).
- [8] H. Tanaka, *J. Phys.: Condens. Matter*, **13**, 4637 (2001).
- [9] H. Jinnai, H. Kitagishi, K. Hamano, Y. Nishikawa, M. Takahashi, *Phys. Rev. E*, **67**, 021801 (2003).
- [10] H. Tanaka, *Phys. Rev. E*, **51**, 1313 (1995).
- [11] H. Tanaka, T. Araki, *Phys. Rev. Lett.* **81**, 389 (1998).



## CHAPTER 4: STRUCTURES IN A ZERO-DIMENSIONAL MOLD

### 1. Introduction

In recent years, porous siloxane gel with bicontinuous structure has been utilized as a separation medium for high performance liquid chromatography (HPLC) [1]. This type of bicontinuous gel can be prepared by inducing phase separation during sol-gel transition of silicon alkoxides such as tetramethoxysilane (TMOS) and methyltrimethoxysilane (MTMS) etc. In the application of such siloxane gel to miniaturized devices, the porous gels can be prepared in an every small confined space as long as the starting sol can be introduced, however, the surface effects become significant and structural deformation often takes place in such a small system.

In Chapters 2 and 3, the phase-separation behaviors in confined geometries were discussed. In the present system hydrodynamic flow in the late stage of spinodal decomposition is revealed to play a crucial role rather than the chemical character of the surface which affects the wetting behavior in diffusive surface-directed spinodal decomposition. In a long cylindrical capillary or a gap between parallel plates, Tanaka *et al.* has revealed that the hydrodynamic flow in liquid polymer blends took an important role in wetting phenomenon which determined the overall morphology of the blends [2,3]. More recently, Moffitt *et al.* demonstrated that the surface-directed spinodal decomposition-like phenomenon has occurred even in a thick film about a hundred micrometers [4]. They showed layered structure of polymer blend film and found hydrodynamic channels for the first time by LSCM which are evidence of wetting by hydrodynamic composition flow.

For inside the random bicontinuous structure and severely low dimensionality, another problem arises. Critical behaviors of a liquid mixture in a porous Vycor glass or a

macroporous glass are intensively studied by lots of physicists [5-11]. They revealed the phase separation kinetics become much slower (usually macroscopic phase separation does not occur) in such a porous medium as termed “critical slowing-down”, and discussed whether randomness of the space, which leads thermodynamic instability and slow diffusion, or wetting truly induce such an effect. However, since the experimental results are limited to the scattering methods or NMR, and no direct observation has been done, the slow dynamics still remains unexplained. Moreover, their confining molds are Vycor glass with pore sizes typically only 7-100 nm, that are comparable to bulk correlation length and it is too small to observe a hydrodynamic effect.

In this chapter, in order to further clarify the relationship between the structural development and the dimension of the mold, we prepared phase-separated siloxane gels in short cylindrical pores (approximately 2.74  $\mu\text{m}$  in diameter) in a porous medium, and then the obtained structures were closely observed under SEM. Some phenomenological discussion was also conducted.

## 2. Experimental

### 2.1 Preparation of the mold

Bicontinuous porous silica gel is used as a porous media in this study. The preparation procedure is as follows. First, 0.65 g of poly(ethylene glycol) (Aldrich,  $M_w=10,000$ ) and 0.90 g of urea (Hayashi Pure Chemical Ind.) were dissolved in 10 mL of 0.01 mol/L acetic acid aqueous solution in a glass sample tube. Then 5 mL of tetramethoxysilane, TMOS (Shin-Etsu Chemical Co., Japan), was added under vigorous stirring and ice-cooled condition. After being stirred for 30 min, the resultant homogeneous solution was transferred to an autoclave and allowed to gel at 40°C in a closed condition. The resultant gel was aged at the same temperature for 24 h followed by a hydrothermal aging at 100°C for 24 h. The aged gel was dried at 40°C for about 24 h,

and then sintered at 1000°C for 2 h. Characterization of the pore structure of the mold gel was performed by mercury porosimetry (PORESIZER-9320, Micrometrics, USA) and the result is shown in Figure 1 with an SEM photograph. The average pore size of the mold can be determined as approximately 2.74  $\mu\text{m}$ .

An as-sintered silica gel was used as a hydrophilic porous medium and octadecylsilylated silica gel was used as a hydrophobic one.

### 2.2 Preparation of siloxane gel (guest gel) in the mold

In the MF system, the compositions of samples are MTMS : FA : H<sub>2</sub>O = 1 :  $f_M$  : 2.5 in molar ratio. The value  $f_M$  is varied from 1.3 to 2.6. In the MM system, the molar ratio is MTMS : MeOH : H<sub>2</sub>O = 1 :  $m$  : 2.0, and the value  $m$  is varied 0.2 through 1.2. In the TMOS-FA system (denoted as TF system), the molar ratio is TMOS : FA : H<sub>2</sub>O = 1 :  $f_T$  : 1.5, and the value  $f_T$  was varied from 1.0 to 2.5. In general, the more the amount of FA is increased, the larger phase separation tendency becomes in these systems.

An appropriate amount of FA or MeOH and 1.0 mol/L nitric acid aqueous solution were mixed in a glass sample tube, and then MTMS or TMOS was added under vigorous stirring and ice-cooled condition. After stirred for 5 min, approximately 0.50 g of the confining mold gel was put in the identical glass sample tube followed by an evacuation with aspirator to introduce the sol into the mold. The sample tube was sealed and allowed to gel at 40°C. After gelation, the samples were aged more than 24 h at the same temperature, and then dried for about 24 h at the same temperature. The obtained gels are observed under SEM (S-2600N, Hitachi, Japan). The pore structure characterization of some of the samples was performed by mercury porosimetry. Hereafter, we denote the guest gel outside the mold as “bulk gel” or more shortly, “bulk”.

## 3. Results and Discussion

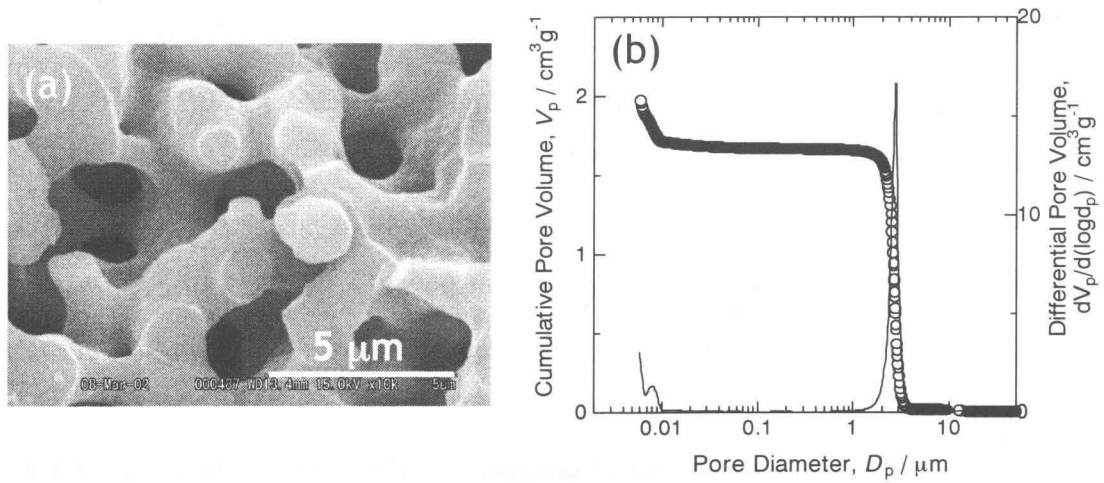


Figure 1 (a) An SEM image of the porous silica medium used as a confining mold in this study. (b) Pore size distribution of the mold characterized by Hg porosimetry. The average pore size is 2.74 μm.

### 3.1 The MF system

Figure 2 shows the phase-separated structure of methylsiloxane gel in hydrophilic 0D molds. In part (a) to (c), 3D bulk gels with different values of  $f_M$  are exhibited, and in part (d) to (f), the corresponding confined gels with identical compositions are shown. A gel with almost homogeneous network has developed in a relatively large value of  $D/\Lambda_m$  ( $\approx 3.2$ ), and transformed to a columnar structure connecting mainly two points on the surface of the mold as is shown in part (e), and then wetting transition occurred (see part (f)). The evidence of the wetting transition is corroborated by mercury porosimetry; both the pore volume and the mean pore size decreased compared to the original mold (Figure 3). These behaviors might be considered to be similar to that in the molds with other dimensions, however, what is intriguing is that the size of the phase-separated structure is quite different from the case of other dimensionalities. Namely, phase-separated structure keeps its “shape”, only varying its own scale in a self-similar manner in a severely confined space.

In Figure 4 the gel structures in hydrophobic 0D molds are indicated. Similarly to those in Figure 2, confined gel structure transforms from homogeneous one to columnar one, and to complete wetting with increasing value of  $f_M$ . The prominent difference between hydrophilic and hydrophobic occasions is the siloxane wetting layer on the surface of the mold. In a hydrophilic mold, tightly bonded wetting layer forms on the surface of the mold as clearly seen in Figure 2 (f). The wetting layer and skeletons of silica mold can be regarded as a united body. On the contrary, wetting layer on a hydrophobic surface exhibits a distinct interface and looks like “skin” layer, suggesting there is no covalent bond between methylsiloxane gel and octadecylsilylated silica gel.

### 3.2 The MM system

Although the structural transition behavior in the MF system in a 0D mold is similar to that of 2D and 1D cases, the MM-derived gel exhibits an extraordinary behavior in a 0D mold. In Figure 5, phase-separated gels in both hydrophilic and hydrophobic 0D molds are

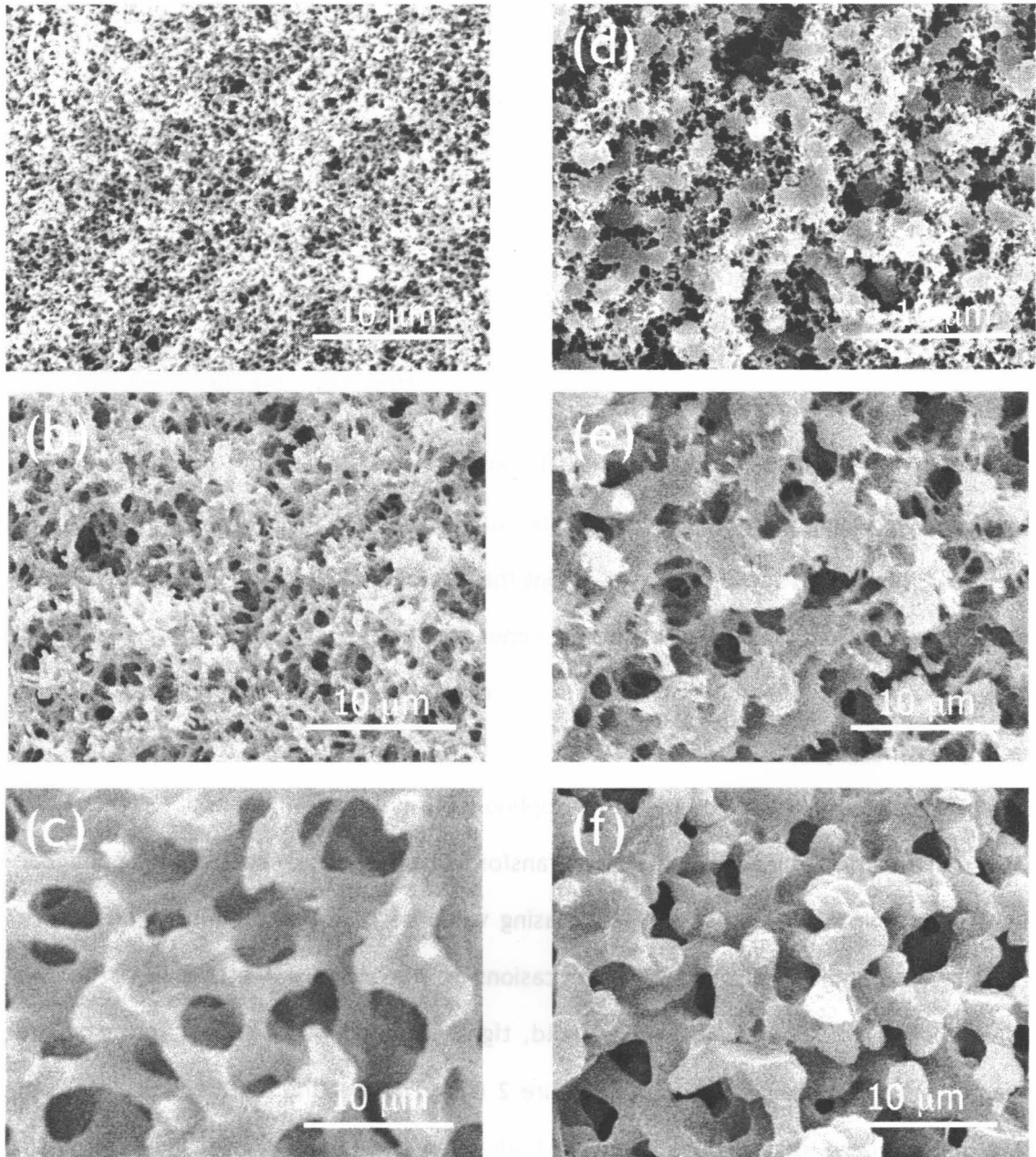


Figure 2 Scanning electron microscope images of 0D confined gels derived from the MF system. (a)-(c) 3D bulk gel in different compositions; (a)  $f_M=2.0$ , (b)  $f_M=2.1$  and (c)  $f_M=2.2$ . (d)-(f) Corresponding confined gel in 0D molds. Almost homogeneous structure formed at the relatively large value of  $D/\Lambda_m$  ( $=3.2$  in part (d)), then transformed to columnar structure when  $D/\Lambda_m=1.2$  shown in part (e), and wetting transition occurred when  $D/\Lambda_m$  became less than unity (part (f)).

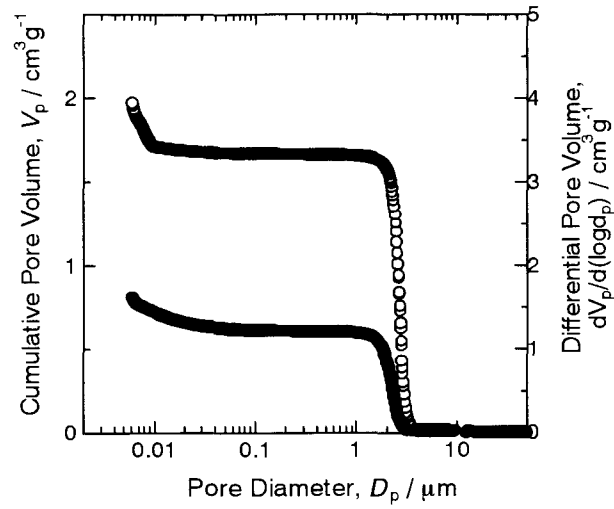


Figure 3 Comparison between the bare silica mold (open circles) and after guest gel ( $f_M=2.2$ ) is included (filled circles). Both pore size and pore volume are reduced after guest gel inclusion, showing the evidence for wetting transition.

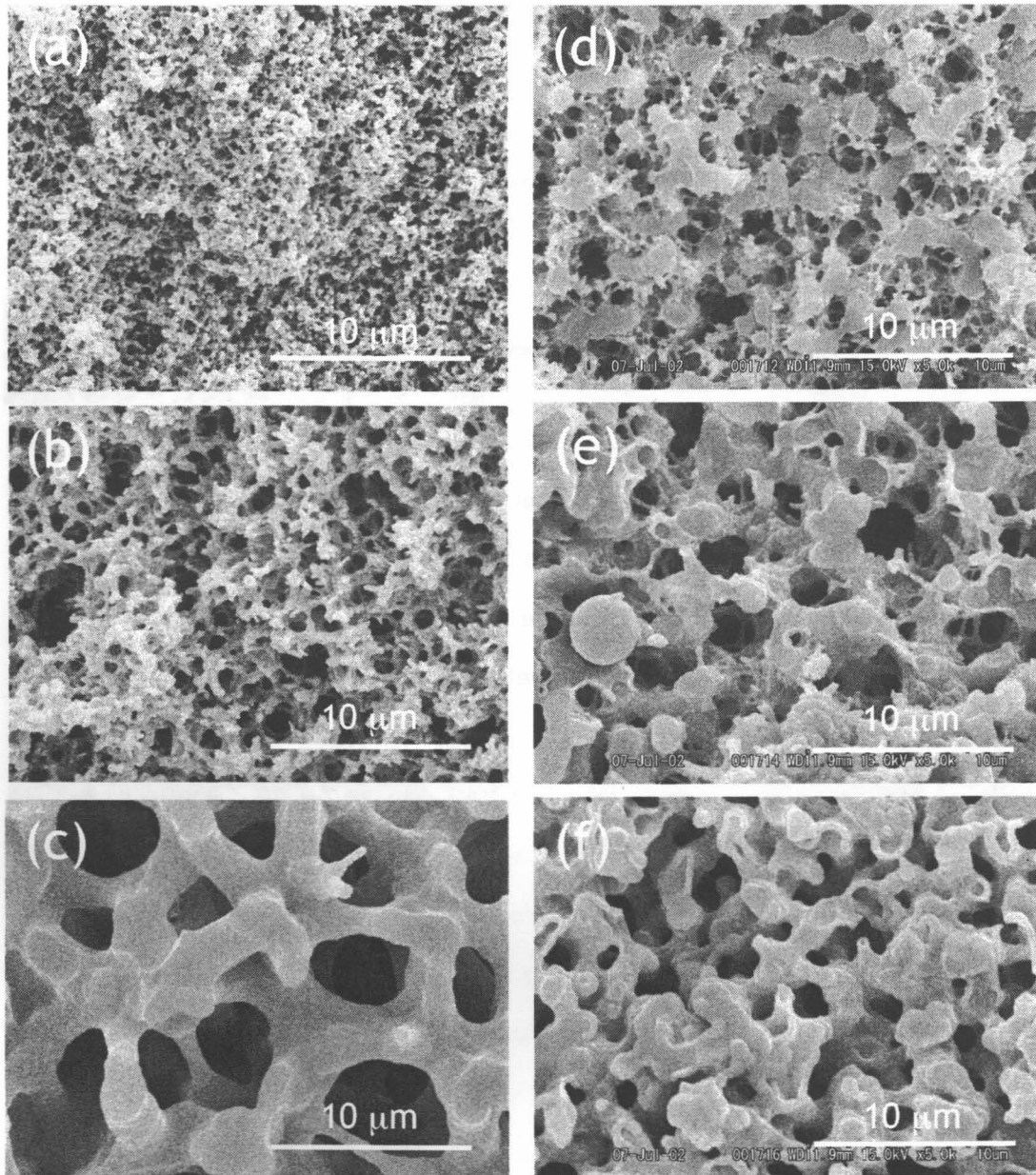


Figure 4 Scanning electron microscope images of OD confined gels derived from the MF system. (a)-(c) 3D bulk gel in different compositions; (a)  $f_M=2.1$ , (b)  $f_M=2.2$  and (c)  $f_M=2.3$ . (d)-(f) Corresponding confined gel in hydrophobic 0D molds. In this case, the same tendency as in Figure 2 is confirmed except for the thick skin layer. Note that the value of  $f_M$  is different because of poor reproducibility, but the bulk characteristic lengths are close to those in Figure 2.

shown  
 (part (f))



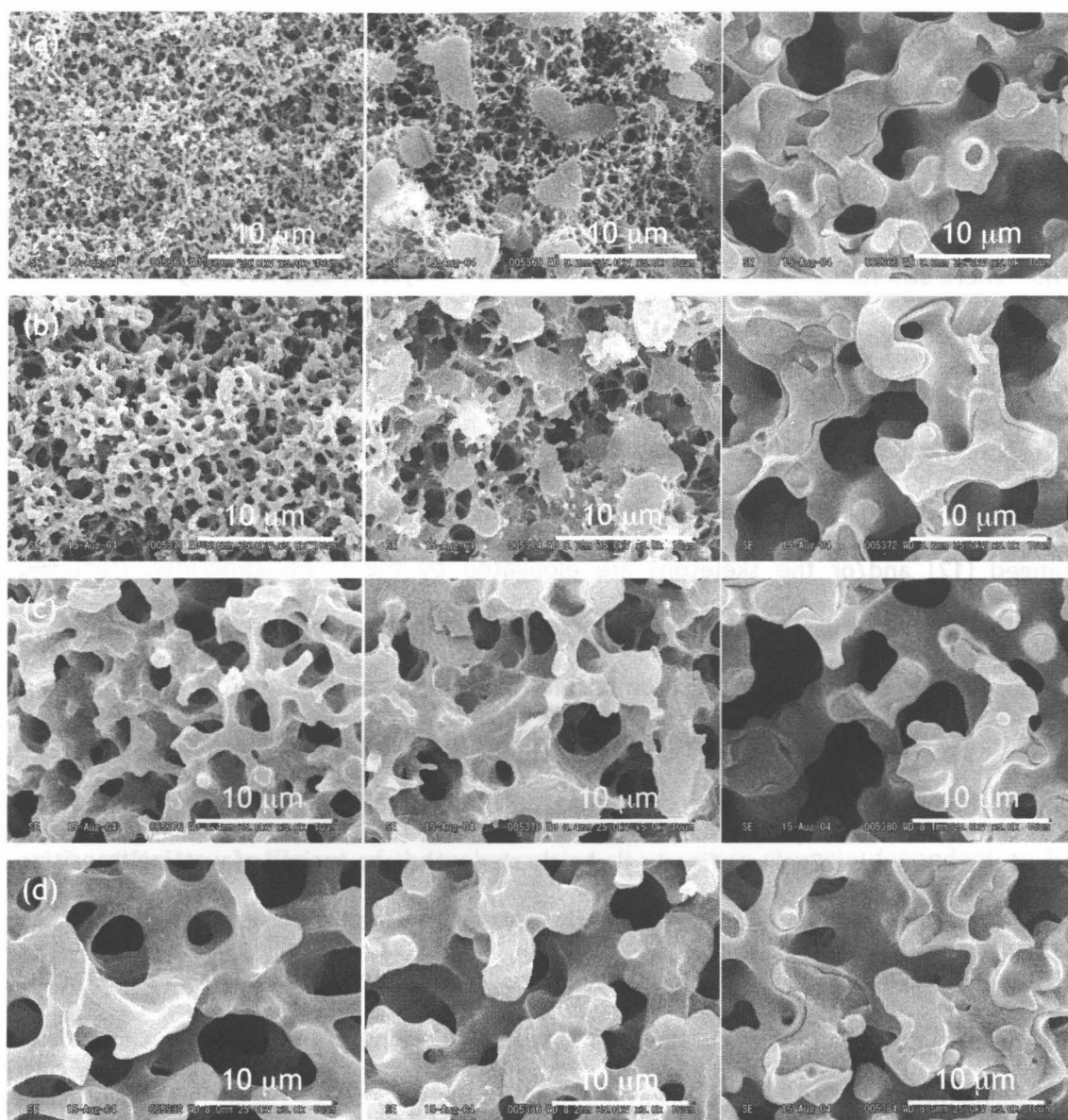


Figure 5 Scanning electron microscope images of gels derived from the MM system confined in hydrophilic and hydrophobic 0D molds. The left images of each row (a)-(d) corresponds to the bulk gel in different compositions; (a)  $m_M=0.9$ , (b)  $m_M=1.0$ , (c)  $m_M=1.1$ , and (d)  $m_M=1.2$ . The center and right images of each row show gels confined in hydrophilic and hydrophobic molds, respectively. The bulk characteristic lengths of part (b) and (c) are  $0.933$  and  $3.43 \mu\text{m}$ , respectively, that is,  $D/\Lambda_m$  becomes less than unity in part (c).

indicated. Confined gels in hydrophilic molds (see center column) exhibits the similar tendency to the case of 1D capillary, and there is no evident difference between the MF and MM systems. The bulk characteristic length  $\Lambda_m$  exceeds the mean pore diameter of macroporous silica (2.74  $\mu\text{m}$ ) in part (c) (for part (b)  $\Lambda_m=0.933 \mu\text{m}$  and part (c)  $\Lambda_m=3.43 \mu\text{m}$ ). There still remains a columnar structure and the system does not fully transform to complete wetting yet, suggesting the early structural freezing in the MM system. In the hydrophilic case the skeleton thicknesses of the confined gels are much thinner than the corresponding bulk. The possibilities are that a little amount of siloxane species is attracted onto the surfaces of a mold making the composition inside the pore slightly changed [12] and/or the skeletons are elongated by the stress generated from the additional condensation, which occurs during aging and drying, under restricted shrinkage. On the other hand, wetting transition occurs in a hydrophobic OD mold even if  $D/\Lambda_m$  is much larger than unity. The right column in Figure 5 shows the confined gels in hydrophobic molds. Bulk characteristic lengths of parts (a) and (b) are shorter than the size of the OD mold. Each confined gel clearly shows the occurrence of wetting transition. There are two confinement effects in this system. One is preferential wetting by diffusion in the early stage of spinodal decomposition, and the other is also preferential wetting by hydrodynamic flow in the later stage. According to the 3D numerical study of hydrodynamic spinodal decomposition (model H in the Hohenberg-Halperin notation [13]) under the influence of a surface [14], though thickening dynamics of wetting layer by early diffusion is slower than that by later hydrodynamic flow ( $t^{1/3}$  for diffusion and  $t$  for hydrodynamic flow), it is anticipated that the wetting completes through diffusion in the early stage of spinodal decomposition because of the strong attractive interaction between polymerizing hydrophobic siloxane and hydrophobic surfaces of the mold. Moreover, the diffusion length is short enough to accomplish the complete wetting in the small, geometrically random porous media. To check the acceleration of coarsening by diffusive wetting, gels with more decreased amount of MeOH, that is, more decreased phase separation tendency, were prepared. Bulk gels show no well-defined porous

structure suggesting the phase separating structures were frozen in the initial stages as seen in Figure 6. In hydrophilic silica molds, the confined gel structures resembled their bulk. However, more coarsened gels were obtained in hydrophobic molds where polymerizing species and the surface of the mold attract more strongly. Again, this fast coarsening phenomena attributes to the fast diffusion resulted from strong hydrophobic attractive interaction and shorter diffusion length inside the random porous network. As shown in Figure 6 (c), the transient structure just before the complete wetting in a hydrophobic mold does not show the deformed structure, which means there is no evidence of hydrodynamic wetting. This is an extraordinary example exhibiting the complete wetting induced only by diffusion.

Then, why this diffusive complete wetting does not occur in the MF system confined in a hydrophobic porous medium? Although the diffusion effect may appear in the hydrophobic MF system, it is much slower due to the higher viscosity in the MF system. Although viscosity arises drastically near the gel point, the overall viscosity of the system and the diffusion coefficient of the polymerizing siloxane are strongly dependent on its composition at the onset of phase separation. The only major difference of starting compositions between the MF and MM system is the kind of solvent; the MF system contains more viscous FA and the MM system does less viscous MeOH (viscosity  $\eta=3.75$  and  $0.611$  mPa·s for FA and MeOH at  $20^\circ\text{C}$ , respectively). Another possibility affecting the initial diffusion is hydrogen bonding between polymerizing MTMS and FA. FA is known to make a hydrogen bond between polymerizing silica, and makes cross-linking density lower [15]. If this is true for MTMS system as well, FA will trap the polymerizing MTMS and make the mobility of it lower. In the initial stage of spinodal decomposition, the compositional contrast between siloxane-rich and solvent (FA)-rich phases is not developed yet. Therefore considerable amount of MTMS-derived species and FA are contacted each other, resulting in a considerable hydrogen bonding between the two.

### 3. The TF system

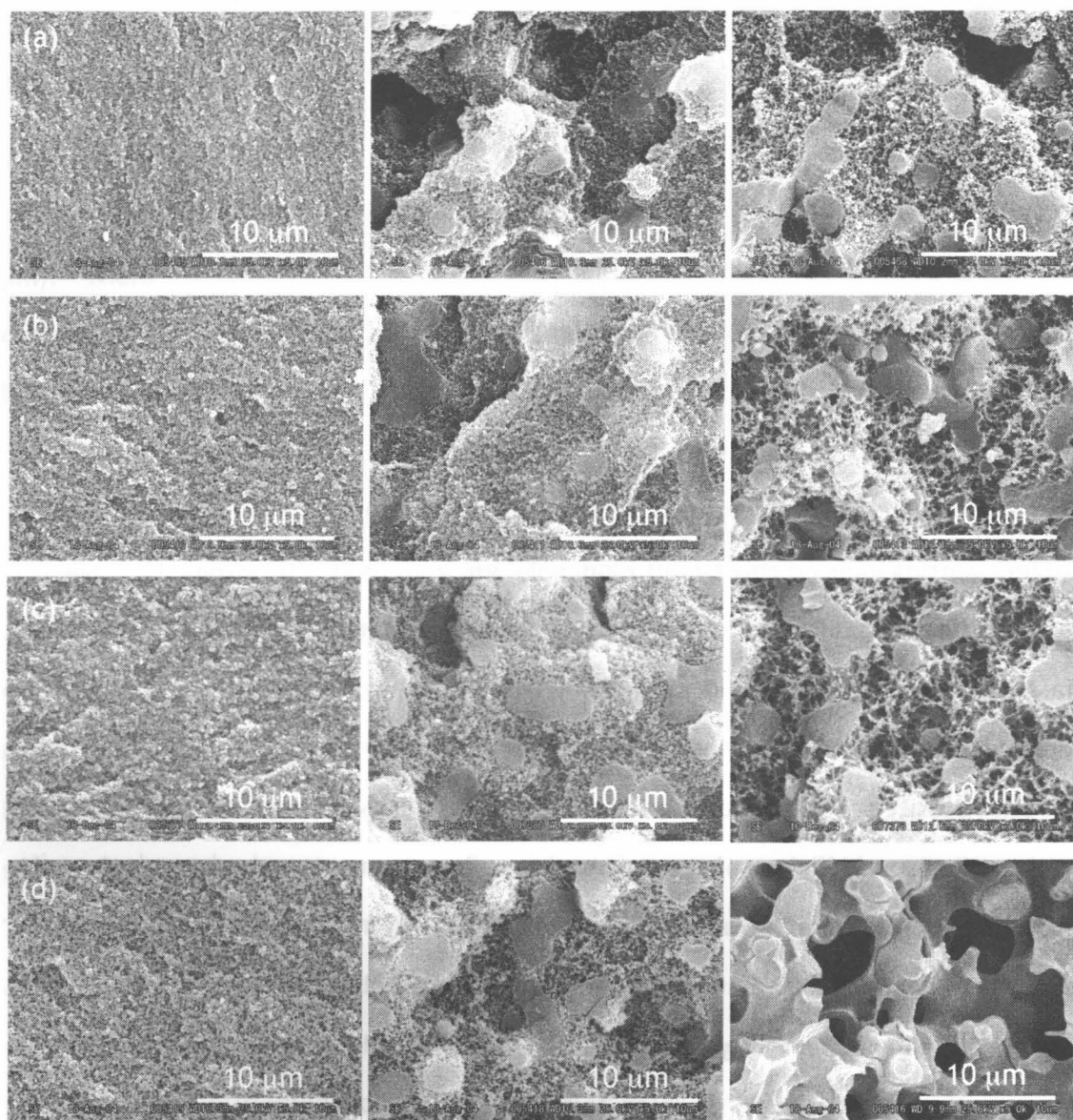


Figure 6 Scanning electron microscope images of gels derived from the MM system confined in hydrophilic and hydrophobic 0D molds with more decreased phase separation tendencies. The left images of each row (a)-(d) corresponds to the bulk gel in different compositions; (a)  $m_M=0.2$ , (b)  $m_M=0.4$ , (c)  $m_M=0.5$ , and (d)  $m_M=0.6$ . The center and right images of each row show gels confined in hydrophilic and hydrophobic molds, respectively.

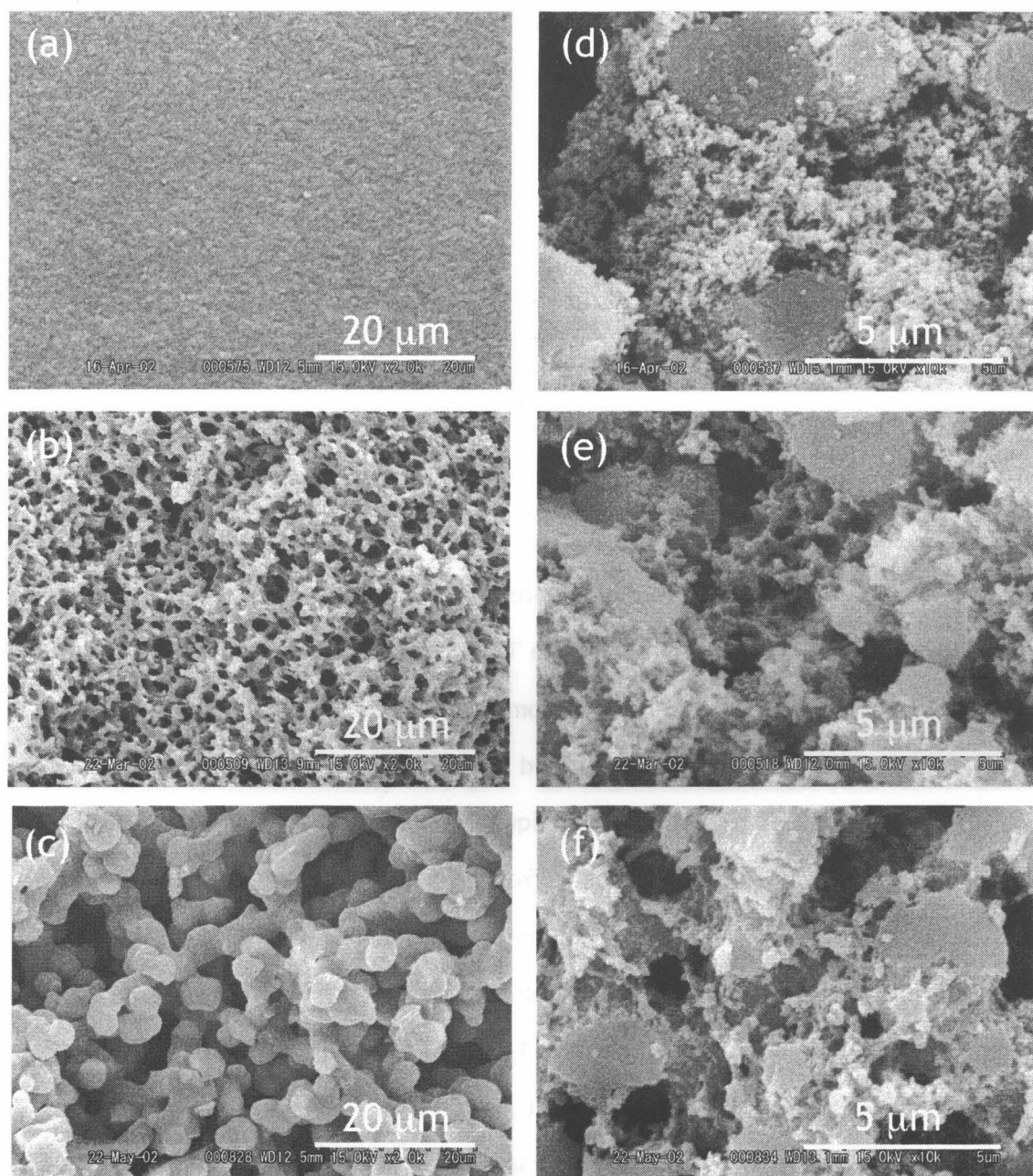


Figure 7 Scanning electron microscope images of 0D confined gels derived from the TF system. (a)-(c) 3D bulk gel in different compositions; (a)  $f_T=1.6$ , (b)  $f_T=1.9$  and (c)  $f_M=2.2$ . (d)-(f) Corresponding confined gel in hydrophilic 0D molds. Fine, disordered structure can be corroborated in all compositions.



Figure 7 shows a curious tendency in the TF system in a hydrophilic 0D mold. Bulk characteristic lengths of parts (a) and (b) are shorter than the size of the mold, and that of part (c) is obviously longer than the pore size of mold silica. However, fine, disordered structure which is quite different from the bulk structure is found in the confining mold. As the disordered structure does not have a well-defined surface, in this case the initial diffusion is also affected by the surfaces of the mold. Bulk gel in part (a) is slightly translucent indicating this composition is on the borderline of phase separation. The corresponding confined gel exhibits the disordered globular morphology and is a little different from the other two samples, which shows the confined gel is frozen as soon as the effect of the surfaces appears, i.e. phase separation starts. The other two shows the similar morphology; fine bicontinuous structure with rough surfaces.

The light scattering experiment of the TF system at 40°C shows that the typical initial dominant wavelength of spinodal decomposition (ca. 3.5  $\mu\text{m}$ ) is longer the size of the bulk (2.74  $\mu\text{m}$ ) [16]. Thus the disordered structure without a well-defined surface is observed for all compositions. If a critical liquid mixture is confined in a porous medium whose pore size is shorter than the initial correlation length, it is known phase separation kinetics is saliently suppressed and no macroscopic phase separation with distinct interfaces takes place. However, some composition variations on macroscopic scales were observed with NMR micro-imaging 14 days following the quenching of the temperature [9]. According to Wiltzius et al., in the case where pore radius of confining mold  $r$  is much longer than the characteristic length  $\Lambda$ , wetting phenomena should dictate the structure. On the other hand, if  $r \ll \Lambda$ , the chemical potential exerted by the internal surface of the mold is random on the relevant length scales in the phase-separating system and should act as a random field [17,18]. The present case (TF system) resembles the latter while the other cases may follow the former. In the practical system the random-field effect and wetting phenomena should not be independently divided but interplay each other and the TF-derived gel confined in a hydrophobic mold exhibits the mixed tendency. Figure 8 shows the interplay between suppression of phase separation

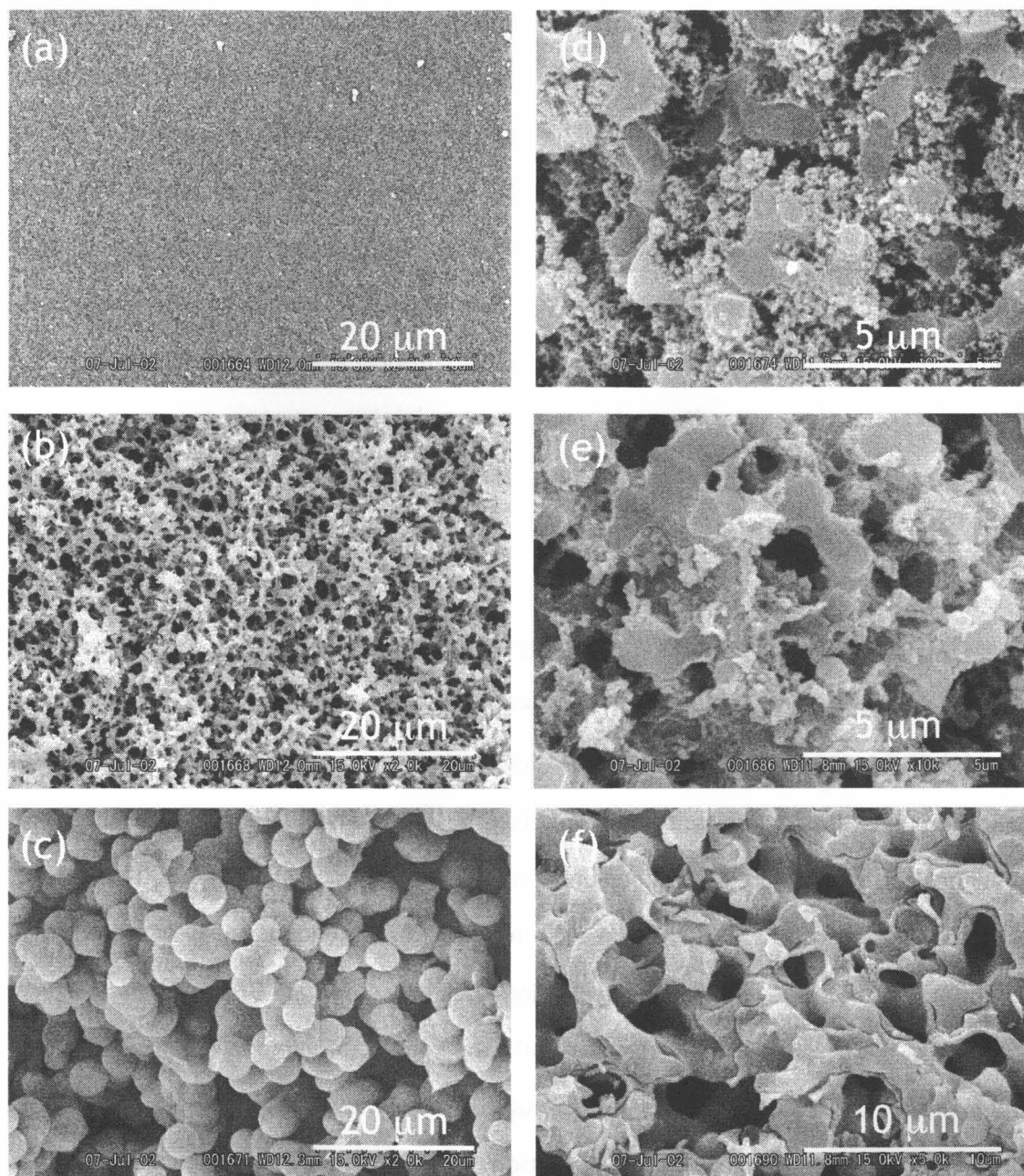


Figure 8 Scanning electron microscope images of 0D confined gels derived from the TF system. (a)-(c) 3D bulk gel in different compositions; (a)  $f_T=1.6$ , (b)  $f_T=2.1$  and (c)  $f_M=2.4$ . (d)-(f) Corresponding confined gel in hydrophilic 0D molds. Bulk characteristic length of par (b) is  $1.56 \mu\text{m}$ , i.e.  $D/\Lambda_m$  becomes less than unity in part (c).

and wetting transition. In part (e) the disordered bicontinuous structure remains in the OD mold, and wetting transition occurs as indicated in part (f). The surfaces of the guest gel structure are rough before the wetting transition, suggesting the suppression of phase separation due to the random-field effect. Due to the attractive interaction between hydrophobic surfaces of the TMOS-derived species and octadecylsilylated surfaces of the mold through hydrophobic interaction, the distinct transition to complete wetting took place.

#### 4. Conclusion

In this chapter the structural observation in a macroporous sintered silica with varied surface characters was performed. In the MF system it was found the overall tendency is similar to the cases of the molds with other dimensionalities. That is, when  $D/\Lambda_m$  is much larger than unity, isotropic bicontinuous structure develops, when  $D/\Lambda_m$  becomes closer to unity, the isotropic nature is broken, and finally, when  $D/\Lambda_m$  becomes less than unity, wetting transition occurs. In the MM system, the similar tendency was observed in a hydrophilic mold; however, wetting transition took place for all  $D/\Lambda_m$  values inside a hydrophobic mold. The TF system exhibits the more curious morphological change. For a hydrophilic mold, fine structure with rough surfaces was observed for all  $D/\Lambda_m$  values, and for a hydrophobic mold, wetting transition occurred when  $D/\Lambda_m$  becomes less than unity.

Two effects are thought to rule the morphological development. One is diffusion in the early stage of spinodal decomposition. The extraordinary behavior observed in the MM system in a hydrophobic mold is elucidated by rapid diffusion during the initial stage. And the other is the effect of random space. If a system is confined in a small space shorter than its initial wavelength, phase separation kinetics is significantly suppressed. The TF system shows this feature in a hydrophilic mold but simultaneously wetting



transition occurs in a hydrophobic mold when the bulk characteristic length becomes longer. This implies interplay between two phenomena.

The effect of confinement is prominent in the case of 0D mold. Namely, the above extraordinary phenomena were not confirmed in the other molds. Still, it should be confirmed in the future experiment whether the dimensionality or simply the size of the mold play an essential role. At least the variation of the initial wavelengths in the other systems (i.e. the MF and MM systems) should be studied by light scattering experiment. Also, the present systems containing FA and MeOH are the two extremities from the viewpoint of the attractive interaction between a solvent and the MTMS-derived species. A series of amide solvents has to be examined with different hydrogen bonding ability to explore the effect of hydrogen bond.

From a practical point of view, wetting transition may be applied as a coating technique. A thick and uniform coating can be performed on the surfaces of a narrow space such as flow channels or macroporous siloxane gel by a simple procedure (see also wetting transition in 1D capillary in Chapter 3).

## References in Chapter 4

- [1] K. Nakanishi, *J. Porous Mater.* **4**, 67 (1997).
- [2] H. Tanaka, *Phys. Rev. Lett.* **70**, 2770 (1993).
- [3] H. Tanaka, *J. Phys.: Condens. Matter*, **13**, 4637 (2001).
- [4] M. Moffitt, Y. Rharbi, H. Li, M. A. Winnik, *Macromolecules*, **35**, 3321 (2002).
- [5] M. C. Goh, W. I. Goldberg, C. M. Knobler, *Phys. Rev. Lett.* **58**, 1008 (1987).
- [6] A. J. Liu, D. J. Durian, E. Herbolzheimer, S. A. Safran, *Phys. Rev. Lett.* **65**, 1897 (1990).
- [7] F. Aliev, W. I. Goldberg, X-l. Wu, *Phys. Rev. E*, **47**, R3834 (1993).
- [8] M. Y. Lin, S. K. Sinha, J. M. Drake, X-l. Wu, P. Thiyagarajan, H. B. Stanley, *Phys. Rev. Lett.* **72**, 2207 (1994).
- [9] S. Lacelle, L. Tremblay, Y. Bussi re, F. Cau, C. G. Fry, *Phys. Rev. Lett.* **74**, 5228 (1995).
- [10] L. Tremblay, S. M. Socol, S. Lacelle, *Phys. Rev. Lett.* **61**, 656 (2000).
- [11] R. Valiullin, I. Fur , *Phys. Rev. Lett.* **66**, 031508 (2002).
- [12] P. Wiltzius, S. B. Dierker, B. S. Dennis, *Phys. Rev. Lett.* **62**, 804 (1989).
- [13] P. C. Hohenberg, B. I. Halperin, *Rev. Mod. Phys.* **49**, 435 (1977).
- [14] H. Tanaka, T. Araki, *Europhys. Lett.* **51**, 154 (2000).
- [15] I. Artaki, T. W. Zerda, J. Jonas, *J. Non-Cryst. Solids*, **81**, 381 (1986).
- [16] H. Kaji, K. Nakanishi, N. Soga, T. Inoue, N. Nemoto, *J. Sol-Gel Sci. Tech.* **3**, 169 (1994).

## CHAPTER 5: APPLICATION TO CAPILLARY HPLC

### 1. Introduction

Porous silica gels with bicontinuous structure can be prepared via sol-gel accompanying phase separation, especially, spinodal decomposition [1]. This kind of silica gel possesses well-defined micrometer-range continuous pores and its porosity reaches typically as high as 80%. After tailoring micrometer-range structure, mesopores with 5-10 nm in diameters can be formed by heat-treating with basic aqueous solution [2]. This process is known as Ostwald ripening [3] in which convex parts with larger curvature dissolve and reprecipitate onto concave parts with larger curvature, making the whole silica gel into that with hierarchical double pore. The double pore structure is favorable in applying the material to separation media for high performance liquid chromatography (HPLC) because it requires high macro-porosity in order to obtain high flow rate and the mesopores which contribute to the separation of the mixture of molecules [4,5].

Recently, much effort has been made to apply bicontinuous silica gel to miniaturized HPLC [6] such as Lab-on-a-chip or micro-HPLC because porous bicontinuous structure can be prepared in a variety of small confined spaces as far as a starting solution can be introduced in. Also, porous bicontinuous organic-inorganic hybrid gels are intensively studied to obtain a variety of surface character and/or functions [7,8]. For one example, such hybrid materials can be tailored from three-functional methyltrimethoxysilane (MTMS) which can provide a hydrophobic surface [9] because the methyl groups are mainly directed outward the gel surfaces [10]. However, the “flexible” MTMS-derived network tends to deform under the influence of surfaces, which makes it difficult to prepare ideal structures in small confined spaces as detailed in the previous chapters. Thus, investigation on the surface effect is highly required.

In polymeric multi-component systems which undergo phase separation, the surfaces

induce a wetting effect during phase separation [11-14]. Especially in bicontinuous spinodal decomposition, more wettable component(s) flows onto the contacting surfaces through bicontinuous pathways in a hydrodynamic manner [13]. This hydrodynamic flow leads to a significant deformation of siloxane gel; the larger the domain size becomes, the more significantly the structure deforms because longer time is needed to obtain the more coarsened structure, which in turn means longer time is allowed for wetting.

In this chapter, tailoring isotropic methylsiloxane structure in a capillary and application to capillary HPLC is described. The wetting-induced deformation in a capillary is already given in Chapter 3.

## 2. Experimental

Methyltrimethoxysilane (MTMS, Shin-Etsu Chemical Ind. Ltd., Japan), Methanol (MeOH), and Nitric acid (Hayashi Pure Chemical Ind., Japan) were used as received.

The MM system with molar ratio MTMS : MeOH : H<sub>2</sub>O=1 : *m* : 2.0 is used because in the previous chapters it is revealed the MM system is not susceptible to micro-surface effects due to its rapid reaction rate.

The experimental procedure is as follows: Appropriate amounts of 1.0 M aqueous Nitric acid and MeOH were mixed in a glass tube and then MTMS was added under vigorous stirring at 0 °C. After stirring for 5 min, the resultant solution was transferred into a polystyrene reaction vessel in which the capillaries were placed, followed by an ultrasonic agitation for 1 min. The diameters of capillaries are 200 and 530 μm. Then the solution was allowed to gel at 40 °C in a closed condition. The resultant gel was aged over 24 h at the same temperature followed by solvent evaporation at 40 °C. The dried samples were subjected to SEM (S-2600N, Hitachi, Japan) observation.

For the purpose of altering the surface polarity, nonionic surfactant Poly(oxyethylene) nonylphenyl ether with 10 and 70 oxyethylene units (NS-210 and NS-270,

respectively) are included in the starting solution before adding MTMS.

In chromatographic characterization, a conventional HPLC system consisting of a pump (LC-10AD, Shimadzu, Japan), an injection valve (Model 7725i, Rheodyne, Berkeley, CA, USA), a UV detector (CE-1570, JASCO, Japan) and a data processor (BORWIN, JASCO, Japan) was used. The overview of the system is exhibited in Figure 1. The mobile phase was hexane/2-propanol (100:2, v/v) and sample mixture contains toluene, 2,6-dinitrotoluene and 1,2-dinitrobenzene as solutes. Toluene is not retained on the siloxane surface and gives dead time  $t_0$  (see below).

Number of theoretical plates  $N$ , Column permeability  $K$  and Separation impedance  $E$  were calculated from the following equations:

$$N = 5.54 \left( \frac{t_R}{w_{1/2}} \right)^2, \quad (5-1)$$

$$K = \frac{u\eta L}{\Delta P}, \quad u = \frac{L}{t_0}, \quad (5-2)$$

$$E = \frac{\Delta P t_0}{\eta N^2}, \quad (5-3)$$

where  $t_R$  and  $w_{1/2}$  are retention time of a solute and peak width at half height, respectively.  $u$  shows linear velocity of mobile phase,  $\eta$  solvent viscosity,  $L$  column length,  $\Delta P$  and  $t_0$  column pressure drop and dead time (time for unretained species to reach the detector), respectively. Retention factor  $k'=(t_R-t_0)/t_0$  is also calculated from the obtained chromatogram.

### 3. Results and discussion

#### 3.1 Important factors that affect the structural development in confined geometry

Here, let us briefly review the important factors that become crucial for tailoring phase-separated siloxane gel inside micro-surfaces. Wetting-induced deformation is

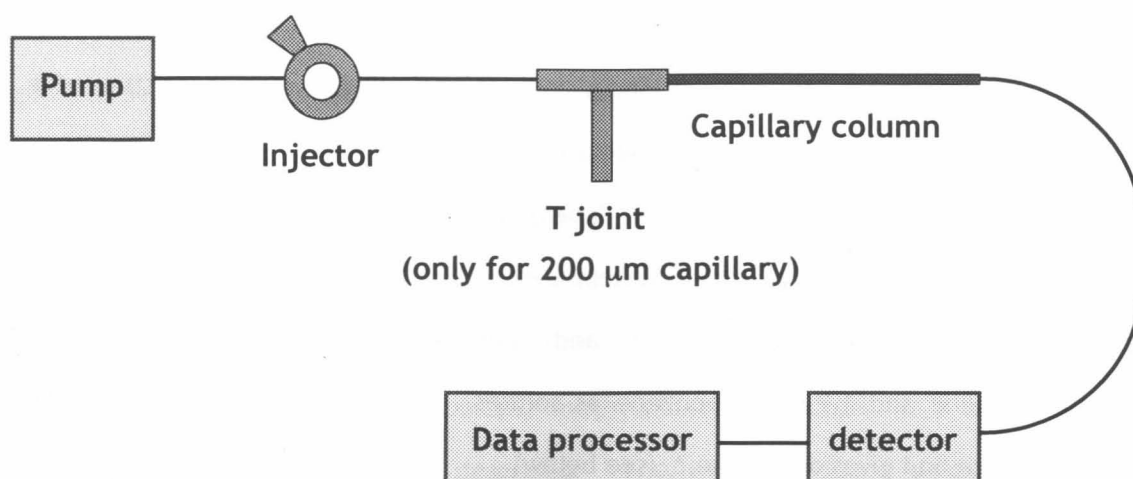


Figure 1 The HPLC system used in this study. A “T joint” splitter is used only for the capillary with diameter of 200 μm in order to lower the back pressure.

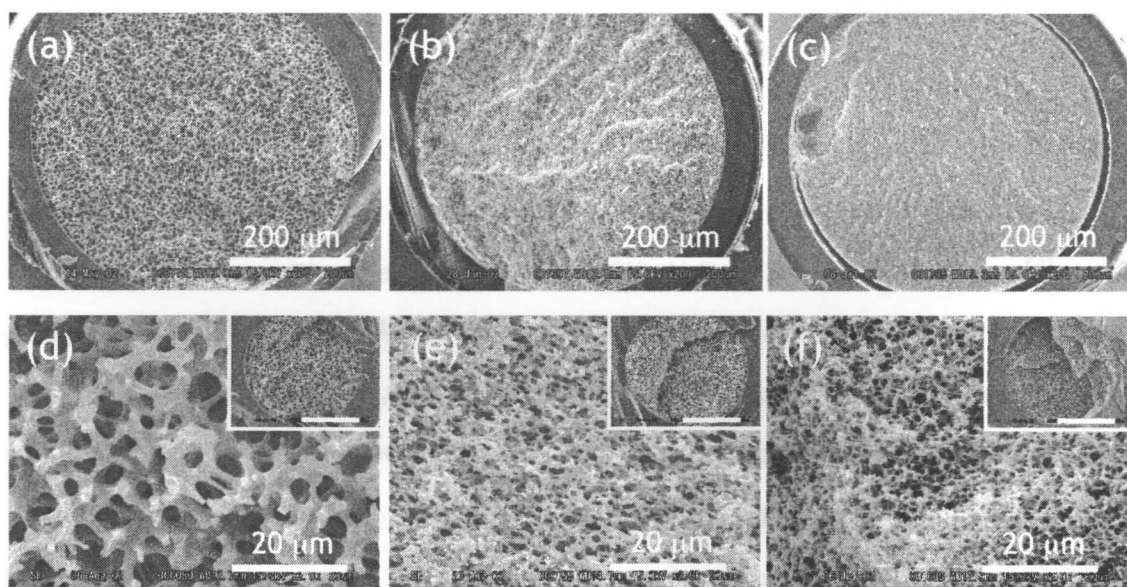


Figure 2 Scanning electron microscopy photographs of phase-separated siloxane gels derived from the MM system in (a)-(c) 530-μm-ID capillaries and (d)-(f) 200-μm-ID capillaries. The starting compositions are as follows: (a) and (d) are  $m=1.1$ , (b) and (e) are  $m=1.0$ , and (c) and (f) are  $m=0.9$ . A saber-like void can be confirmed near the surface in part (c), however, there is no void in 200-μm-ID capillaries.

persistently described in the previous chapters, so it is not explained here again.

In the course of spinodal decomposition, when the separating two phases possess far different dynamics, e.g. if “A” phase has a high viscosity and “B” phase has a low viscosity, the system phase-separates in a very unique manner called “viscoelastic phase separation” [15-17]. In the conventional theory for spinodal decomposition, bicontinuous structure can develop when the volume fractions of separating phases are close enough [18,19]. However in the viscoelastic phase separation, the more viscoelastic “A” phase can be elongated and keep connectivity even if the volume fraction of “A” phase is far less than 0.5. Siloxane sol-gel system described here is a typical example of viscoelastic phase separation because one phase usually consists of low molecular solvent and the other phase contains siloxane polymer which will lose mobility during sol-gel reaction. That is, the more viscoelastic “A” phase corresponds to the siloxane-rich phase. Jinnai et al. have also studied an organic polymer blend system consisting of deuterated polybutadiene (dPB) and polybutadiene (PB) [20], which is an ideal fluid phase separation model, that is, the both separating phases have almost the same characters (for example, viscosity, interfacial energy etc.). The more wettable PB-rich phase gradually wets the surface in a 2D mold separated by ca. 55  $\mu\text{m}$ , however, the structural deformation is far less than siloxane sol-gel system. Since dPB/PB polymer blend system does not undergo viscoelastic phase separation, elongated portion of PB phase with larger curvature easily breaks up while siloxane gel phase can deform into columnar shape in siloxane sol-gel system. Besides, the wetting transition does not take place even if  $D/\Lambda_m$  becomes less than unity in dPB/PB blend system. Instead of that, spatial symmetry of bicontinuous structure is significantly broken, and transforms into pillar-like structure connecting two wetting layers (see Fig. 4c in ref. 20). The difference comes from the symmetric property of wettability. Namely, in dPB/PB system, both the separating phases have almost the same interfacial energy so that the driving force of wetting is not so large. In contrast to that, there is a large difference of interfacial energy in siloxane system leading to the acceleration of wetting.

Chemical character, especially hydrophobicity of the surface is another important factor. However, when the surface of a mold is octadecylsilylated, the wetting behavior is hardly affected in MTMS-derived system which is already well-discussed in the previous chapters. The reason is still unclear but the possibility is that the surface energy of methylsiloxane phase is low enough that the wetting behavior is less susceptible to the interfacial energy change of the surface. Chemically, MTMS-derived polymer can interact with hydrophilic/hydrophobic surfaces using hydroxyl/methyl groups, respectively. The methylsiloxane polymer forms Si–O–Si chemical bonds with hydrophilic surface on which silanol groups exist. While with hydrophobic surface, methylsiloxane polymer does not make a chemical bond, but attracts each other through hydrophobic interaction. Hydrophobic interaction is much weaker than a chemical bond, thus the resultant gel is subjected to free shrink during aging and drying especially when the volume/surface ratio becomes larger.

### *3.2 Structural modification for capillary HPLC*

In order to apply the bicontinuous siloxane-based gels to capillary HPLC, generation of voids around the internal surface can be a critical problem because a large fraction of the sample flow possibly goes through the voids, which results in deterioration of separation efficiency. The formation of the voids is related mostly to two factors: One is shrinkage during synthesis, and the other is adhesiveness to the internal surface of a mold.

Shrinkage is the inevitable phenomenon as far as the polymerization reaction proceeds as the “condensation” reaction. After the homogeneous gelation, the unreacted silanol or alkoxide groups condense each other, leading to the shrinkage to some extent during the aging and drying step. In the MTMS-derived siloxane gel, the unfavorable shrinkage can be suppressed probably because of the steric hindrance by the methyl group. Besides, gels prepared from tetrafunctional alkoxides such as TEOS or TMOS is “rigid but brittle” while gels prepared from trifunctional alkoxides such as MTMS



or MTES is “flexible” due to the low cross-linking density. This flexibility enables the gel to endure the stress generated by the shrinkage and can suppress the formation of the voids.

Adhesiveness is another important factor to suppress the voids. MTMS-derived gel has a lower polarity compared to a TMOS-derived one, so it is thought to have lower interfacial energy, which helps the gel phase flows onto the surface and spread itself there. Then the gel and the surface connect through Si–O–Si chemical bonds tightly. Thus the MTMS-derived gel can endure the stress toward the center of the capillary using its tight “footholds” as well as the flexibility.

From these points of view, we have tried to prepare the spatially isotropic bicontinuous siloxane-based gels without the voids in a capillary with internal diameter (ID) of 200 and 530  $\mu\text{m}$ . From the preceding discussion, the MM system is more favorable because the shorter time is allowed for wetting, which results in the more homogeneous structure. Figure 2 (a)-(c) shows the gel structure in a 530- $\mu\text{m}$ -ID derived from the MM system. Although gels without voids can be prepared when the characteristic length of the structure is relatively large ((a) and (b)), the formation of the voids can be confirmed in part (c). As the capillary force resulted from solvent evaporation becomes stronger when the pore size becomes smaller, the voids tend to be generated as shown in part (c). Figure 2 (d)-(f) shows the gel structure in a 200- $\mu\text{m}$ -ID capillary derived from the MM system. In contrast to the case of 530- $\mu\text{m}$ -ID capillaries, no voids can be recognized even in the case of the smallest pore size. Since the volume/surface ratio becomes smaller in the 200- $\mu\text{m}$ -ID capillary, the stress of shrinkage becomes much smaller, which restrains the formation of the voids. Phase-separated gels derived from surfactant-incorporated MM system are shown in Figure 3. In this system, well-defined porous monolith without a void can be prepared as well. In the MM system without a surfactant, gel tends to be deformed when the characteristic length becomes longer, however, coarsened gels without the deformation is obtained in parts (b) to (d). This result may be related with the fact that EOPEO-incorporated system shows less deformation as indicated in Section 2.2.

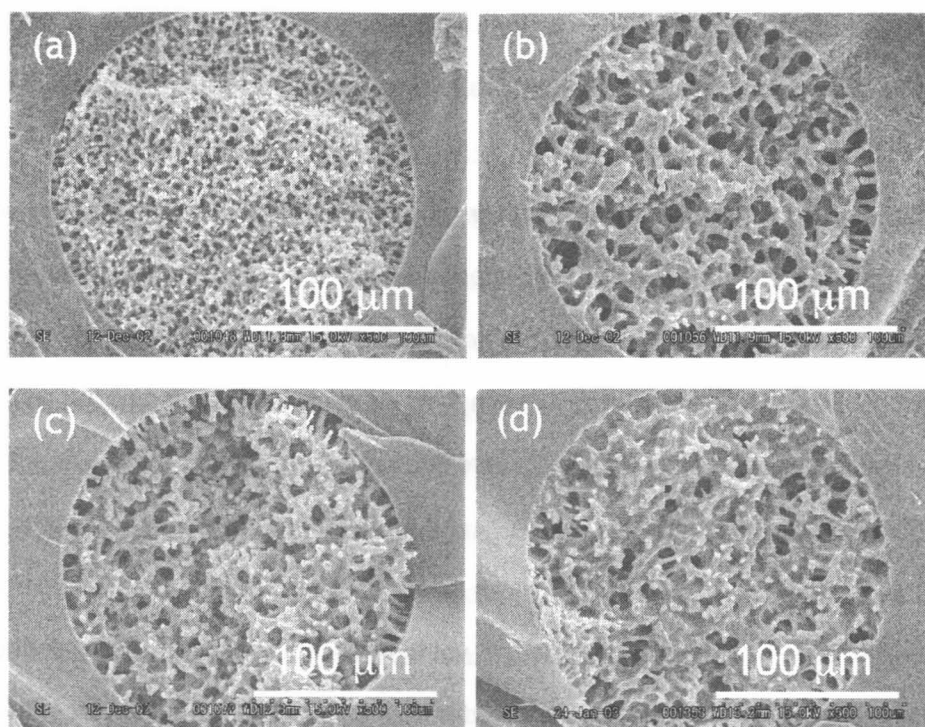


Figure 3 Scanning electron microscopy photographs of phase-separated siloxane gels derived from the MM system incorporated with nonionic surfactants. The starting compositions are MTMS : MeOH : H<sub>2</sub>O=(a) 1 : 1.1 : 2.0, (b) 1 : 0.9 : 2.2, (c) 1 : 1.3 : 2.0, and (d) 1 : 0.9 : 2.0 in molar ratios. Surfactants are (a)-(c) NS-210 and (d) NS-270. The weight ratios of surfactant/MTMS are (a) and (b) 0.021, (c) 0.042, and (d) 0.021.

### 3.3 Results of capillary HPLC characterizations

Up to now we have been studying formability and applicability to miniaturized HPLC of silica monoliths [6,21-23], here we briefly show the application of methylsiloxane monoliths. It is difficult to prepare well-defined structure of silica gel in a capillary, however, we can easily prepare well-defined MTMS-derived siloxane gel in confined spaces as described above. Figure 4 shows the resultant chromatogram for the MM system in a 200- $\mu\text{m}$ -ID capillary. A mixture of toluene, 2,6-dinitrotoluene and 1,2-dinitrobenzene was used as a solute. The features of gels and the obtained chromatographic characters are listed in Table 1. Although inside of the skeletons of MTMS-derived siloxane gels are non-porous, the chromatographic efficiencies of methylsiloxane monoliths are comparable to the conventional particle-packed columns. Numbers of theoretical plates ( $N$ ) become larger with decreasing size of the phase-separated structure. However, since the samples with finer pore structures represent high back pressures, the values of permeability ( $K$ ) becomes smaller, resulting in giving a minimum of separation impedance ( $E$ ) at  $m=1.0$ . The thinner gel skeletons lead to better separation, which corresponds to smaller particle beds in the conventional particle-packed columns. Thus similar to the conventional particle-packed columns, finer pore structures lead to the better separation efficiency, whereas the flow resistance becomes higher and much longer time will be needed for analysis. However, the most important thing is, since sol-gel method starts with liquid precursors, it provides a high formability even in a capillary with 10  $\mu\text{m}$  of inner diameter.

Figure 5 shows the relationship between oxyethylene chain length and retention factors  $k'$  of MTMS-derived gels incorporated with NS-210 (Figure 3(a)) and NS-270 (Figure 3(d)) in normal phase. Since these kinds of nonionic surfactants have attractive interaction with silanol groups through hydrogen bonding, large amount of them are distributed in methylsiloxane gel phase, which was confirmed using TG-DTA analysis [24]. The retention factors of 1,2-dinitrobenzene/toluene are 0.75 (NS-210) and 0.82 (NS-270),

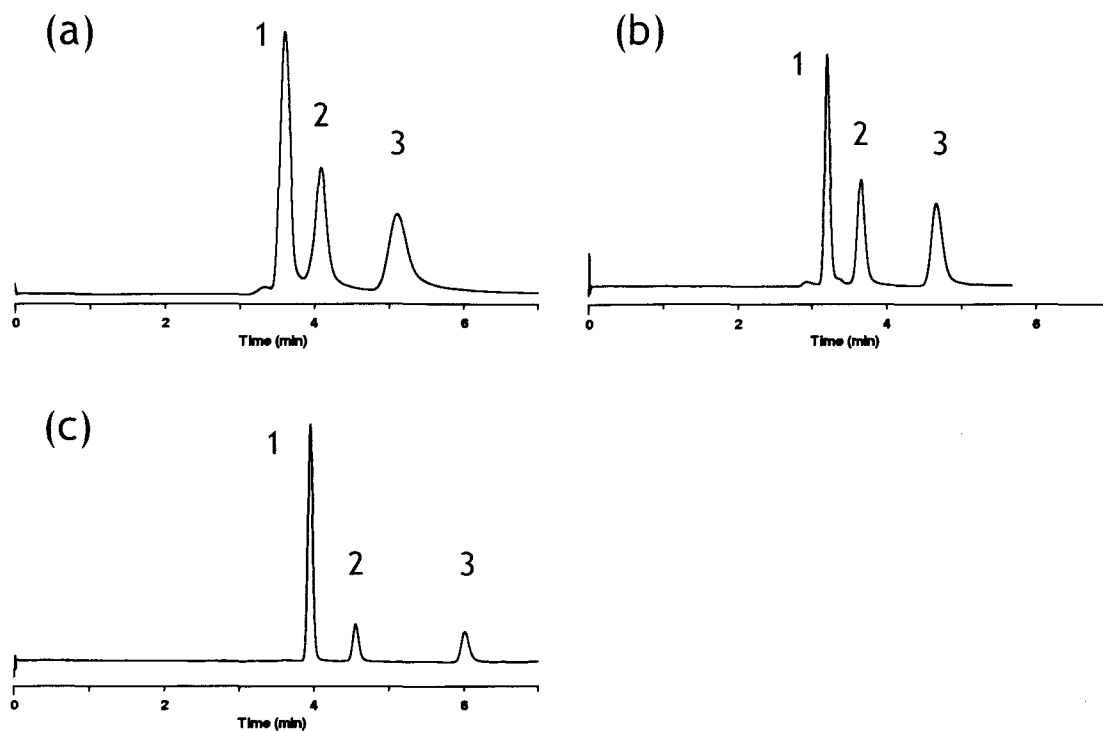


Figure 4 Normal phase-chromatograms obtained with methylsiloxane gel columns. (a)  $m=1.1$ , (b)  $m=1.0$  and (c)  $m=0.9$ . The capillary diameter is 200  $\mu\text{m}$  and the sample mixture contains 1: toluene, 2: 2,6-dinitrotoluene, and 3: 1,2-dinitrobenzene. See also Fig. 2 (d-f) and Table 1.

Table 1 Results of the chromatographic characterization of methylsiloxane gels.

MeOH/MTMS (molar ratio)	Skeleton Size ( $\mu\text{m}$ )	Pore size ( $\mu\text{m}$ )	Characteristic length ( $\mu\text{m}$ )	Column length (mm)	Back pressure (kgf)	$N$ (1/m)	$K \times 10^4$ ( $\text{m}^{-2}$ )	$E$
1.1	1.5	3.3	4.8	143	1	11,000	340	2,500
1.0	0.54	1.8	2.3	146	6	32,000	66	1,600
0.9	0.19	0.67	0.86	155	53	96,000	10	1,900

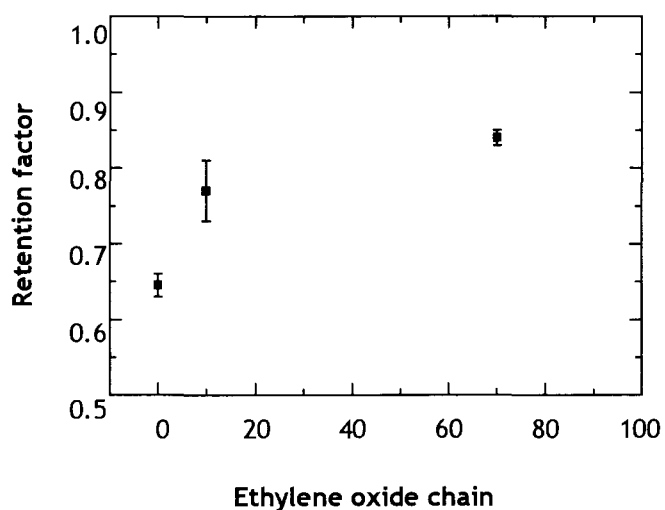


Figure 5 Relationship between retention factor and the length of ethylene oxide chain. The structures of surfactant-incorporated gels are shown in Figure 3(a) and (d). Retention factors are calculated using the peaks of toluene and 1,2-dinitrobenzene. The surface of the gel skeletons becomes hydrophilic when the ethylene oxide chain becomes longer.

indicating that the surface with longer oxyethylene units shows higher polarity. These values of retention factor were not changed by varying the amount of surfactant, which suggests that the surfaces of methylsiloxane gels are saturated with the surfactant. Thus we can easily alter the surface character simply by adding a surfactant into the system. Chromatograms obtained from nonionic surfactant-incorporated methylsiloxane gels are shown in Fig. 6. Although the column lengths are different from those listed in Table 1, separation of polar species (2 and 3) is improved and the widths of the peaks are sharper than monoliths without any surfactants. Although further research is needed, 3-functional MTMS-based bicontinuous siloxane gel will become one of the most prevailing candidates for analytical devices because we can easily create a crack-free monolithic structure without effective surface-directed deformation and the surface character can be altered using various types of surfactant in the near future.

#### 4. Conclusion

We have been trying to tailor a unique porous structure using spinodal decomposition and have obtained various kinds of phenomenological knowledge about surface effect in a confined geometry. The main factor that decides the final structure is wetting of siloxane gel phase during phase separation and gelation. Since the more polar silanol groups are consumed in the course of polycondensation reaction, the polarity of siloxane phase becomes smaller and siloxane gel phase always wets the surface preferentially. This speculation is not fully checked yet, but we believe it is true to all the phase-separating sol-gel systems because siloxane gel phase always loses polar silanol groups and then turns into gel. In any case, the consistent thing is that wetting of methylsiloxane gel phase onto the existing surface induces the structural deformation, which accelerates wetting in the hydrodynamic pumping mechanism. When the spinodal wavelength becomes larger than the dimension of a confining space, wetting transition occurs. This phenomenon is

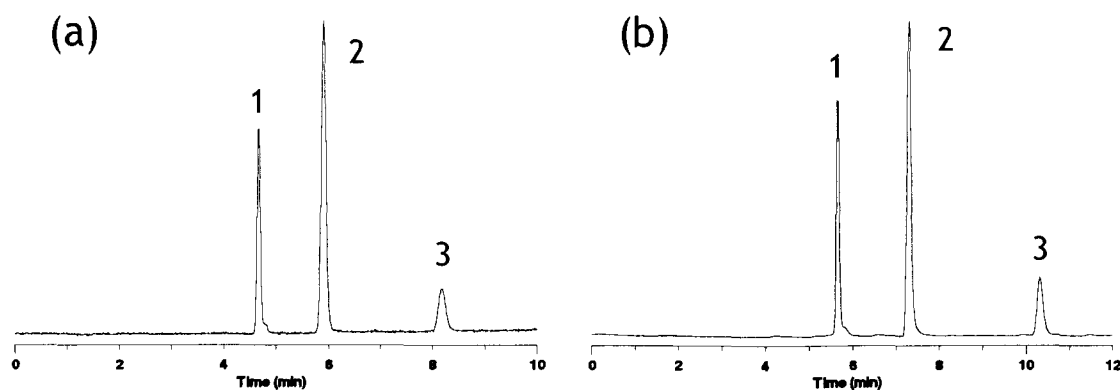


Figure 6 Chromatograms obtained with surfactant-incorporated methylsiloxane gel columns. (a) MTMS : MeOH : H<sub>2</sub>O=1 : 1.1 : 2.0 and the weight ratio of NS-210/MTMS is 0.021 (see also Figure 3 (a) for the SEM photograph), and (b) MTMS : MeOH : H<sub>2</sub>O=1 : 1.1 : 2.0 and the weight ratio of NS-270/MTMS is 0.021 (see also Figure 3 (d) for the SEM photograph). The capillary diameter is 200  $\mu$ m and the sample mixture contains 1: toluene, 2: 2,6-dinitrotoluene, and 3: 1,2-dinitrobenzene. The column length of each monoliths are 300 mm. Back pressures are: (a) 6 kgf and (b) 19 kgf. The calculated values of  $N$  are: (a) 6,100 /m and (b) 6,200 /m.

universal for all the “closed” confined system, but can not be applicable to the “open” system.

The MTMS-Methanol system is less susceptible to the structural deformation due to the rapid reaction. Capillary columns made with the MM system showed an excellent ability of fast and efficient separation of nitrobenzenes in normal phase. Surfactants can alter the surface character of MTMS-derived gel easily, which will contribute to the further development of MTMS-derived micro-separation media.



## References in Chapter 5

- [1] K. Nakanishi, *J. Porous Mater.* **4**, 67 (1997).
- [2] K. Nakanishi, R. Takahashi, T. Nagakane, K. Kitayama, N. Koheiya, H. Shikata, N. Soga, *J. Sol-Gel Sci. Tech.* **17**, 191 (2000).
- [3] R. K. Iller, *The Chemistry of Silica, Solubility, Polymerization, Colloids and Surface Properties, and Biochemistry*, Wiley Interscience, New York (1979).
- [4] N. Tanaka, H. Kobayashi, K. Nakanishi, H. Minakuchi, N. Ishizuka, *Anal. Chem.* **73**, 420A (2001).
- [5] F. C. Leinweber, D. Lubda, K. Cabrera, U. Tallarek, *Anal. Chem.* **74**, 2470 (2002).
- [6] N. Tanaka, H. Nagayama, H. Kobayashi, T. Ikegami, K. Hosoya, N. Ishizuka, H. Minakuchi, K. Nakanishi, K. Cabrera, D. Lubda, *J. High Resol. Chromatogr.* **23**, 111 (2000).
- [7] A. Itagaki, K. Nakanishi, K. Hirao, *J. Sol-Gel Sci. Tech.* **26**, 153 (2003).
- [8] K. Nakanishi, T. Yamato, K. Hirao, *Mat. Res. Soc. Symp. Proc.* **726**, Q9.7.1 (2002).
- [9] N. J. Shirtcliffe, G. McHale, M. I. Newton, C. C. Perry, *Langmuir*, **19**, 5626 (2003).
- [10] C. Della Volpem, S. Diré, E. Pagani, *J. Non-Cryst. Solids*, **209**, 51 (1997).
- [11] U. Steiner, J. Klein, E. Eiser, A. Budkowski, L. J. Fetters, *Science*, **258**, 1126 (1992).
- [12] J. Bodensohn, W. I. Goldberg, *Phys. Rev. A*, **46**, 5084 (1992).
- [13] H. Tanaka, *J. Phys.: Condens. Matter*, **13**, 4637 (2001).
- [14] M. Moffitt, Y. Rharbi, H. Li, M. A. Winnik, *Macromolecules*, **35**, 3321 (2002).
- [15] I. S. Polios, M. Soliman, C. Lee, S. P. Gido, K. Schmidt-Rohr, H. H. Winter, *Macromolecules*, **30**, 4470 (1997).
- [16] H. Tanaka, *J. Phys.: Condens. Matter*, **12**, R207 (2000).
- [17] A. Onuki, *Phase Transition Dynamics*, Cambridge University Press, Cambridge (2002), pp. 444.
- [18] K. Binder, in: *Materials Science and Technology, A Comprehensive Treatment*, R. W. Cahn, P. Haasen, E. J. Kramer (Eds.), VCH, Weinheim (1990), Vol. 5, pp. 405.
- [19] pp. 403 in ref 25

[20] H. Jinnai, H. Kitagishi, K. Hamano, Y. Nishikawa, M. Takahashi, *Phys. Rev. E*, **67**, 021801 (2003).

[21] N. Ishizuka, H. Minakuchi, K. Nakanishi, N. Soga, K. Hosoya, N. Tanaka, *J. High Resol. Chromatogr.* **21**, 477 (1998).

[22] N. Ishizuka, H. Minakuchi, K. Nakanishi, N. Soga, H. Nagayama, K. Hosoya, N. Tanaka, *Anal. Chem.* **72**, 1275 (2000).

[23] N. Ishizuka, H. Kobayashi, H. Minakuchi, K. Nakanishi, K. Hirao, K. Hosoya, T. Ikegami, N. Tanaka, *J. Chromatogr. A*, **960**, 85 (2002).

[24] K. Nakanishi, T. Nagakane, N. Soga, *J. Porous Mater.* **5**, 103 (1998).

## SUMMARY

The present thesis deals with the effect of micro-surface on the micrometer-range structural formation of siloxane gel via phase separation. Shape, size and chemical character of the mold are systematically studied.

Chapter 1 was devoted to the model sol-gel systems together with Laser Scanning Confocal Microscopy (LSCM) and its related image analysis techniques. Methyltrimethoxysilane (MTMS)-formamide (FA)-H<sub>2</sub>O system (denoted as MF system) and MTMS-methanol (MeOH)-H<sub>2</sub>O system (denoted as MM system) are suitable for tailoring micro-devices since the gels derived from such systems show excellent formability; they show little cracks and shrinkage. This fact is quite important for both structural observation and application. All the techniques introduced in Chapter 1 are sufficiently complete and well-established. However, the observation methods shown in “Case 1” through “Case 4” are just the examples and the author hopes easier and more reliable methods are contrived in the near future.

In Chapter 2, phase-separated structures in two dimensional (2D) molds were examined by Laser Scanning Confocal Microscopy (LSCM). Conspicuous deformation was observed in the near-surface regions in the MF system for both hydrophilic and hydrophobic surfaces. On the contrary, tetramethoxysilane (TMOS)-FA-H<sub>2</sub>O system (denoted as TF system) showed only a slight deformation. In Section 2.1 the origin of deformation was discussed from the viewpoints of chemical characters of the surface of the mold and that of polymerizing species. In the MF system, the following was concluded: Since hydrophilic surface and MTMS-derived species can form chemical bonds, MTMS-derived phase wetted preferentially, resulting in a significant deformation. In the case of hydrophobic surfaces, MTMS-derived phase wetted preferentially as well by hydrophobic interaction, and again, resulted in a significant deformation. From SEM observation, the gel interfaces contacted to hydrophilic and hydrophobic surfaces showed

different features; skin layer was formed only in the hydrophobic interfaces. Since the chemical interaction between gel and hydrophobic surfaces is quite weak, the gel was stripped off at the interfaces, while in the case of hydrophilic surfaces the gel was broken at the structurally weak deformed regions. In the TF system, the deformation was critically suppressed since the gel network is rigid and does not stretch. However, there were a lot of cracks and shrinkage which make it difficult to prepare intact samples. In Section 2.2 the origin of the deformation was discussed from the viewpoint of hydrodynamic effects. The local analysis clearly showed the undesirable deformation with larger curvatures and it can be deduced that “hydrodynamic pumping” process plays an important role. Namely, from the early stage of spinodal decomposition siloxane-rich phase preferentially wetted the surface which makes elongated columnar structure in the proximity of the surface. Then the wetting will be accelerated by the pressure difference between inside the elongated skeleton and the surface wetting layer. When the bulk characteristic length exceeded the spacing of the mold, transition to complete wetting was observed (wetting transition). The extent of deformation became larger when the characteristic length of the bulk becomes longer and/or the size of the mold becomes smaller. In the MM system the deformation was much smaller than the MF system due to its rapid reaction rate. That is, the MF system allows a considerable time for wetting during phase separation, on the contrary, the MM system freezes soon after the onset of phase separation. Since wetting proceeds between the onset of phase separation and gelation, the MM system is less susceptible to the deformation. Gravity and viscosity were also found to affect the gel formation in addition to the hydrodynamic wetting. In the thicker samples the deformation becomes much salient due to the gravitational effect, and when more viscous water-soluble polymer was introduced in the solvent-rich phase the deformation is significantly suppressed.

In Chapter 3, the structural deformation in a long cylindrical capillary or a rectangular-sectioned open groove was studied. For a long cylindrical capillary the overall tendency in the MF system is closely resembles the case of 2D mold, which was

described in Section 3.1. In the MM system, the deformation was much suppressed in the hydrophilic capillaries as was seen in the 2D case. In the hydrophobic capillary, however, the deformation was promoted compared to the hydrophilic case. Hydrophobic interaction is also affecting this phenomenon. In Section 3.2 a markedly different structure was observed in an open groove. The web-like isotropic bicontinuous structure inside the groove was transformed into the pillar structure with decreasing the width of the groove. This phenomenon is named as "web-to-pillar transition". Special conditions that the confined gelling material is connected to the bulk reservoir and the shape of the surfaces are responsible to it.

In Chapter 4, more extensive study on the essential effects of confinement was described. A macroporous silica gel with mean pore diameter  $2.74\ \mu\text{m}$  was used as a OD mold. Although the MF-derived gels showed a similar behavior to the former cases, the other resultant gels exhibited a more complicated tendency. The MM system showed a similar tendency in the hydrophilic OD mold, however, in the hydrophobic mold complete wetting occurs even when the bulk characteristic length, i.e. the phase separation time, is very short. A swift diffusion during the early stage of spinodal decomposition is thought to be responsible for the rapid transition. In the TF system, the appearance of the confined gels did not bear the slightest resemblance to the corresponding bulk. The rough surfaces of the confined gels are the evidence of the effect in the early stage. Since the initial spinodal wavelength in the TF system is longer than the size of the mold, phase separation kinetics was significantly suppressed. The effect of random-field and wetting in the early stage is thought to become important.

In Chapter 5, an example of application to capillary HPLC is demonstrated. Since the MM system is less deformed by the contacting surface, and shorter characteristic length and larger size of the space are preferred to prepare homogeneous gel, the MM-derived gels with finer structures were prepared in  $530$  and  $200\ \mu\text{m}$  capillaries. Since the  $530\ \mu\text{m}$  capillary was found to form voids,  $200\ \mu\text{m}$  capillary was used for the HPLC characterization. Also, incorporation of a surfactant into the starting solution

successfully modified surface polarity. Both methylsiloxane gels with and without a surfactant showed an excellent separation of nitrobenzenes in normal phase.

The present thesis dealt the first study about the surface effects on the phase separation in sol-gel systems. Some aspects resembled the linear polymer blend system but there were a lot of unique contributing factors related to sol-gel. Phenomenological experiments gave a sufficient insight and will be quite useful for various applications whereas the most parts concerning dynamic aspect are still unexplored. Nevertheless the author wishes this work will contribute and be helpful to both application and phase separation physics.

## LIST OF PUBLICATIONS

### CHAPTER 1 and CHAPTER 5

“Structural formation of hybrid siloxane-based polymer monolith in confined spaces”

Kazuyoshi Kanamori, Hideyuki Yonezawa, Kazuki Nakanishi, Kazuyuki Hirao, Hiroshi Jinnai  
*Journal of Separation Science*, **27**, 874-886 (2004).

### CHAPTER 2

“Phase separation in methylsiloxane sol-gel systems in a small confined space”

Kazuyoshi Kanamori, Norio Ishizuka, Kazuki Nakanishi, Kazuyuki Hirao, Hiroshi Jinnai  
*Journal of Sol-Gel Science and Technology*, **26**, 157-160 (2003).

“Three-dimensional observation of phase-separated silica-based gels confined between parallel plates”

Kazuyoshi Kanamori, Kazuki Nakanishi, Kazuyuki Hirao, Hiroshi Jinnai  
*Langmuir*, **19**, 5581-5585 (2003).

“Phase separation in siloxane sol-gel confined in a two-dimensional space: Effect of wetting, gravity, and viscoelasticity”

Kazuyoshi Kanamori, Yoshitaka Suzumura, Kazuki Nakanishi, Kazuyuki Hirao, Hiroshi Jinnai  
to be submitted to *Langmuir*.

“Three-dimensional observation of phase-separated siloxane sol-gel structures using Laser Scanning Confocal Microscopy (LSCM)”

Kazuyoshi Kanamori, Kazuki Nakanishi, Kazuyuki Hirao, Hiroshi Jinnai  
H. Morawiec, D. Stróż eds. “Proceedings of the XIX Conference of Applied Crystallography”,  
pp. 367 (2004).

### CHAPTER 3

“Three-dimensional observation of phase-separated siloxane sol-gel structures in confined spaces using Laser Scanning Confocal Microscopy (LSCM)”

Kazuyoshi Kanamori, Kazuki Nakanishi, Kazuyuki Hirao, Hiroshi Jinnai

*Colloids and Surfaces A: Physicochemical Engineering Aspects*, **241**, 215-224 (2004).

“Interface-directed web-to-pillar transition of microphase-separated siloxane gels”

Kazuyoshi Kanamori, Kazuki Nakanishi, Kazuyuki Hirao, Hiroshi Jinnai

*Langmuir*, **19**, 9101-9103 (2003).

“Tailoring spontaneous pillar structure using phase-separating organosiloxane sol-gel systems in micro-fabricated grooves”

Kazuyoshi Kanamori, Kazuki Nakanishi, Kazuyuki Hirao, Hiroshi Jinnai

Submitted to *Journal of Sol-Gel Science and Technology*.

“Interface-directed web-to-pillar transition of phase-separating siloxane sol-gel systems in micro-fabricated grooves”

Kazuyoshi Kanamori, Kazuki Nakanishi, Kazuyuki Hirao, Hiroshi Jinnai

XX International Congress on Glass Proceedings, O-11-002, 2004.

### CHAPTER 4

Phase separation in siloxane sol-gel systems in a macroporous medium

Kazuyoshi Kanamori, Kazuki Nakanishi, Kazuyuki Hirao, Hiroshi Jinnai

to be submitted to *Langmuir*.



The structural control of methylsiloxane gels and their chromatographic behavior described in Chapter 5 received first prize in “HPLC 2004 Best Poster Awards” at HPLC 2004 (Philadelphia, USA).

---

## HPLC 2004 Best Poster Paper Award First Prize

**P-0710 “Structural Control of Phase-Separated Methylsiloxane Polymer Monoliths in Confined Spaces”, K. Kanamori, Hideyuki Yonezawa\*, Kazuki Nakanishi, Kazuyuki Hirao, and Hiroshi Jinnai#, Graduate School of Engineering, Kyoto University, Kyoto, Japan; \* Nitto Denko Corp., Osaka, Japan; #Kyoto Institute of Technology, Kyoto, Japan**

**Award: \$750 Amazon.com gift Certificate**



## ACKNOWLEDGEMENT

The present dissertation has been carried out under the direction of Professor Kazuyuki Hirao at Graduate School of Engineering, Kyoto University.

Many people are responsible for my completion of this thesis, far too many to name, but a few of them deserve singling out. First of all, the author wishes to express his sincere gratitude to Professor Kazuyuki Hirao for his continuous encouragement and valuable advice all through the duration of the present work. The author is also grateful to Professor Toshinobu Yoko and Professor Katsuhisa Tanaka for their useful suggestions on the present thesis. The author also thanks Professor Teiichi Hanada, Professor Setsuhisa Tanabe, Dr. Koji Fujita, and Mr. Shunsuke Murai in Kyoto University.

The author is greatly indebted to Professor Kazuki Nakanishi for his critical discussions, experimental directions and sincere supports. Most of the present work had not been accomplished without him. Many experimental instructions concerning LSCM and fruitful discussions on phase separation in confined geometry are contributed by Professor Hiroshi Jinnai, Dr. Yukihiro Nishikawa and the students at Kyoto Institute of Technology.

Many thanks also to the member of Hirao's laboratory for their collaboration and everyday activities. Especially, the author's colleagues, Mr. Atsushi Itagaki, Mr. Masayuki Nishi and Mr. Yoshinori Yonesaki have greatly contributed to my happiest time.

An acknowledgement is extended to the financial support by a Grant-in-Aid for Scientific Research (No. 16000836) from the Ministry of Education, Culture, Sports, Science and Technology, Japan.

Last but not least, the author expresses his sincere gratitude to his parents, Yasuo Kanamori and Keiko Kanamori, for their understanding, visible and invisible supports, and hearty encouragements so far.

Kyoto, Winter 2005

Kazuyoshi Kanamori



## APPENDIX: ACCURACY OF LSCM OBSERVATION AND OTSU THRESHOLDING

It is necessary to investigate the accuracy of LSCM observation by comparing to other methods. Here, a comparison between LSCM and mercury porosimetry is described. Although all the results in the present thesis were derived from thresholding with human eye, the validity of Otsu thresholding, one of the best methods to decide a binarization threshold, described in Chapter 1 is also examined.

### Otsu's thresholding [1]

The principle of Otsu's thresholding is very simple. Let the pixels of a given picture be represented in  $L$  gray levels  $[1, 2, \dots, L]$ . The number of pixels at level  $i$  is denoted by  $n_i$  and the total number of pixels by  $N=n_1+n_2+\dots+n_L$ . The gray-level histogram  $n_i$  is normalized by the total number of pixels into  $p_i$  and regarded as a probability distribution:

$$p_i = \frac{n_i}{N} \quad (\text{A-1})$$

Now, suppose the histogram is divided into two classes  $C_0$  and  $C_1$  (background and objects, or vice versa) by a certain threshold  $k$ . Here  $C_0$  denotes a group of pixels with levels  $[1, \dots, k]$  and  $C_1$  with  $[k+1, \dots, L]$ . Then the probabilities of class occurrence and the class mean levels, respectively, are given by

$$\omega_0(k) = \sum_{i=1}^k p_i, \quad \omega_1(k) = \sum_{i=k+1}^L p_i \quad (\text{A-2})$$

$$\bar{\mu}_0(k) = \sum_{i=1}^k ip_i / \omega_0(k), \quad \bar{\mu}_1(k) = \sum_{i=k+1}^L ip_i / \omega_1(k). \quad (\text{A-3})$$

The class variances are given by

$$\sigma_0^2(k) = \sum_{i=1}^k (i - \bar{\mu}_0(k))^2 p_i / \omega_0(k), \quad \sigma_1^2(k) = \sum_{i=k+1}^L (i - \bar{\mu}_1(k))^2 p_i / \omega_1(k). \quad (\text{A-4})$$

The total mean level of the original picture and the total variance of levels, respectively, are

$$\bar{\mu}_T = \sum_{i=1}^L i p_i = \sum_{j=1,2} \omega_j(k) \bar{\mu}_j(k), \quad \sigma_T^2 = \sum_{i=1}^L (i - \bar{\mu}_T)^2 p_i = \sigma_W^2(k) + \sigma_B^2(k), \quad (\text{A-5})$$

where  $\sigma_W^2(k) = \omega_0(k) \sigma_0^2(k) + \omega_1(k) \sigma_1^2(k)$  and  $\sigma_B^2(k) = \omega_0(k) (\bar{\mu}_0(k) - \bar{\mu}_T)^2 + \omega_1(k) (\bar{\mu}_1(k) - \bar{\mu}_T)^2$  exhibit the within-class variance and the between-class variance, respectively. The most appropriate threshold is given by the maximum of the following criterion;

$$\eta(k) = \sigma_B^2(k) / \sigma_T^2. \quad (\text{A-6})$$

Since  $\sigma_T^2$  is independent of  $k$ , the above thresholding is equivalent to maximizing  $\sigma_B^2(k)$ .

### Experimental

The sample used in validation is the MF-derived siloxane gel at MTMS : FA : H<sub>2</sub>O = 1 : 2.3 : 2.5. In LSCM observation, uranine/DMA solution (denoted as U/DMA) and fluorescein/FA solution (F/FA) were employed as contrast-matching solutions containing a fluorescent dye. For the thresholding of LSCM images, human-eye determination (denoted as E) and Otsu's method (denoted as O) were employed. That is, U/DMA/E, U/DMA/O, F/FA/E, and F/FA/O are compared.

In mercury porosimetry, a cell with known volume  $V_c$  was used. Bulk volume (skeleton plus pore) of the sample  $V_b$  is given by  $V_b = V_c - V_{Hg}$ , where  $V_{Hg}$  is the volume of mercury introduced in the cell at a low pressure. Note that this sample does not have a large pore and is not intruded by mercury below ambient pressure. Macropore volume  $V_p$  is equivalent to the cumulative pore volume, which is chosen at the pore diameter around the resolution of LSCM (553 nm in lateral resolution). Then the porosity  $\phi$  is given by  $\phi = V_p / V_b$ . The values of porosity derived from both mercury porosimetry and LSCM are compared.

## **Results and Discussion**

A slight difference of appearance was observed between the samples contrast-matched by DMA and FA. Since the refractive index of methylsiloxane gel is closer to that of DMA, the U/DMA sample was obviously more transparent compared to the sample F/FA. In Figure A1, raw LSCM images of the D/DMA and F/FA samples at the similar depths are shown. The F/FA sample in part (b) suffers from low contrast and the two peaks in the histogram are close together. On the other hand, two peaks in the histogram of the sample U/DMA is well separated and it is better for the binarization.

Figure A2 and A3 shows the reconstructed images of the samples U/DMA and F/FA, respectively. In part (a) thresholding was performed by human eye (U/DMA/E in Figure A2 and F/FA/E in Figure A3), and part (b) by Otsu's method (U/DMA/O in Figure A2 and F/FA/O in Figure A3). There is no visible difference between the two thresholding methods. Table A1 summarizes the geometrical parameters derived from mercury porosimetry, LSCM with human thresholding and Otsu's method. With regard to the porosity, though there is a little difference between the samples and the thresholding methods, these are in good agreement and LSCM is proved to be an excellent reliable method. In particular, an appropriate contrast-matching method results in better contrast images, and thresholding with human eye is the most reliable. However, since thresholding with human eye is dependent on an experimenter, Otsu's method should be used in the future. A slight difference of porosity between mercury porosimetry and Otsu's method may be within the experimental error. However, it is better to check the optical distortion or blur in LSCM images resulted from the geometry of the confocal ray path and/or mismatch of refractive indices. Deconvolution of images using the "point spread function" has to be examined in particular [2].

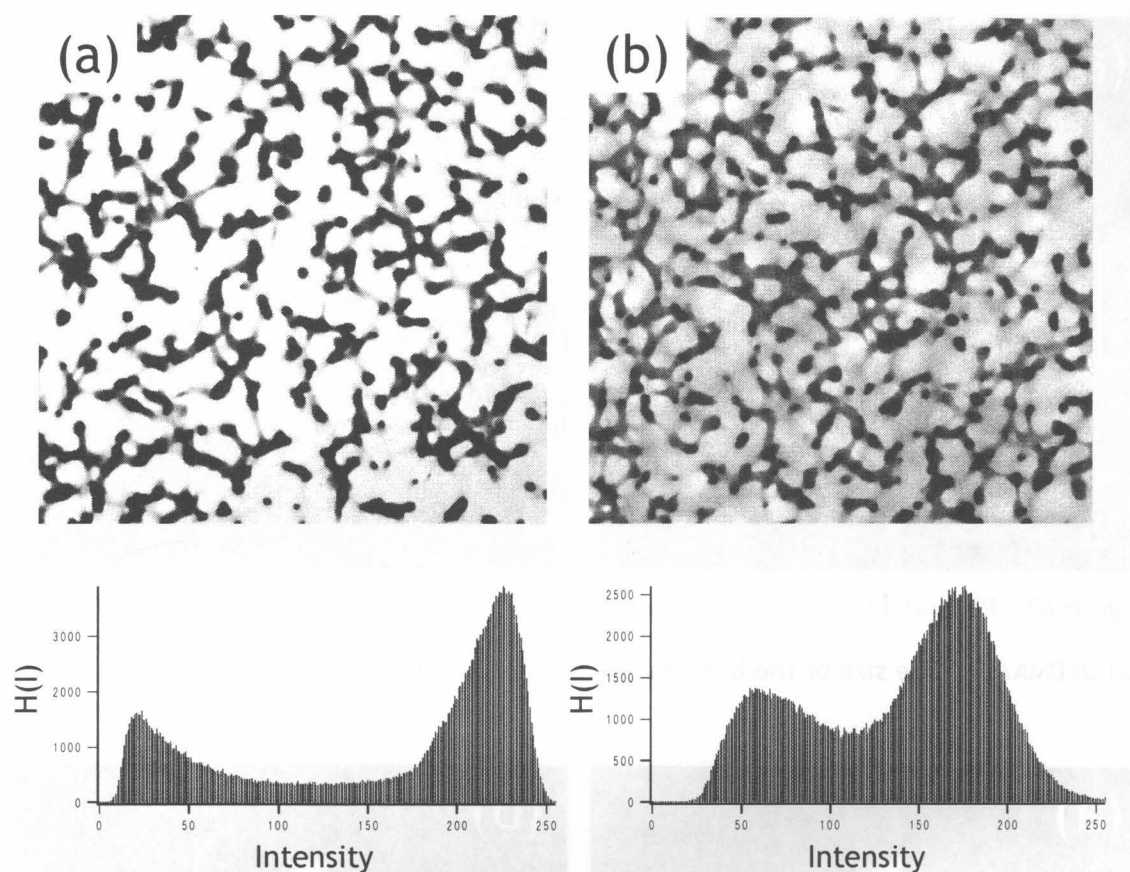


Figure A1 RAW LSCM images of the (a) U/DMA and (b) F/FA samples at the similar depth. The depth is ca.  $40\ \mu\text{m}$  beneath the surface of the coverslip. The graphs below the images are corresponding histograms of pixel intensities.

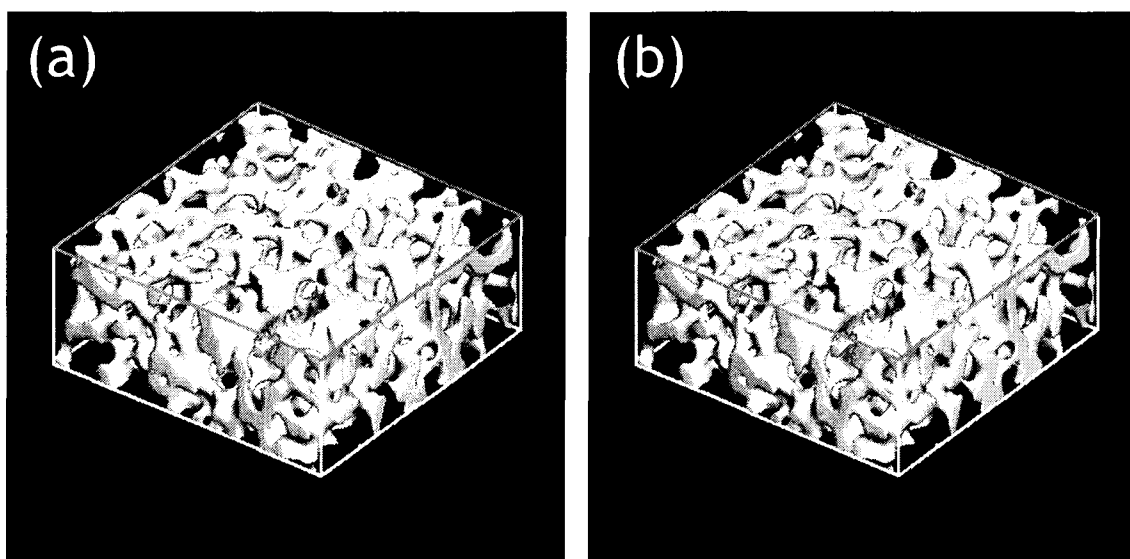


Figure A2 Reconstructed images of the sample of the same volume. (a) U/DMA/E, and (b) U/DMA/O. The size of the both images are  $731. \times 73.1 \times 29.75 \mu\text{m}^3$ .

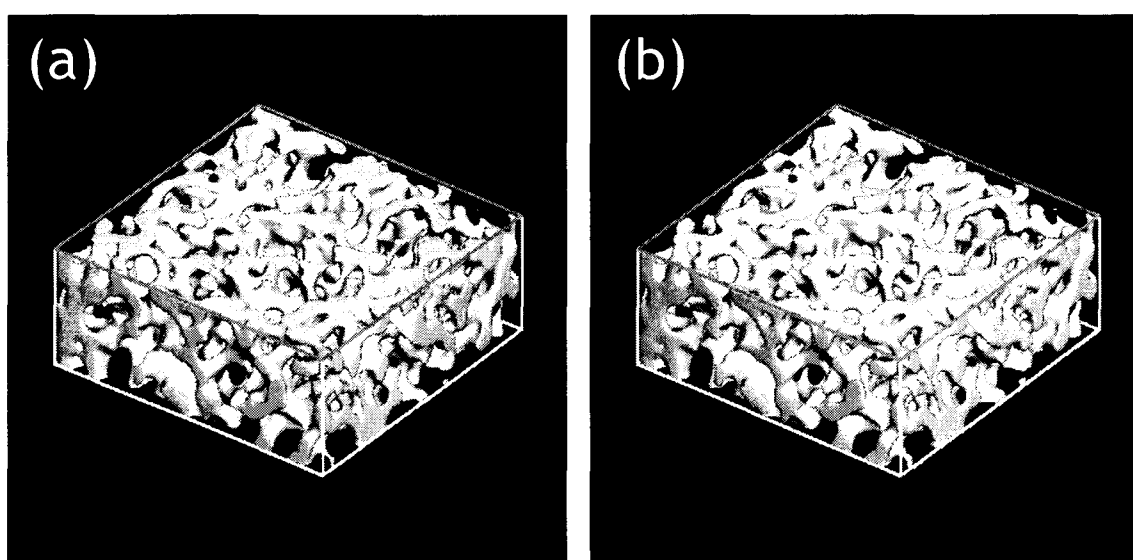


Figure A3 Reconstructed images of the sample of the same volume. (a) F/FA/E, and (b) F/FA/O. The size of the both images are  $731. \times 73.1 \times 29.75 \mu\text{m}^3$ . The sample is the same as in Figure A1, but the volume is different.



Table A1 Parameters obtained from different procedures

	Porosity $\phi$	Characteristic length ( $\mu\text{m}$ )	$\langle \tilde{H} \rangle$	$\langle \tilde{K} \rangle$
Hg porosimetry	0.674*			
U/DMA/E	0.668	12.9	-0.252	-1.85
U/DMA/O	0.664	13.0	-0.241	-1.85
F/FA/E	0.664	13.5	-0.251	-1.84
F/FA/O	0.642	13.7	-0.191	-1.79

\*Calculated using the value of cumulative pore volume at 557.8 nm.